AN EXPERIMENTAL APPARATUS FOR MEASUREMENT OF PRESSURE DROP, VOID FRACTION, AND NON-BOILING TWO-PHASE HEAT TRANSFER AND FLOW VISUALIZATION IN PIPES FOR ALL INCLINATIONS

By

WENDELL L. COOK

Bachelor of Science in Mechanical Engineering

Oklahoma State University

Stillwater, Oklahoma

2004

Submitted to the Faculty of the
Graduate College of the
Oklahoma State University
in partial fulfillment of
the requirements for
the Degree of
MASTER OF SCIENCE
December, 2008

AN EXPERIMENTAL APPARATUS FOR MEASUREMENT OF PRESSURE DROP, VOID FRACTION, AND NON-BOILING TWO-PHASE HEAT TRANSFER AND FLOW VISUALIZATION IN PIPES FOR ALL INCLINATIONS

Thesis Approved:

Dr. Afshin J. Ghajar

Thesis Adviser

Dr. Frank W. Chambers

Dr. David G. Lilley

Dr. A. Gordon Emslie

Dean of the Graduate College

ACKNOWLEDGMENTS

I would like to thank my graduate advisor, Dr. A. J. Ghajar for his guidance support and patience and most of all for his friendship throughout my studies as a master's student as well as through the completion of this thesis. I would like to thank all of the colleagues who have worked with me on this research, Clement Tang, Melkamu Woldesemayat, Pranav Godbole, and Nishant Mathure. Special thanks go to Clement without whose hard work and friendship this research would not have been possible.

Very special thanks go to my parents, George and Susan Cook, for their unwavering love and support throughout my college career. This document is dedicated to them for there is little doubt that it is they who instilled me with the perseverance and determination to see this part of my schooling through to closure.

TABLE OF CONTENTS

Chapter Page

LIST OF TABLES

Table Page

LIST OF FIGURES

Figure Page

Figure Page

NOMENCLATURE

English Letter Symbols

A	Amperes or area
AWG	American Wire Gauge
Btu	British thermal units
C	Celsius
cc	Cubic centimeter
c_f	Fanning friction factor
C_p	Specific heat
D	Diameter
Eo	Eötvös number
F	Fahrenheit
f	Darcy friction factor
F_p	Flow pattern factor
F_s	Shape factor
ft	Feet
g	Grams or acceleration due to gravity
h	Heat transfer coefficient
gal	Gallons
hr	Hours
Hz	Hertz

I	Inclination factor or current
ID	Inner pipe diameter
in	Inches
IPS	Iron pipe size
K	Kelvin
k	Thermal conductivity
L	Liters
l	Length
lbm	Pounds mass
m	Meters
$\dot{m}$	Mass flow rate
min	Minutes
Nu	Nusselt number $Nu = hD / k$, dimensionless
P	Pressure
Pa	Pascals
psi	Pounds per square inch
Pr	Prandtl number $\mathrm{Pr} = C_p \mu / k$, dimensionless
$\dot{q}$	Heat transfer rate
$\dot{q}$"	Heat Flux
Re	Reynolds number $\mathrm{Re} = \rho VD / \mu$, dimensionless

R_t	Thermal resistance
s	Seconds
T	Temperature
$\overline{T}$	Average temperature
U	Velocity
V	Velocity or Voltage
V_D	Voltage drop
VDC	Direct current voltage
W	Uncertainty
W	Watts
x	Quality $x = m_G / m_{tot}$, dimensionless

Greek Letter Symbols

α	Void fraction
Δ	Change in …
θ	Inclination angle
μ	Absolute viscosity
μ_b	Absolute viscosity evaluated at bulk temperature
μ_w	Absolute viscosity evaluated at inner wall temperature
ρ	Density
σ	Surface tension

Subscripts and Superscripts

atm	Atmosphere
b	Bulk
cal	With respect to calibration
D	With respect to diameter
G	Gas
i	Inner
in	At the inlet or input
GM	Derived from mass with respect to gas
liq	Liquid
L	Liquid
o	Outer
out	At the outlet or output
rms	Root mean square
SG	Superficial gas
SL	Superficial liquid
system	With respect to the system
tk	With respect to tank
tot	Total
TP	Two-phase
wi	Inner wall
wo	Outer wall

CHAPTER I

INTRODUCTION

By definition, two-phase flow is the simultaneous movement of two differing phases, where the phase refers to the state of the matter (i.e. solid, liquid or gas). Two-phase flows can occur as either single-component flow or multi-component flow. Single-component two-phase flows occur when both the phases are of the same chemical composition. This type of flow typically involves some sort of phase change such as melting or boiling. Multi-component two-phase flow involves the simultaneous movement of two different phases with differing chemical compositions. Phase changes are generally not associated with multi-component two-phase flow. It is towards the latter of these types of two-phase flow with which the present investigation will be directed.

Multi-component two-phase flows are commonly associated with the oil and natural gas industry. Transport of crude oil to the surface involves the simultaneous movement of oil and natural gas through the associated pipelines. As the hydrocarbon fluids move towards the surface, their temperature will drop to some value between the reservoir temperature and the temperature of the surrounding medium. The temperature change is directly related to the heat lost from the hydrocarbon fluids to the earth surrounding the well. Several design problems arise in petroleum production which necessitate the calculation of a flowing temperature profile. One of these is the

calculation of two-phase flowing pressure traverses that are necessary in tubing design, artificial lift design and productivity testing (Shiu and Beggs, 1980).

This temperature change associated with the heat transfer between the hydrocarbon fluids and the surrounding earth is also directly related with the buildup of hydrocarbon waxes in oil pipelines. In the case of sub-sea oil production, oil may leave the reservoir at a temperature of 75˚C and experience a temperature drop at the pipeline wall to roughly 4˚C. This drop in temperature combined with pressure changes associated with extraction can cause the accumulation of paraffin precipitates around the outer wall of the pipeline (Singh et al., 2000). This wax accumulation can result in reduced flow efficiency and even total blockage of petroleum transport lines. The U.S DOE (2001) estimated the cost of clearing sub-sea blockages at $1 million per mile. A specific example of monetary losses associated with wax buildup is that of the Lasmo Company (U.K.). In this particular case, a platform had to be abandoned at a cost of $100 million (Singh et al., 2000).

The build up of wax in petroleum pipelines is not restricted to sub-sea operations. One particular study of 69 oil fields in 19 U.S. states showed that paraffin was present in oil from 59 of the fields in 18 states (Woo et al., 1984). Overall, the problem costs the petroleum industry billions of dollars annually, in terms of cost of treatment, reduced production, wells shut-in, inefficient use of production capacity, choking of flow lines, premature abandonment, and increased manpower (Yong, 1996).

A second phenomena associated with the two-phase flow moving though oil and natural gas pipelines is hydrate plug formation. Gas hydrates are ice-like crystalline compounds composed of nano-scale water cages that enclose gas molecules of

appropriate diameters. Due to the frequent presence of water and light hydrocarbons, such as methane, in oil production, hydrate formation is of serious concern. Hydrate formation is of particular concern in sub-sea operations where high pressures and low temperatures are often encountered (Gao et al. 2005). Thus, it is critical to develop a knowledge of two-phase heat transfer phenomena in oil and natural gas pipeline so as to prevent gas hydrate and wax deposition blockages (Furuholt, 1988).

Two-phase mixtures can also be of interest in planned space operations. Knowledge of the phase distribution is of particular importance in the design of piping systems, separators and other associated units. The design of such systems is, by nature, limited in terms of size, causing the prediction of heat transfer characteristics to be of particular importance (Fore et al., 1996). Flow pattern mapping and transition criteria in reduced gravity situations have been of particular interest (Dukler et al. 1988; Zhao and Rezkallah, 1993; Bousman and Dukler, 1994). Also of interest have been measurements of void fraction and pressure drop in slug flow (Boussman, 1994). Studies of two-component heat transfer have been conducted by Rite and Rezkallah (1994) and Fore et al. (1996, 1997) using air and water. However, these studies have been limited to slug and annular flows.

Wang et al. (2004) pointed out that while two-phase single-component heat transfer correlations are relatively abundant; the literature is sparse in terms of two-phase multi-component research. Due to the limited number of studies available, convection heat transfer research was conducted on the shell side of a TEMA-F horizontal heat exchanger using 60% aqueous glycerin and air. This research ultimately resulted in the recommendation of a correlation for two-phase heat transfer coefficient. The correlation

developed was applicable for stratified, intermittent, and annular flows in shell and tube heat exchangers.

Research at the Oklahoma State University heat transfer laboratory has been directed towards the further enhancement of knowledge in these areas for the past several years. An extensive literature review by Kim et al. (1999) identified a total of 38 different two-phase flow heat transfer correlations as well as several experimental data sets for forced convective heat transfer. The validity and range of applicability of the correlations identified was in most cases documented by the original authors. In the majority of the cases, the correlations presented were generated using small sets of experimental data. The range of applicability of the correlations identified in terms of flow pattern and gas-liquid combinations was found to be quite limited. Of the data sets identified, the majority were for forced convection during two phase liquid gas flow in vertical pipes. Only very limited data was obtained for two-phase non-boiling heat transfer in horizontal pipes and non-boiling two-phase heat transfer data for inclined flows was lacking entirely. Continued work in the area of two-phase non-boiling heat transfer resulted in the development of a general correlation for two-phase non-boiling heat transfer in pipes in a vertical orientation (Kim et al., 2000).

In the interest of broadening the work of Kim et al. (2000), it proved desirable to develop a robust heat transfer correlation that is capable of spanning all or most of the fluid combinations, flow patterns, flow regimes, and pipe orientations (i.e. vertical, horizontal, and inclined). In order to collect the data necessary to develop this correlation, a state-of the-art experimental facility was developed for systematic heat transfer data collection in horizontal and inclined positions (up to 7˚). This experimental

setup was capable of producing a variety of flow patterns and included two transparent flow visualization sections for the purposes of detailed flow pattern visualization and flow pattern mapping. The general heat transfer correlation developed through the use of this experimental apparatus has been published in numerous papers and is published most recently in Ghajar and Tang (2008).

Through the extensive use of the aforementioned experimental test facility, certain limitations began to present themselves. The first of these was that the test facility had a maximum angle of inclination of 7˚. This limitation was primarily rooted in the size of the experimental apparatus. When all of the necessary components were incorporated into the experimental apparatus, it was simply too long to achieve an angle of inclination higher than 7˚ within the dimensions of the laboratory. As previously mentioned, it was intended that the correlation developed would be applicable for any angle of inclination. Thus this limitation on inclination angle proved quite problematic.

The second major limitation associated with the experimental apparatus was its inability to take measurements of void fraction. The majority of the heat transfer correlations in the literature as well as the in house correlation developed are dependent on void fraction as a parameter. Originally, the void fraction correlation of Spedding and Chen (1984) was used for the purpose of obtaining void fraction values. However, the heat transfer correlation developed has the robustness that it can be utilized with multiple void fraction correlations. In an attempt to investigate the accuracy of the void fraction correlations available in the literature, an extensive literature review was conducted by Woldesemayat and Ghajar (2007), resulting in the proposal of an improved void fraction correlation. Ultimately, it is desirable to have the ability of accurate void fraction

measurement for the purposes of use in combination with the heat transfer correlation as well as for the purposes of further development of the void fraction correlation.

Flow visualization and flow pattern mapping are also matters of critical importance. While the flow visualization sections fore and aft of the heat transfer section in the experimental apparatus were sufficient to generate quality flow pattern images and provided the ability to develop flow pattern maps, it proved desirable to have a dedicated flow visualization test section with optical quality clear tubing in order to further enhance the quality of the images obtained.

In order to further extend research capabilities and address some of the aforementioned limitations, an entirely new experimental apparatus has been developed. This experimental apparatus has two separate test branches. The first of these is a clear test branch dedicated to obtaining void fraction and pressure drop data as well as flow visualization. A separate branch is capable of taking two-phase heat transfer measurements as well as pressure drop measurements. Both test sections are half the inner diameter of the original experimental apparatus, allowing the length of the testing area to be reduced to the point that data can be taken at any angle of inclination, ranging between ±90˚. This state-of-the-art experimental apparatus is the first of its kind, allowing for flow visualization, void fraction measurements, pressure drop measurements, and heat transfer measurements at any inclination between ±90˚ all in one compact unit.

This document is intended to detail the design, construction and the validation of this new experimental apparatus. Toward that end, four chapters will follow:
Experimental Setup, Calibration of Experimental Setup and Experimental Procedure,

Results and Discussion, and Conclusions. The Experimental Equipment chapter will detail the components of the experimental apparatus. Calibration of the Experimental Setup and Experimental Procedure will detail the calibration process and give a detailed description of the operation of the experimental apparatus. The Results and Discussion section will present the results of the validation of the experimental apparatus in terms of pressure drop, void fraction, and heat transfer measurements. The Conclusions chapter will present both the conclusions derived from the validation of the experimental apparatus as well as recommendations for further research.

CHAPTER II

EXPERIMENTAL SETUP

This chapter provides a discussion of all of the critical components of the experimental test setup. It is necessary to discuss the characteristics of the experimental setup in order to facilitate a greater understanding of the function of the test branches as well as the instrumentation used. An overall system schematic is depicted in Figure 2.1. Figure 2.2 is a photograph of the experimental setup in its fully vertical position. More extensive diagrams of the individual test sections will be provided later on in the chapter.

As the experimental setup is made to serve three different major research purposes and is comprised of two separate test branches, it is going to be beneficial to discuss each test branch independently. The first half of this chapter will discuss the components of the test setup that are shared between the two test branches. These sections include Test Platform, Variable Inclination Frame, Water Transport, Air Transport, Coriolis Flow Meters, Data Acquisition, Pressure Transducer, and Connections to the Test Area. Later in the chapter, individual components unique to each of the test branches will be discussed. The Heated Branch will be broken into four different sections in order to facilitate discussion. These sections are Mixing Sections, Flow Visualization Sections, Heated Test Section, and Thermocouple Array. The Flow Visualization / Void Fraction Branch will also be discussed in terms of four different major components.

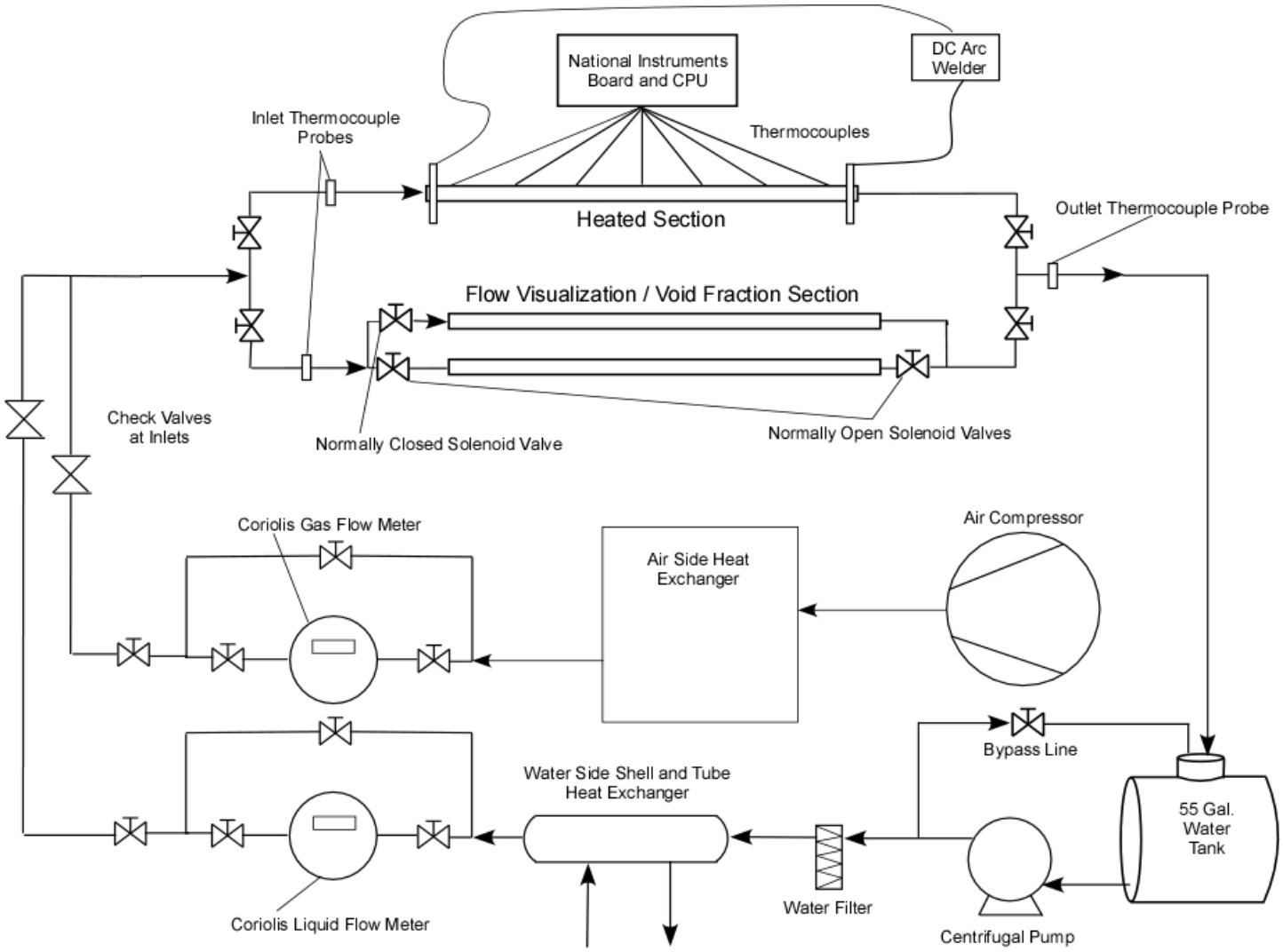

Figure 2.1: Schematic of the Experimental Setup

Figure 2.2: Experimental Setup in the Fully Vertical Position

These are the Mixing Section, Thermocouple Array, Void Fraction System, and Flow Visualization Section. A full listing of all equipment associated with the experimental apparatus can be found in Appendix A.

2.1 Test Platform

Both the heated and void fraction / flow visualization branches rest in the same test platform. The platform itself consists of an aluminum I-beam fabricated from 2.381mm (3/32in) aluminum sheet and 3.175mm (1/8in) by 50.8mm (2in) aluminum angle. The platform measures 3.353m (11ft) in length and 0.61m (2ft) in width. The flat portion constructed from the aluminum sheet measures 3.05m (10ft) by 0.61m (2ft). In order to construct the I-beam, the sheet was sandwiched between two 3.353m (11ft) lengths of aluminum angle on either side. The sheet was centered along the lengths of angle in order to leave 15.24cm (6in) areas at each end of the platform allowing for necessary plumbing. Small holes have also been cut along the length of the platform in order to allow for various components to pass to the underside of the platform. The test sections are fastened to the platform using a combination of 5.08cm (2in) by 15.24cm (6in) blocks and leather strapping. The blocks are used as risers to get the test branches up off of the platform. The leather strapping proved an effective method of fastening the test section down to the risers. The platform itself is attached to the variable inclination frame.

2.2 Variable Inclination Frame

The variable inclination frame is one of the key components of the experimental setup. One of the design constraints for this project was that the test sections be able to articulate from positive 90˚ all the way down to negative 90˚. Thus every design feature of this frame caters towards achieving this high degree of articulation while maintaining a high degree of rigidity. Figure 2.3 depicts a schematic of the variable inclination frame.

As can be seen in the figure, the variable inclination frame actually consists of two frames; a heavy outer frame and a lighter internal rolling frame. The large heavy outer frame measures 4.57m (15ft) in length, 3.66m (12ft) in height and 0.84m (33in) in width. The 3.66m (12ft) height is necessary in order to allow the test sections and platform to become completely vertical. The length of the frame is longer than that of the test platform. This was done in order to leave room for any possible unforeseen additions to the experimental setup. While it would have been beneficial to leave extra space at the top of the frame, the height of the frame was constrained by the ceiling in the lab. The outer frame is constructed of 3.175mm (1/8in) by 50.8mm (2in) by 101.6mm (4in) rectangular steel tubing. Large gussets made out of 4.76mm (3/16in) steel plate were attached at the corners of the outer frame in order to ensure rigidity. The outer frame is also bolted into the concrete floor in order to provide increased stability and rigidity. The inner rolling frame is constructed entirely out of 3.175mm (1/8in) by 38.1mm (1.5in) steel angle. The vertical portion of the internal frame consists of a guide made out of two pieces of steel angle facing each other. The test platform is attached to the rolling frame via a bolt and plastic bushing combination. When tightened, the point of attachment is rigid. When the bolt is loosened, movement along the axis of the guide can be achieved.

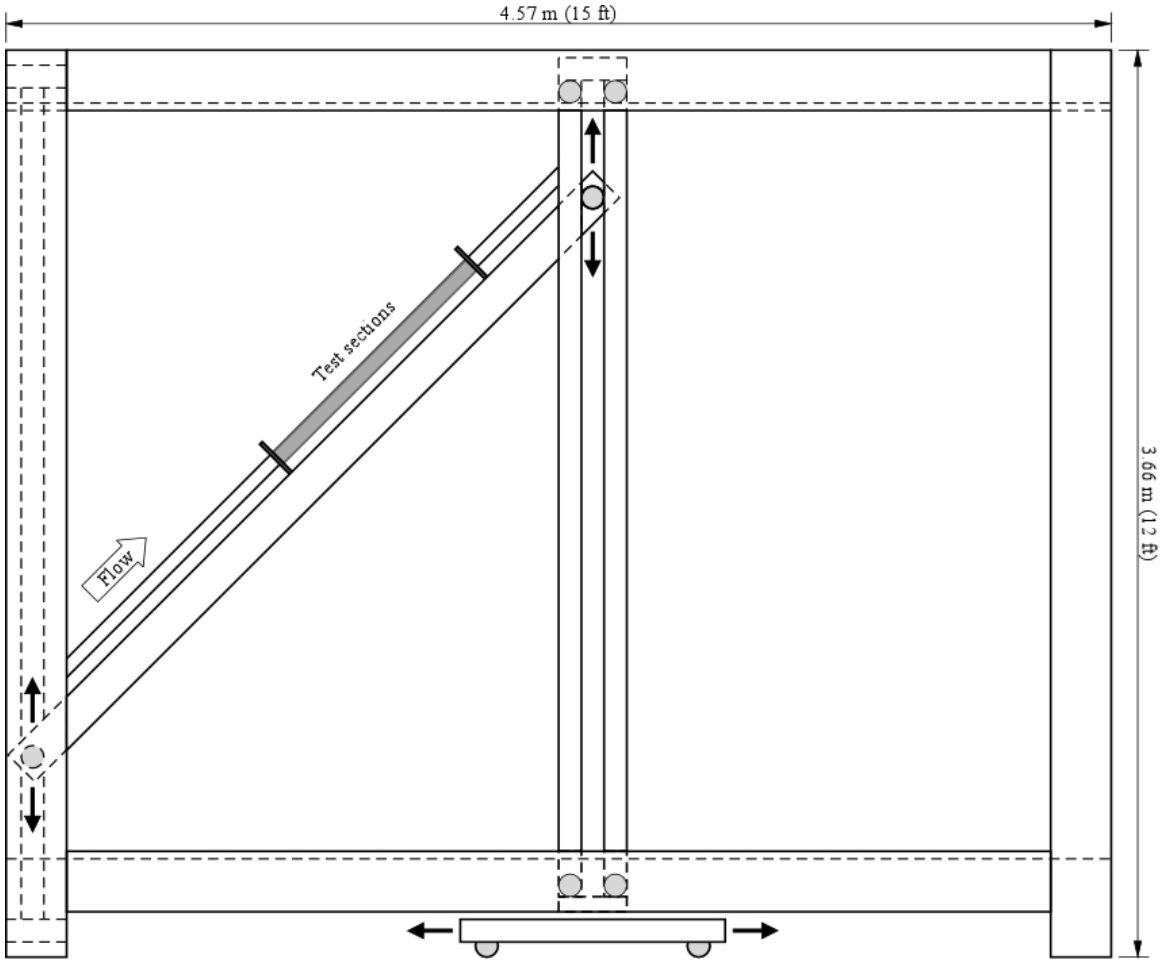

Figure 2.3: Test Platform and Variable Inclination Frame

Guides made out of 3.175mm (1/8in) by 38.1mm (1.5in) steel angle are attached to the upper and lower lengthwise crossbeams as well as to the vertical supports at one end of the frame. The vertical guides are used to allow for vertical movementat the end of the test platform opposite of the end attached to the inner rolling frame. The inner frame is attached to the horizontal guides along the length of the outer frame. Here too, a bolt and bushing combination is used. Loosening the bolts allows for movement of the inner frame in the horizontal direction. Once tightened, the bolts provide a rigid attachment point. Using this mechanism, increasingly positive or negative angles of inclination can be achieved as the rolling frame is moved towards the fixed vertical supports. Angle of incline is measured using a simple contractor's angular scale.

2.3 Water Transport

The working fluids used in research conducted with the experimental setup are air and purified water. The water is filtered via reverse osmosis by the Chemistry Department at Oklahoma State University. The purified water is stored in a 208.2L (55gal) cylindrical tank. Water transport is achieved via a closed system. Thus, the polyethylene drum serves not only as a storage tank, but also as a fluid reservoir for the system.

Water is pulled from the tank via a Bell and Gosset series 1535 Coupled Centrifugal Pump. The pump model number is 3545 D10. The pump generates mass flow rates that are more than acceptable for the purposes of this experimental setup. When pushing water through each individual test section the pump can achieve mass flows up to 0.226kg/s (30lbm/min).

After passing through the pump, the water passes through an Aqua-Pure AP12T water purification system. This system has been included within the setup in order to prevent the growth of organics as well as to trap any foreign objects that might be introduced into the system. The pleated paper filters will trap objects down to the size of 20μm (7.87E-04in). The filtration system has a maximum operating temperature of 38˚C (100˚F) and a maximum operating pressure of 862kPa (125psi). For additional filtration, a bypass line with a small Oberdorfer Model 600 F13 pump and Bio Logic BIO-1.5 UV filter has also been included. Water is passed through this UV filter on a weekly basis to further ensure that it remains free of organic impurities.

The next step in the water cycle is a heat exchanger. It is necessary to implement a heat exchanger in the experimental setup so that water is consistently passed to the test sections at a constant temperature. The heat exchanger used is an ITT Standard model BCF 4063 one shell and two-tube pass heat exchanger. The heat exchanger has a shell area of 1.97 m^2 (12.2ft^3) and a maximum duty of 19.7kW (18.67Btu/s). Cooling water for the heat exchanger is obtained from a tap located in the lab area. The temperature of the cooling water averages about 22˚C (71.6˚F). However, due to the use of tap water, the cooling water temperature will vary depending on the outside temperature. Temperatures of the cooling water will range between 18˚C (64.4˚F) and 26˚C (78.8˚F). The cooling water is supplied to the heat exchanger at a rate of approximately 45.5L/min (10gal/min).

Beyond the heat exchanger, the water passes through one of two Coriolis flow meters that will be discussed later on in this document. Control over the water flow rate is achieved by a gate valve located just after the flow meter assembly. The water then

mixes with the air supply as it passes through one of the test sections and eventually returns to the 208.2L (55gal) reservoir. Air escapes from the reservoir via a curved vent on its upper surface, allowing air but not water to exit the tank.

2.4 Air Transport

The airflow to the system is provided by a large air compressor located in an outbuilding located adjacent to the lab. It was deemed necessary to locate the compressor in a separate area due to the considerable noise and heat generated by its operation. The compressor used is an Ingersoll-Rand T30 Model 2545 Industrial Air compressor. The maximum pressure that the compressor can achieve is 862kPa (125psi). Air is supplied to the system at a maximum mass flowrate of 0.25kg/min (0.55lbm/min). The compressor has also been fitted with both a dump valve and an unloader valve in order to facilitate a more consistent air pressure.

Air passes from the compressor room into the lab and immediately into a 1379kPa (200psi) regulator / filter-drier assembly. This allows for some initial control over the air pressure inlet to the setup as well as providing added air pressure consistency. The filter-drier removes foreign objects from the air flow as well as unwanted condensation produced by the compressor.

After passing through the regulator, the compressed air is sent through a copper coil submerged in running tap water. This simple heat exchanger is used to remove heat generated by the compressor as well as high outdoor temperatures. As tap water is used as the cooling water, the temperature of the air exiting the coil is very close to that of the water exiting the shell and tube heat exchanger.

After passing through the copper coil, the compressed air passes through yet another filter-drier assembly and into a Parker Model 24NS 82(A)-V8LN-SS Needle Valve, used for flow control. This metering valve provides for very fine adjustment of the air mass flow rates that are necessary for this setup. The meter through which the air passes is controlled by system of ¼ turn ball valves. Once again, the Coriolis flow meter assembly will be discussed later in this document. After passing through one of the meters, the air moves in to the desired test section where it is mixed with the water. After leaving the desired test section, the air moves back to the 208.2L (55gal) reservoir where it is expelled from the system.

2.5 Coriolis Flow Meters

All of the Coriolis flow meters used in the experimental laboratories are of the Micro Motion brand. Three have been more than generously donated by Emerson Process Management, while the fourth was sold to the university at a reduced price. Special thanks must be given to Martin Mabry, the Oklahoma sales representative for Micro Motion. Two Micro Motion meters are currently in use amongst the two fluids / heat transfer labs run by this research team. Both of these meters are of the Micro Motion Elite series, the most accurate produced by Micro Motion. The meters are accurate to ±0.05% of rate for liquid flow, and ±0.20% of rate for gas flow. The larger of these two meters, a Model CMF100, is used to measure mass flow on the water side. This meter is made to accept liquid mass flow rates ranging from 1360kg/hr (2998lbm/hr) to 27,200 kg/hr (59,966lbm/hr). The CMF100 meter utilizes a Micro Motion Model RFT9739

Field-Mount Transmitter to give readouts of mass flow and other various properties as well as transmit mass flow data to the data acquisition system via milliamp outputs.

The second meter, a Model CMF025, is used to monitor the mass flow rates on the airside. The CMF025 meter is intended to measure mass flow rates for liquids or gases ranging from 54kg/hr (119lbm/hr) to 2180kg/hr (4806lbm/hr). This meter uses a more modern Micro Motion Model 1700 transmitter. As is the case with the CMF100, this transmitter provides a display of mass flow data as well as other physical properties and transmits mass flow data to the data acquisition system via milliamp outputs.

2.6 Data Acquisition

In this experimental setup, data is recorded via a National Instruments Data Acquisition system and stored on a CPU. There are three major types of components to the National Instruments data acquisition system. These are the chassis, modules, and terminal blocks.

The chassis is the housing for all of the other components. The particular chassis used for this experimental setup is a SCXI 1000. This chassis serves as a low noise area containing components for signal conditioning, power supply, and circuitry control. The chassis is AC powered and has four slots for modules and accompanying terminal blocks.

Connected directly to the chassis are the modules. These modules perform the signal conditioning process and are the point of attachment for the terminal blocks. Two 32 channel analog modules and one eight channel analog module were used for the purposes of this test section. The 32 channel modules are National Instruments Model SCXI 1102s. These modules are intended for high accuracy signal conditioning of

thermocouples. They can also be used to acquire data via millivolt, 0 to 20 mA, and 4 to 20 mA current signals. Each of the input channels includes a 2 Hz lowpass filter in order to reduce noise from the 60Hz power source. Each channel also has an amplifier with a gain that can be varied from 1 to 100.

The eight channel analog module is a National Instruments Model SCXI 1125. This module allows for isolated analog signal input conditioning through its eight channels. As was the case with the Model 1102 modules, this module is designed for gathering data from thermocouples. Each channel has a lowpass filter that can be configured for either 4 Hz or 10 kHz. In addition, each of the eight channels has 12 programmable gain settings ranging from 1 to 2000.

The terminal blocks serve as the direct connection to the various devices being monitored. In the case of this experimental setup, thermocouples, a differential pressure transducer, and the Coriolis flow meters are wired into the terminal blocks. Twin shielded SCXI 1303 32 Channel Isothermal Terminal Blocks were used to connect to the SCXI 1102 modules. These terminal blocks are front mounted and provide direct connection to the modules via screw terminals. They have an isothermal construction for high accuracy thermocouple measurement. In order to further increase the accuracy of measurement, these terminal blocks contain an onboard temperature sensor for cold junction compensation.

In order to connect to the eight channel module, a SCXI 1313 8 Channel High Voltage Attenuator Terminal Block was used. This terminal block is very similar to the 32 channel blocks with the exception of the addition of a 100:1 resistive voltage divider. This allows for the terminal block to accept voltage inputs up to 300 V_{rms} or ±300 VDC

when the terminal block is used in conjunction with the SCXI 1125 module. This block is used to read voltage across the test section, and current through the test section.

Data recording and storage is performed through the use of a CPU. In order to facilitate this part of the data acquisition process, the graphical interface program, LabVIEW designed by National Instruments, was used. Using LabVIEW, a data acquisition program had to be written. The original program was written by Jae-yong Kim, a former Ph.D. candidate. However, the original program was written for a different two phase flow setup. Modifications to the program to make it functional for this setup were performed by Clement Tang, current Ph.D. candidate and member of the research team.

2.7 Pressure Transducer

In both test branches, pressure drop is measured across the test sections. This is done in order to collect data for the purposes of developing a pressure drop correlation. Pressure drop measurements are taken in the non-heated branch in order to provide a correlation between pressure drop and the two-phase flow pattern exhibited. Measurements are taken in the heated branch in order to associate pressure losses with both the flow pattern and the heat transfer achieved. The pressure drop measurements from the two branches are compared for the purposes of validation. Pressure drop measurements are achieved using a Validyne model DP-15 pressure transducer in combination with a CD15 carrier demodulator. The Validyne pressure transducer is able to cover a very high range of pressure drops due to the fact that it utilizes interchangeable diaphragms. With the diaphragms currently in use at the laboratory facilities, differential

pressures ranging from 0.862kPa (0.125psi) to 1379kPa (200psi) can be measured with accuracies of ±0.25% full scale of the diaphragm in use.

2.8 Connections to the Test Area

Air and water are brought into the testing area via reinforced flexible tubing. Standard 3/8in nominal air compressor hose was used in order to bring air to the inlet of the test area. Water is provided via 1 1/8in nylon reinforced flexible clear PVC tubing. This is also the material that is used in the return line from the exit of the test area to the 208.2L (55gal) reservoir.

The water and air enter the test area via a 1/2in IPS plastic tee. As soon as they enter the tee they begin to mix. However, mixing is further enhanced through the use of static mixers. This will be discussed later in this chapter. After the air and water are brought together into the same pipe, the pipe once again splits. One arm of the pipe goes to the void fraction / flow visualization section, while the other leads to the heated section. Flow into these two different branches is controlled by 1/2in quarter turn ball valves. Thus, the two phase mixture is allowed to follow only one branch at a time. At the end of the testing area, the two branches once again converge. Portions of the plumbing that may be exposed to the high temperatures generated by the heated branch are constructed out of 1/2in CPVC. The rest of the exit area is constructed out of PVC of the same nominal diameter. All of the 1/2in and 3/8in PVC used in the experimental setup are schedule 40. The CPVC, however, is schedule 80 as that was what was readily available in iron pipe sizes.

As at the beginning of the test area, two ball valves are placed at the exit of the testing area as well. These are in place to prevent back flow into the unused test branch during experimentation. The orientation of these valves can be observed if Figure 2.1 is referenced.

2.9 The Test Branches

As previously mentioned, this experimental setup consists of two separate test branches, one for heat transfer measurements, the other for flow visualization and void fraction measurement. The main thrust behind the design of this experimental setup was the ability to achieve flows at inclination angles ranging from positive 90˚ to negative 90˚. In order to do this, the test branches had to be shorter than the 3.78m (12ft 4in) ceiling of the laboratory facilities. The largest internal diameter that could be used while still remaining under this length constraint was found to be 1.27cm (1/2in). As a result, all of the critical portions of these two branches are constructed with pipe media of internal diameters at or very near 1.27cm (1/2in). In the case of the portions made from clear PVC and stainless steel, 3/8" nominal schedule 40 IPS was used. This provides an internal diameter of 1.252cm (0.493in). Certain portions of the testing area had to be constructed using polycarbonate tubing due to either temperature constraints or a necessity for visual clarity. The polycarbonate tubing used in these instances is sold in specific internal diameters. Thus, these polycarbonate sections have internal diameters of exactly 1.27cm (0.50in). All fittings used in the connection of the various aspects of the testing area are either made of PVC or brass in a 3/8" nominal IPS size, or were constructed such that they have a 1.27cm (0.50in) diameter. Both test branches have

inlets and exits constructed of 1/2" nominal PVC and CPVC. However, this size of material was used in these areas simply because of availability issues.

2.10 The Heated Branch

The first of the two test branches included in the experimental setup is the heated branch. Figure 2.4 depicts the heated branch in detail. The heated section consists of four major components, mixing sections, flow visualization sections, a heated section, and a thermocouple array. It will be beneficial to discuss each of these major components independently.

2.10.1 Mixing Sections

Two different mixing sections are employed in the heated test branch. The major purpose of the mixing sections is to churn the air / water mixture enough that an accurate temperature of the mixture can be taken via a thermocouple probe. In addition, the mixer at the inlet of the test branch helps to ensure that the two phase flow patterns observed are not influenced by the entry configuration. Mixers are in place at both the entry and the exit of the test branch. Mixing at the entry of this test branch is facilitated by the use of a Koflo 3-Vane static mixer manufactured from 3/8in nominal clear PVC. The specific designation for this component is Model 3/8-40C-4-3V-2. Figure 2.5 depicts a schematic of the mixer used from Koflo. The air and water enter the beginning of both the test branches via a 1/2in nominal PVC tee. While passing through the tee, the water and air

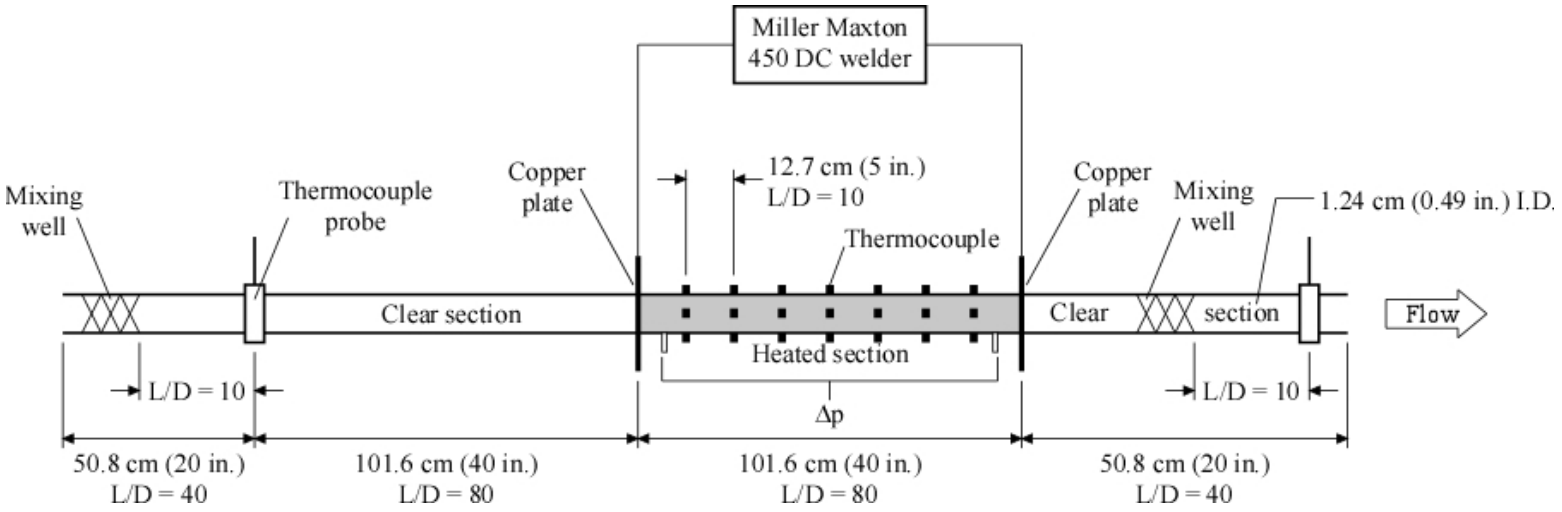

Figure 2.4: Schematic of Heated Branch

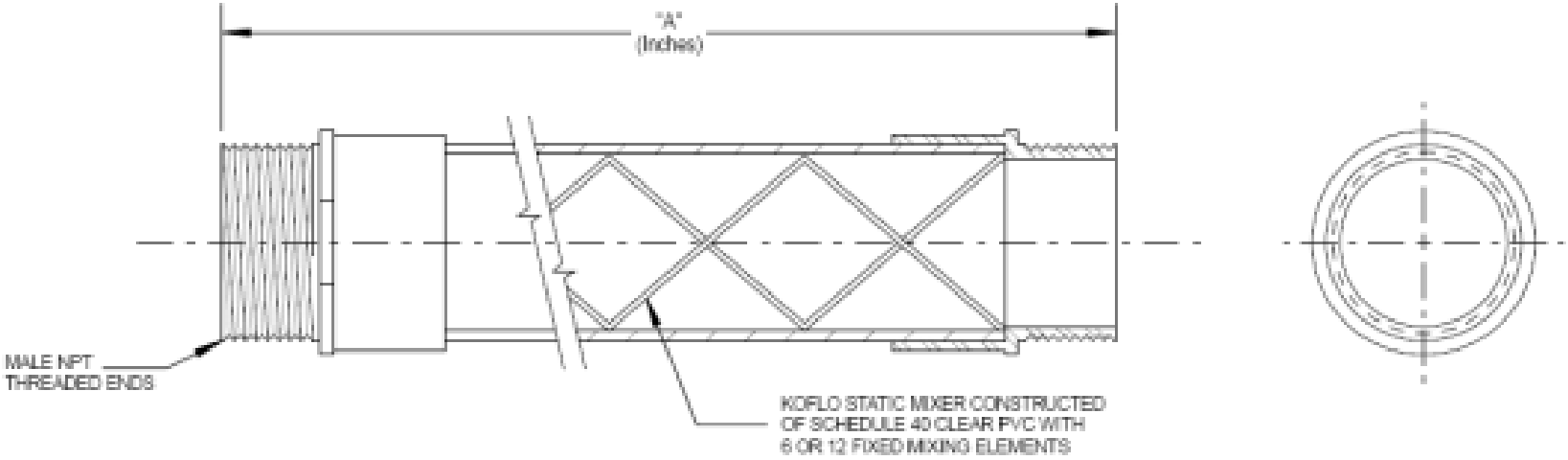

Figure 2.5: Schematic of Koflo Static Mixer

already begin to mix. The aforementioned valve system then directs the flow into the desired test branch. After passing through the mixer, the temperature of the two-phase mixture is taken. Similarly, at the exit of the test branch, another mixer is in place. This mixer is placed after the two test branches have converged. Thus, it is a shared mixer. Since the fluid is hot after leaving the heated test branch, a CPVC mixer has been employed in order to prevent loss of integrity. The mixer used at the exit is a Koflo 1/2-80-4C-3-2. As with the inlet, the temperature of the mixture is taken via thermocouple probe directly after the fluid leaves the mixer. These thermocouple probes will be discussed in more depth in the section covering the thermocouple array.

2.10.2 Flow Visualization Sections

Flow visualization sections have been employed directly fore and aft of the test section. These sections serve two main purposes. The first is simply to allow the user to determine what type of flow pattern is entering the heated test section. The second is to determine whether or not the flow pattern has changed during the heating process. The flow visualization sections are made out of 1.27cm (0.50in) ID polycarbonate tubing. The wall thickness of the tubing is 1.59mm (1/16in). Polycarbonate was used as the material for the flow visualization sections for two reasons; optical clarity, and resistance to heat. Optical clarity was necessary in order to ensure that clear photos could be taken of the flow patterns moving through the test branch. Temperature resistance was necessitated by the fact that the flow visualizations sections are in direct contact with the heated test section. The polycarbonate flow visualization sections will resist temperatures of up to 132˚C (270˚F). The PVC of which the majority of the test section

was constructed cannot easily be connected to the polycarbonate visualization sections via a glued joint. As standard sizing of the two different types of tubing is slightly different, simple threaded fittings were not a viable solution either. Thus, flanges had to be developed in order to make these connections. Flanges that were not to come into direct contact with the heated test section or the heated fluid mixture were constructed out of 2.54cm (1in) thick PVC stock. Those that needed temperature resistance were constructed out of 2.54cm (1in) thick nylon stock, giving them a temperature resistance of 110˚C (230˚F). Figure 2.6 demonstrates the design of the flanges constructed. Each of the flange halves is 2.54cm (1in) in thickness and 15.24cm (6in) in diameter. The flanges clamp down on a lip that is adhered to the polycarbonate visualization sections. Sealing of the flanges is facilitated by a dual O-ring system. One of the O-rings sits behind the polycarbonate lip, the other sits on the face of one of the flanges. As the flanges are bolted together and compressed, the flanges seal both the area behind the polycarbonate lip and between the two flanges. Attachment to the PVC pipe and the heated test section is achieved via a threaded joint. A PVC (or CPVC depending on temperature requirements) female threaded union was turned on a lathe until it could be easily glued into the side of the flange system to be joined with the PVC pipe. With this design, a simple male PVC nipple could be used to attach the PVC to the flange. The ends of the stainless steel heated test section were also threaded so that they could be attached to the flanges in the same manner as the PVC piping.

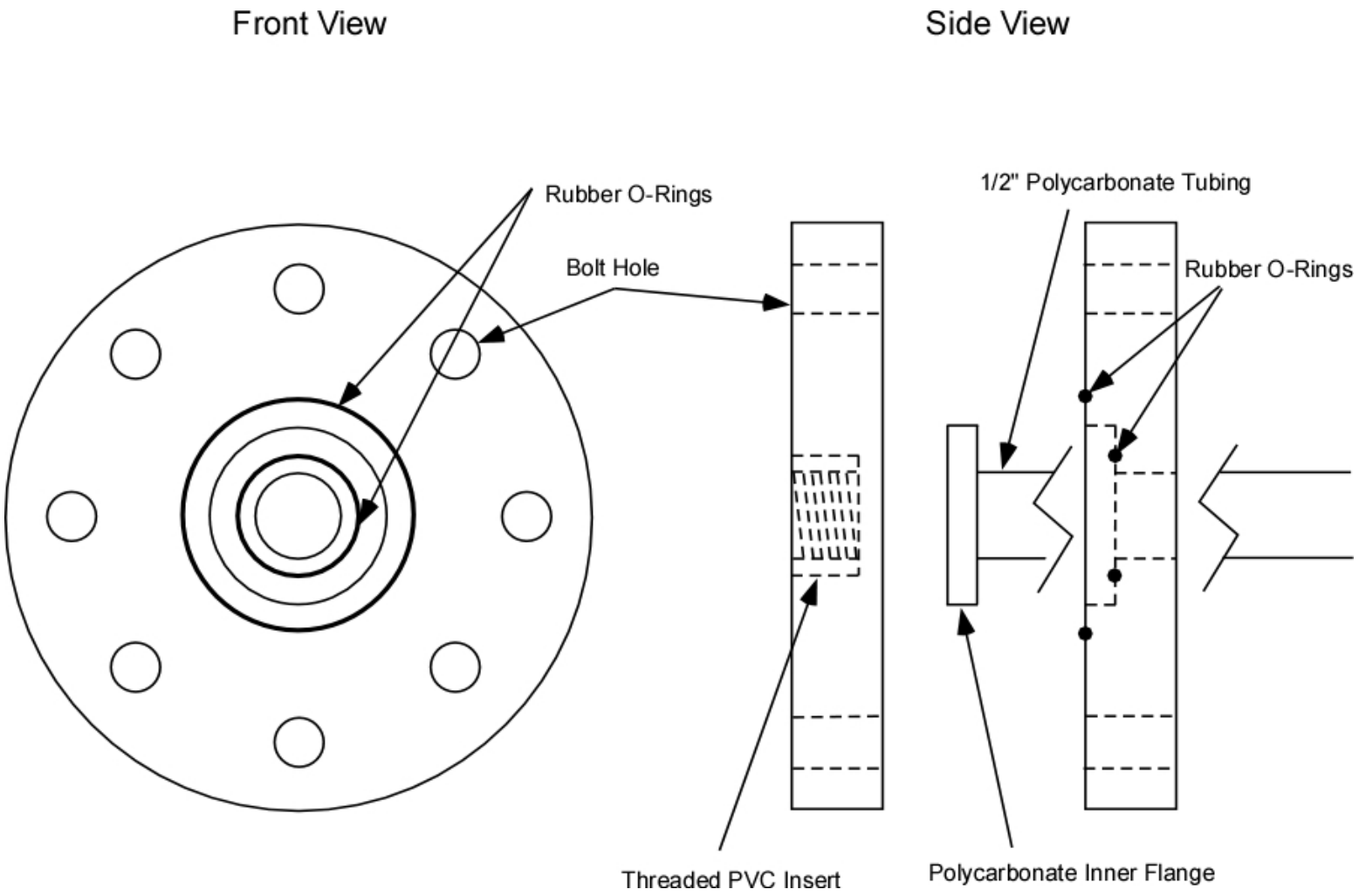

Figure 2.6: Schematic of PVC / Nylon Flange

2.10.3 Heated Test Section

Figure 2.7 demonstrates a detailed schematic of the heated test section as well as thermocouple layout. The heated test section was constructed of 3/8in nominal schedule 40 IPS alloy 304 stainless steel. Thus, the heated section has an actual inner diameter of 12.52mm (0.493in). The test section has a length of 80 diameters or 101.6cm (40in). Stainless steel was used due to its favorable resistance properties when compared with other commonly available metals. The section is heated by passing current through it at high amperages. This type of heat generation is beneficial since it produces a uniform wall heat flux. Current is supplied via one of two welders. The first of these is a Miller Maxtron 450 arc welder, producing up to 450A at a 100% duty cycle. This means that the welder will produce steady output at currents of up to 450A. The second welder utilized is a Lincoln Idealarc DC-600 three phase rectified electric welder, capable of producing steady output at currents of up to 750A. The Miller welder provides better control over output at lower amperages. However, it is necessary to use the Lincoln welder in cases where higher amperages are necessary.

Large 6.35mm (1/4in) thick copper plates were silver soldered at either end of the test section for use as electrical connections. The plates completely encircle the test section and are 17.8cm by 17.8cm (7in by 7in) in order to achieve an even distribution of current input. On the sides of the plates facing away from the heated section, 1.27cm (0.5in) thick phenolic resin board has been used to help prevent loss of heat from the heated test section to the non-heated portions of the test branch.

Connection between the plates and the welder is achieved via 4/0 AWG welding cable. On the connection plate at the exit of the heated test section, a 1000 amp shunt has

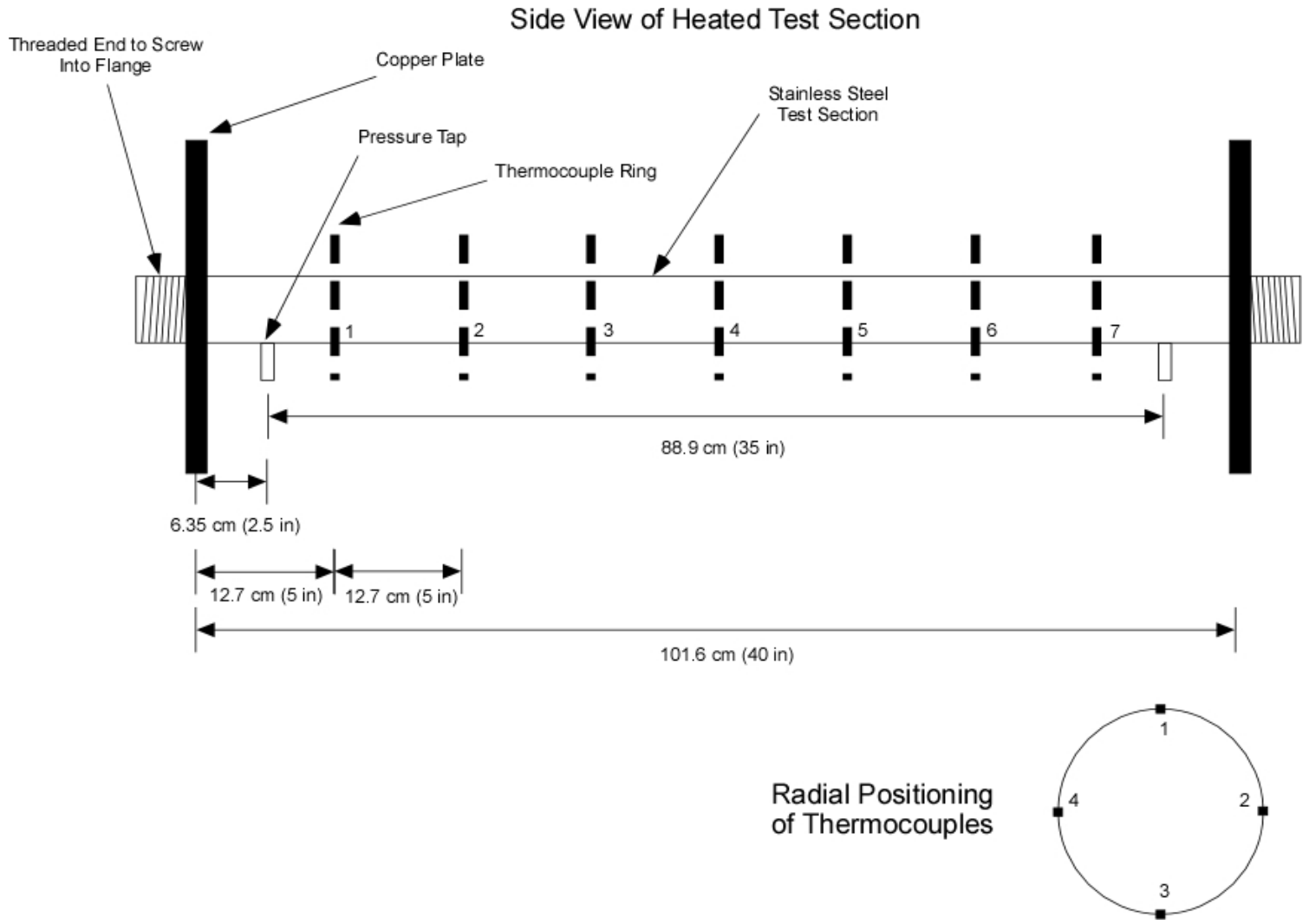

Figure 2.7: Heated Test Section Dimensions and Thermocouple Placement

been connected in line with the circuit. This shunt is manufactured by Empro Shunts and has model number B-1000-50. The shunt is essentially a transducer that produces a mV output that varies linearly with current. This particular shunt produces 50 mV at 1000 A. At either end of the heated test section, pressure taps have been drilled in order to allow measurement of pressure drop across the heated test section. These taps were drilled at a diameter of 0.813mm (0.032in) in order to prevent them from disturbing the flow through the test section. The distance between the pressure taps is 88.9cm (35in) or 70 test section diameters. The taps are placed 12.7cm (5in) or 10 diameters from the inlet and exit of the heated test section. The distance between the taps is kept relatively large in order to generate larger pressure drop values. This, in turn, allows for more accurate pressure drop measurements. In order to further ensure accurate pressure drop readings, the pressure taps were carefully deburred using a combination of an EZ-Burr Micro Series Rotary Deburring Tool and a fine cylindrical file. The pressure taps are regulated via clamp on gate valves and are connected to the Validyne pressure transducer via 1/4" nominal Teflon tubing.

2.10.4 Thermocouple Array

Temperatures are monitored at the inlet and exit of the heated test branch as well as along the length of the heated test section using a combination of thermocouple probes and glue-on thermocouples. All of the thermocouples used are of type T, giving an accuracy of the greater of either ±1.0˚C (1.8˚F) or ±0.75% of the measured value. These thermocouples have a working temperature range of between -250˚C (-418˚F) and 350˚C (662˚F). In addition, all of the thermocouples and thermocouple probes are wired to the

data acquisition system using 6.1m (20ft) lengths of Omega 24 gauge Type T thermocouple wire. The designation for the particular wire used is EXTT-T-24-SLE. The probes used at the inlet and exit of the heated test branch are Omega TMQSS-062U-6 Thermocouple Probes. These thermocouple probes are 1.59mm (1/16in) in diameter and are ungrounded. They are inserted into the test branch extending downwards until they are just above the bottom of the inner wall of the branch. This is done in combination with the use of the static mixers in order to ensure that a representative temperature for the two-phase mixture is achieved even in stratified flows. The probes are sealed into the test branch using compression fittings.

The glue-on thermocouples used were Omega CO1-T Thermocouples. These thermocouples are laminated between two thin layers of phenolic resin, providing a shielding from electrical disturbance. This is beneficial since current is passed through the test section to which they are affixed. In previous test sections, a thick layer of thermocouple epoxy was used in order to shield the exposed thermocouples from the test section. This caused problems as the calibration of thermocouples became inaccurate with curing of the epoxy layer. The use of these shielded thermocouples allowed for a very thin layer of epoxy to be used, alleviating the calibration woes.

The thermocouples were affixed to the heated test section using Omegabond 101 Two-Part Thermocouple Epoxy. This type of epoxy has a high thermal conductivity of 1.038W/(m-K) (7.2BTU-in/hr-ft^2-˚F), and a continuous temperature rating of 105˚C (221˚F). Thermocouples were attached in sets of four, constituting a North, South, East, West placement scheme at each point of measurement. Beginning 12.7cm (5in) from the first copper connection, seven sets of thermocouples were placed at intervals of 12.7cm

(5in) across the entire length of the test section. The placement of the thermocouples was symmetrical along the length of the test section. For an example of the thermocouple placement, please reference Figure 2.7. This type of thermocouple array allows for temperature observation around the circumference of the heated section as well as along its length.

When the heated branch is in operation, it is covered in insulation in order to prevent as much heat loss to the surroundings as possible. The test section itself is covered in a length of 7.62cm (3in) thick Micro-Lok Fiber Glass Pipe Insulation available through Johns Manville. The insulation used is actually made to fit on 1in nominal diameter piping. This extra size is necessary in order to cover all of the leads to the thermocouple array. The insulation used has a conductivity 0.042W/m-˚C (0.29Btu-in/(hr-ft^2-˚F)) at 93˚C (200˚F). The rest of the heated test branch is wrapped in three layers of Thermwell Fiber-Glass Pipe Insulation Wrap. Each layer of this insulation has an R-value of 1.6.

2.11 Flow Visualization / Void Fraction Branch

The second of the two branches in the experimental setup is the flow visualization / void fraction branch. This section has four different major components. These are the mixing sections, flow visualization section, void fraction system, and the thermocouple array. It will once again be beneficial to discuss each of these sections independently. Figure 2.8 depicts the flow visualization / void fraction section in detail.

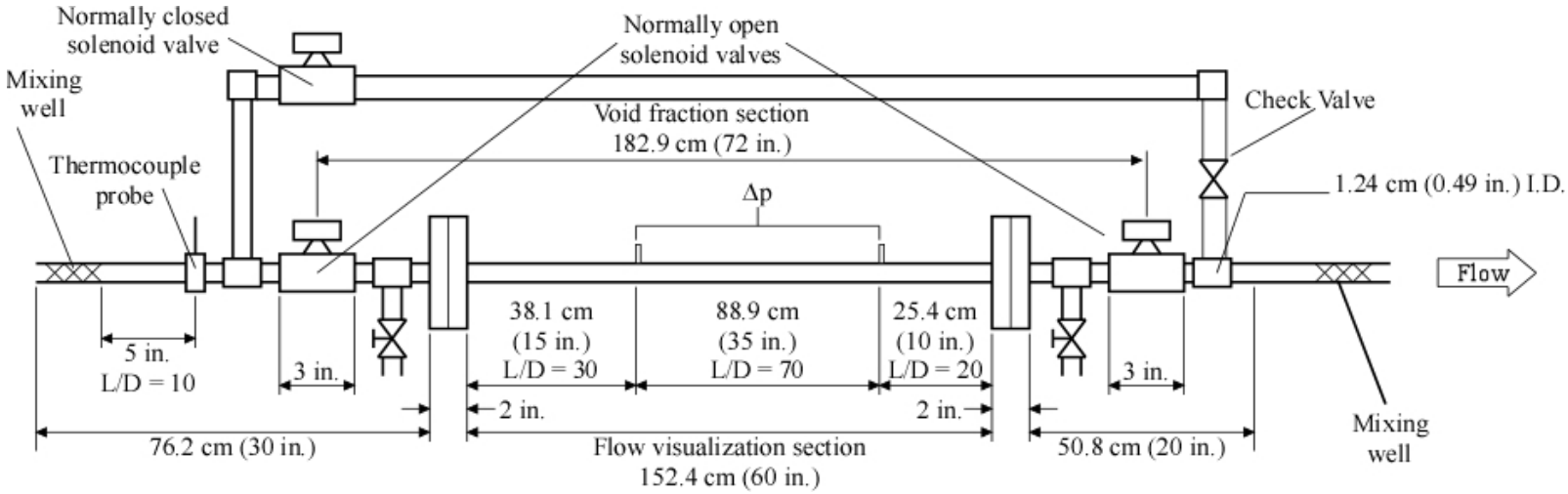

Figure 2.8: Schematic of Flow Visualization/Void Fraction Test Branch

2.11.1 Mixing Sections

Like the heated branch, the flow visualization / void fraction branch uses two different static mixers, one at the inlet of the branch, and one at its exit. The inlet static mixer serves the dual purpose of ensuring that the flow patterns observed in the visualization section are not influenced by the inlet geometry and enabling the thermocouple at the inlet to measure a representative temperature for the two-phase mixture. The mixer at the exit serves the latter purpose as well. The non-heated branch utilizes a Koflo model 3/8-40C-4-3V-2 3/8in clear PVC mixer at the inlet. The exit static mixer is shared between the two test branches.

2.11.2 Thermocouple Array

The thermocouple array for this branch is relatively simple, consisting of two thermocouple probes. These probes are Omega Model TMQSS-06U-6 thermocouple probes, the same type used in the heated section. In fact, the exit thermocouple probe is shared between the two sections. Processes occurring within this section are to be constant temperature. The thermocouple probes are in place simply to verify that this is the case.

2.11.3 Void Fraction System

The purpose of the void fraction section is to trap a sample of the two-phase mixture passing through the non heated branch in order to measure the volume of the liquid portion. Given this value and a known volume for the void fraction section, the value for void fraction of the particular trapped two-phase flow can be determined.

The trapping of the two-phase mixture in the void fraction section is achieved through the use of three quick closing valves. Two normally open quick closing valves are used to control fluid movement at the inlet and exit of the void fraction section. A normally closed quick closing valve is utilized to control entry of fluid into a bypass line. When the valves are triggered, the two normally open quick closing valves shut and the normally closed quick closing valve opens simultaneously. In this manner, a two-phase sample is trapped in the void fraction section while the air-water mixture is allowed to continue flowing through the bypass line. Backflow from the mainline into the exit of the bypass line is prevented through the use of a check valve.

The quick closing valves used are W. E. Anderson Model ABV1DA101 Pneumatic Ball Valves. These valves exhibit a positive seal when closed and have a closing time of 0.03 seconds. The valves connect into the branch via 3/8 nominal female threading. In fact, all three of the valves are identical. It is the solenoid controllers used to monitor the air inlet to the valves that determines whether they are normally open or normally closed. The solenoid controllers used in combination with the pneumatic ball valves are from Dynaquip Controls and have designation 145750.01. Air pressure at 689.5kPa (100psi) is run to the solenoid controllers from the lab air compressor. The four-way solenoid controllers pressurize and exhaust the pneumatic actuators to open and close the ball valves. Thus, air input to the pneumatic valves can be controlled electronically. In order to make a valve normally open, the solenoid controller is mounted in the standard orientation. If the valve is to be normally closed, the orientation is reversed.

After a representative sample of the two-phase flow under observation has been captured, the next step is to drain the liquid portion in order to measure its volume. The void fraction section has an overall length of 219.075cm (88.25in). The central portion of the void fraction section serves as the flow visualization section and is constructed out of 1.27cm (0.50in) ID polycarbonate tubing. This central portion has a length of 152.4cm (60in). The remaining part of the void fraction section is made from 3/8" IPS clear PVC pipe, giving an ID of 1.252cm (0.493in). Using these dimensions, the volume of the void fraction section can be calculated to be 277.5cc ($16.93in^3$). Thus, the void fraction is the measured liquid volume subtracted from this volume.

In order to collect the drained fluid for measurement purposes, an 8L (2gal.) high-density polyethylene tank manufactured by Nalgene is used. The tank has excellent properties of impact resistance and chemical resistance. The tank is of a low profile design in order to minimize size and prevent interference of the collection system with the overall function of the experimental apparatus. Fluid is drained from the void fraction system via a series of four 3.175mm (0.125in) diameter ball valves which are saddle mounted to the void fraction section. The draining fluid passes through a series of 9.525mm (0.375in) outer diameter clear PVC tubes before it moves directly into the tank. In cases where fluid remains in the test section after the initial draining, one or more of the clear PVC tubes is disconnected from the collection tank and compressed air is utilized to remove the trapped fluid.

2.11.4 Flow Visualization Section

The flow visualization section is located in the central portion of the void fraction section. This section is intended to as closely mimic the heated test section as possible. It allows observation of the type of two-phase flow that the opaque portion of the heated section is experiencing under comparable conditions. It is also crucial for the further development of the flow pattern map. As previously stated, this section is constructed from 0.27cm (0.50in) ID clear polycarbonate tubing. The flow visualization section is 152.4cm (60in) in length. The optical clarity of the polycarbonate tubing made it a natural choice for the flow visualization. In this section, as in the heated section, it proved difficult to connect the polycarbonate tubing to the PVC pipe. Thus, PVC flanges of the type previously discussed and shown in Figure 2.5 were used to make the connections.

Included in the flow visualization section are pressure taps used to measure pressure drop across the section. As in the heated section, the taps are 88.9cm (35in) apart and are 0.813mm (0.032in) in diameter. Due to the softness of the material in this section, deburring was done solely with the EZ-Burr Micro Series Rotary Deburring Tool. As previously stated, the pressure drop measurements in the non-heated section are intended to be compared against those from the heated section for validation purposes. Thus, it was necessary to make the two sets of taps as close to identical as possible.

Flow visualization was achieved through the use of either a Nikon D50 digital SLR or a Sony Handycam DCR-VX2100 Digital Video Camera Recorder. Still images were taken using the Nikon D50 while videos were taken using the Sony Handycam. The Nikon D50 is a CCD camera with a maximum shutter speed of $1/4000^{th}$ of a second and a

resolution of 6.0 megapixels. The Sony Handycam is a 3 CCD video camera that has the ability to film with shutter speeds up to 1/10,000th of a second, has a maximum frame rate of 1/60th of a second, and records video at a resolution of 3.8 megapixels.

The most important feature of the photography setup was the lighting and backdrop arrangement. Several different arrangements were experimented with before the final arrangement was developed with assistance from the Oklahoma State University Department of Art. This arrangement is depicted in Figure 2.9. Two 500 Watt photographic lights were used to illuminate the flow visualization section. These lights were oriented at 45 degree angles to the test section in order to reduce glare and the appearance of shadows. In order to further reduce shadows, the lights were set at a position slightly higher than that of the flow visualization section. In a continuing effort to reduce glare and shadows, Roscolux #105 Tough Spun Gel Diffusers were placed in front of the lighting. These types of diffusers are often used in theatrical applications in order to provide diffuse light. The camera was placed slightly behind the lighting in order to reduce the appearance of reflections of the camera and operator in the photographs taken of the flow visualization section. A white muslin backdrop was placed behind the flow visualization section in order to give a bright and crisp, but non-reflective background.

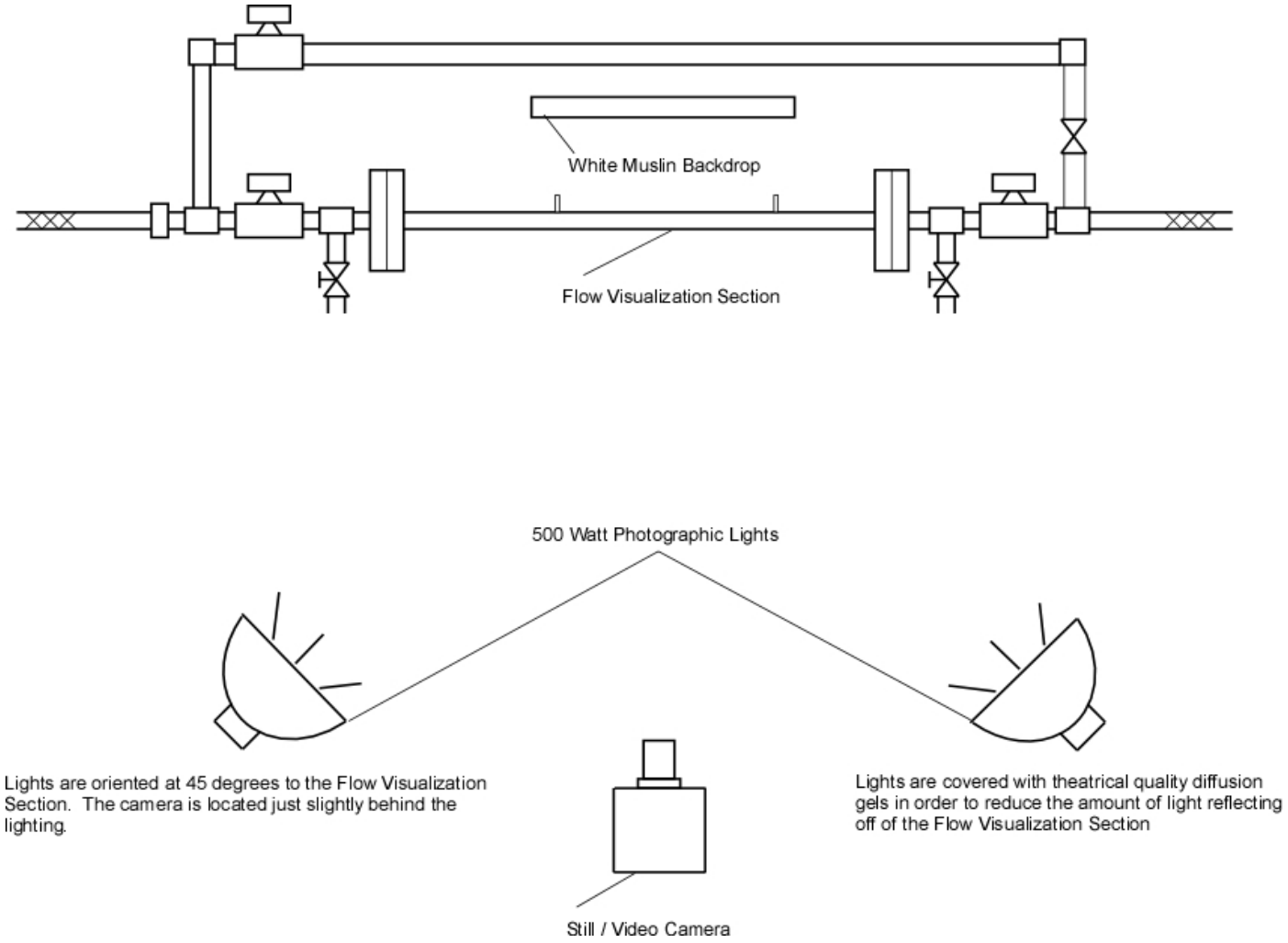

Figure 2.9: Photography Lighting and Backdrop Arrangement

CHAPTER III

CALIBRATION OF EXPERIMENTAL SETUP AND EXPERIMENTAL PROCEDURE

This chapter will delve into the steps involved in the calibration and standard operation of the experimental apparatus. It will be broken into two major sections, Calibration of Experimental Setup, and Experimental Procedure. The first of these sections will detail the calibration of the major components of the experimental apparatus, including the pressure transducer, thermocouple array, Coriolis flow meters and void fraction section. The Experimental Procedure Section will delve into the necessary steps for preliminary checks and system warm up, flow visualization, collection of pressure drop data, collection of void fraction data, and collection of heat transfer data. Each of the modes of data collection will be discussed in separate subsections.

3.1 Calibration of Experimental Setup

This section delves into a discussion of the calibration of the instrumentation utilized by the experimental apparatus. There are four major instrumentation components that require attention in terms of calibration. These are the pressure transducer, thermocouple array, Coriolis flow meters, and void fraction section. An independent

discussion of the calibration procedure for each of the four major instrumentation components will ensue in this chapter. A brief discussion of the uncertainty associated with each of the components will also be presented in this chapter. A more in depth discussion of the experimental uncertainty associated with the apparatus as a whole can be found in Appendix B.

3.1.1 Pressure Transducer

Calibration of the Validyne pressure transducer is a relatively straightforward affair. The calibration process differs very little from what would be expected of any other pressure measurement device. However, the pressure transducer calibration can also be considered the most intensive. Three different diaphragms are used in conjunction with the pressure transducer in order to accurately cover the entire range of pressure drops encountered by the experimental apparatus. Specifically, the three different diaphragms used are Validyne pressure range number 26, 32, and 36, corresponding to maximum pressures of 3.5kPa (0.5psi), 14.0kPa (2.0psi), and 35.0kPa (5.0psi), respectively. These diaphragms are changed relatively often in the experimental process, each instance necessitating calibration of the transducer. In addition, the pressure transducer is calibrated on a daily basis when the experimental apparatus is under heavy use. Thus, while the calibration process is simple by comparison to some of the others that will be discussed in this chapter, it is performed far more often.

Calibration consists of generating a linear equation that relates the voltage output of the pressure transducer to the differential pressure that is applied. In order to accomplish this, it is necessary to generate pressures at regular intervals and record the

output voltage of the transducer. Pressures are applied to the positive side of the pressure transducer while the negative side is left exposed to the atmosphere. Input pressures to the transducer are generated using one of two hand pumps. The first of these pumps is from Si Pressure instruments and is capable of pressures ranging up to 276 kPa (40 psi). The second of these pumps is from Metek and is capable of pressures ranging up to 1724 kPa (250 psi). In calibration, either of the two pumps is connected in parallel with both the Validyne pressure transducer and one of three calibration gages. Two of these calibration gages are Wika calibration grade analog gages. The smaller of the Wika gages has a pressure rating of 103.4 kPa (15 psi). The larger of the two gages is rated up to 1103 kPa (160 psi). Both of these gages have an accuracy of ±0.25% full scale. The third calibration gage used is a Cole Palmer digital manometer with a range of 103.4 kPa (15 psi). This digital manometer has an accuracy of ±0.3% full scale and a resolution of 0.069 kPa (0.01 psi). Due to its excellent resolution, this digital manometer is used for calibration of the smaller diaphragms.

A small LabView program written by Jae-Yong Kim (former Ph.D. student) is used to record both input pressures to the transducer and the coinciding output pressures. These values can then be transferred to an Excel spreadsheet where a calibration equation is generated. This calibration equation is then input to the data acquisition program used in conjunction with the experimental apparatus. Figure 3.1 depicts an example calibration plot for the Validyne pressure transducer.

As previously stated, the coefficients generated by the graphing program are used to generate the linear equation for the calibration. Calibrations are generally performed with between 9 and 12 data points. If there are concerns about the accuracy at the lower

pressure end of the data set, more data points may be taken. The number of data points taken is of little concern so long as the calibration data set is highly linear.

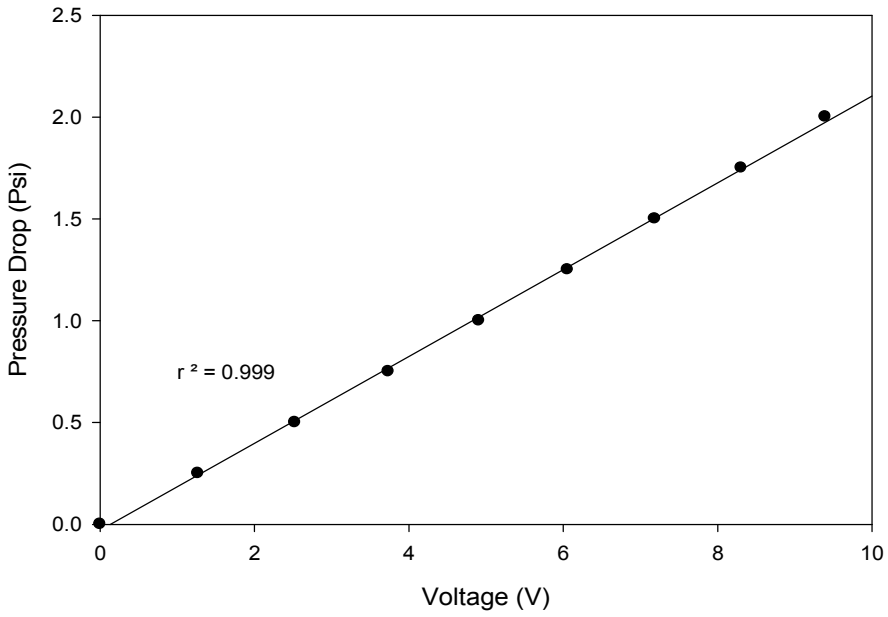

Figure 3.1: Calibration of Validyne Pressure Transducer for 2 psi (3-32) Diaphragm

3.1.2 Thermocouple Array

As discussed in the Experimental Setup chapter, the thermocouple array utilized by the experimental apparatus consists of both cement-on thermocouples and thermocouple probes. All of the thermocouples used are factory calibrated and are specified to an accuracy of the greater of either ±1.0˚C (1.8˚F) or ±0.75% of the measured temperature value. The lesser tolerance of ±0.75% of the measured temperature value will never come into effect during the normal operation of the experimental apparatus. Subsequently, this tolerance will not be discussed throughout the remainder of this chapter.

Despite the factory calibration of the thermocouples, it was necessary to perform a series of calibration runs to ensure that all of the thermocouples included in the array were providing temperature values that were within their specified accuracy. These calibration runs were performed after all of the thermocouples had been placed in their respective working positions on the experimental apparatus. It should be noted that calibration runs for the thermocouple array were done with insulation in place in order to ensure that the data obtained would be free from the influence of temperature gradient and/or outside heat sources. In order to investigate the factory calibration, numerous isothermal liquid phase test runs were conducted. Data from the runs was collected using the National Instruments data acquisition system in combination with the associated LabView data acquisition program. Investigation of the factory calibration of the thermocouples was conducted in two different phases.

The first of these phases involved performing a series of isothermal runs with Reynolds number as the manipulated variable. The test section was heated between each of the runs in order to determine the effects of heating upon the output of the thermocouples. It was of particular interest to investigate the continuity of the temperature readings of each of the 28 cement on thermocouples and 2 thermocouple probes in the thermocouple array of the heated test section. By varying Reynolds number in this mode of testing, it was also possible to investigate the possibility of dependence of the temperature values obtained on Reynolds number. In this mode of testing, Reynolds number was varied from 30,000 to 10,000 with data collected at intervals of 5000. Between each run, the test section was heated to a temperature of 40ºC and allowed to

return to steady state. Figures 3.2 and 3.3 show the raw data collected at Reynolds numbers of 30,000 and 10,000, respectively.

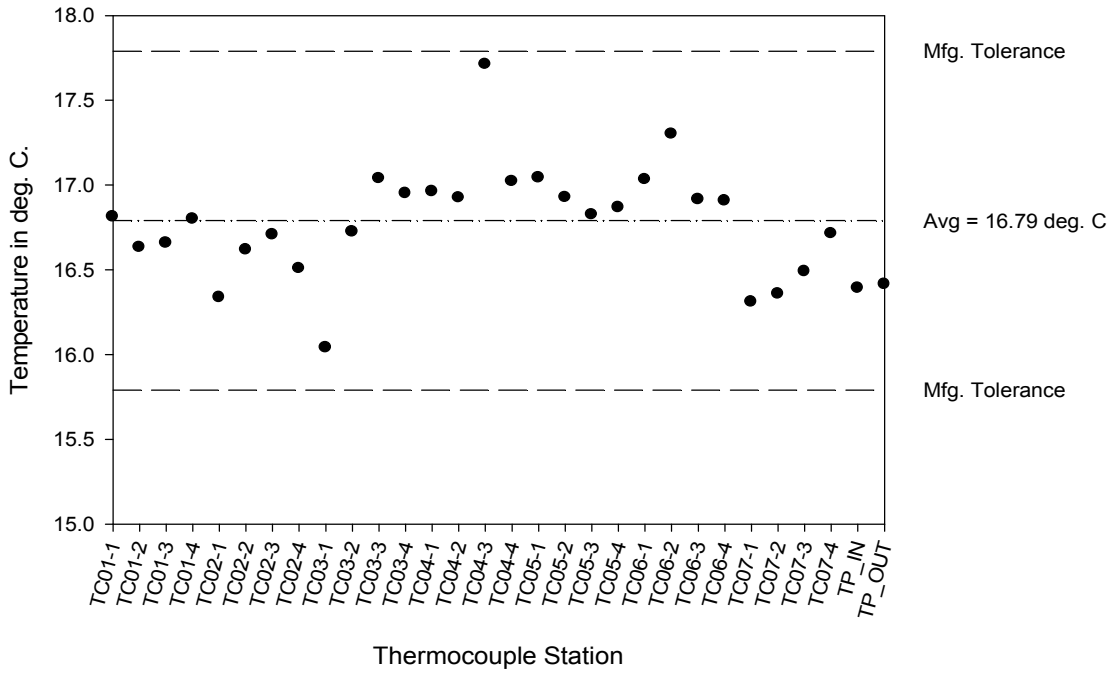

Figure 3.2: Temperature Distribution for Re = 30,000

It should be noted in these figures that all of the temperature values obtained from the thermocouple array are within the specified manufacturer's tolerance of ±1.0ºC. It was also noted through this mode of experimentation that the deviation from the mean of the temperature values recorded for each thermocouple showed a high degree of consistency over the entire series of isothermal runs. In order to illustrate this point, the deviation from the mean for each thermocouple over the first series of five isothermal runs is depicted in Figure 3.4.

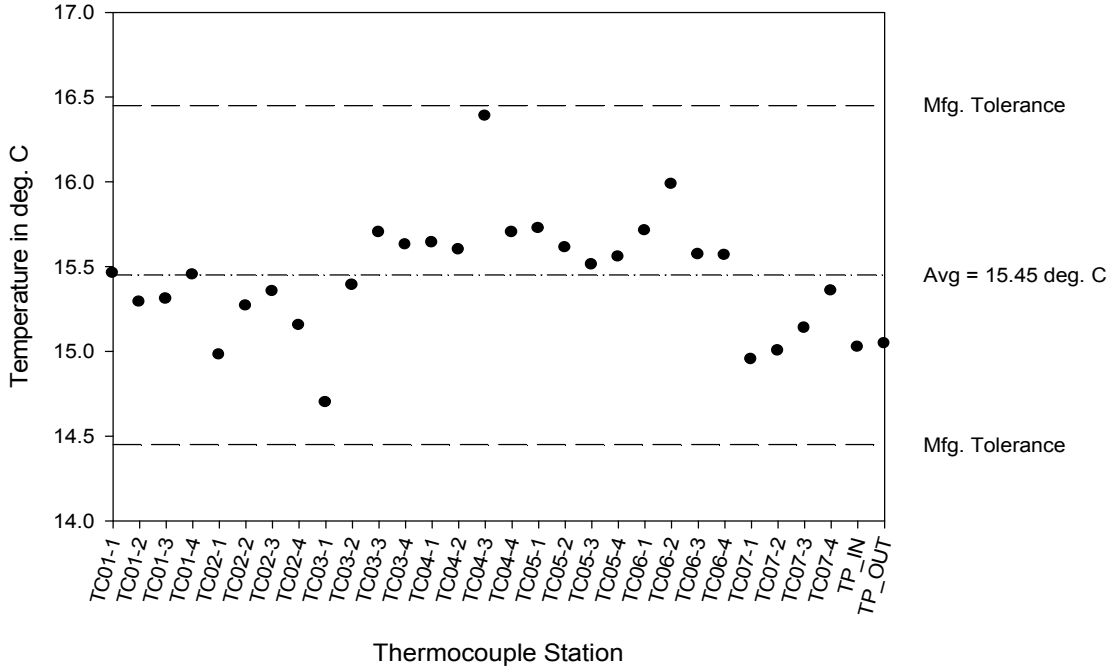

Figure 3.3: Temperature Distribution for Re = 10,000

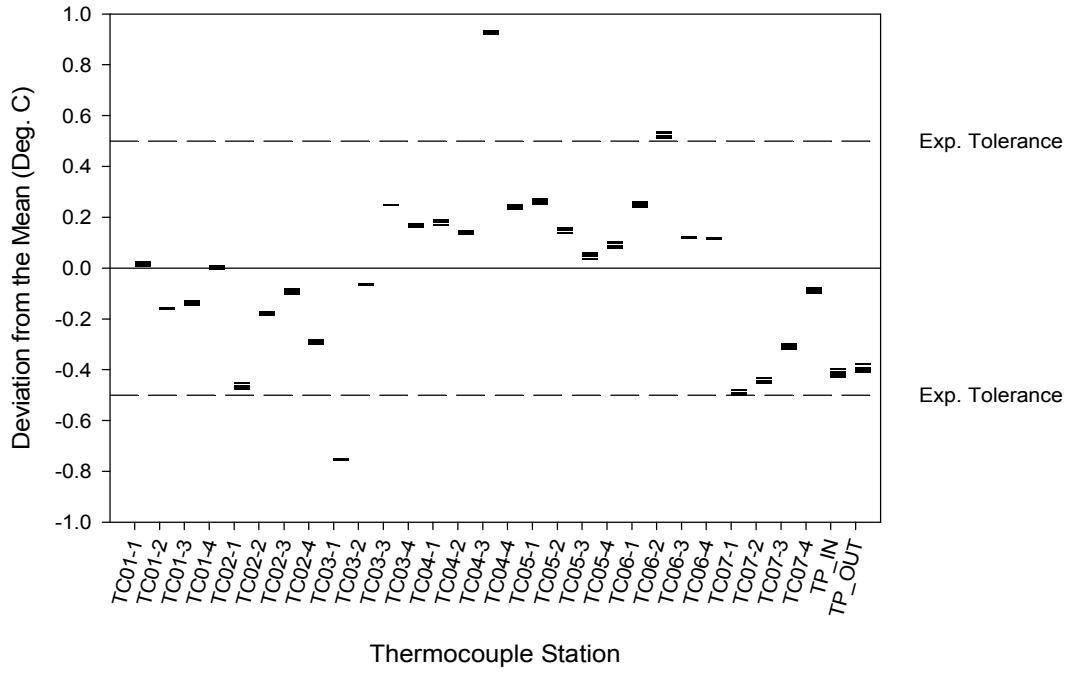

Figure 3.4: Deviation from the Mean for the First Series of Isothermal Runs

From this plot, it can be seen that the deviation from the mean for each of the thermocouples remained highly consistent. This was the case for the cement-on thermocouples as well as the thermocouple probes. In addition, it can be seen that the majority of the thermocouples showed deviations from the mean below ±0.5ºC. It was also noted that the larger deviation values seemed independent of the location of the corresponding thermocouples on the test section. Based on the consistency of the deviation from the mean and the observation that the majority of the thermocouples showed deviations of less than ±0.5ºC, it was deemed prudent to impose an experimental tolerance on the thermocouple output. This experimental tolerance was set at a value of ±0.5ºC. A correction factor was applied to those thermocouples that consistently read outside of or very near to the imposed experimental tolerance. This correction factor was implemented in such a manner that the thermocouple readings were brought just within the boundaries of the experimental tolerance. This was done in order to bring the temperature values within the experimental tolerance without manipulating the thermocouple output to the extreme. A constant was generated for each of the outlying thermocouples. When subtracted from the raw output, this constant brings the temperature value for each of the outlying thermocouples within the experimental tolerance by approximately 0.1ºC. This was done so that the correction factors not only brought the outlying thermocouples within the experimental tolerance, but also provided a small margin for error. It should be noted that the inlet and exit thermocouple probes were not included in the correction. These thermocouples are expected to provide slightly different measurements as they are of a different type from the rest of the thermocouples in the array and measure internal fluid temperature rather than the outside

wall temperature of the test section. In all, six different thermocouples were corrected. Table 3.1 shows the corrected thermocouples with their respective correction factor values.

Table 3.1: Corrected Thermocouples with Associated Correction Factors

Thermocouple	Correction (ºC)
TC02-1	-0.1
TC03-1	-0.35
TC04-3	0.53
TC06-2	0.13
TC07-1	-0.1
TC07-2	-0.1

In order to test the functionality of the correction factors developed, a second series of isothermal runs was conducted. This second series of runs was conducted in order to ensure the proper performance of the correction factors developed outside the range of conditions in which they were developed. In this series of tests, isothermal runs were conducted at varying Reynolds numbers as well as varying temperatures. Between each of the runs, the test section was once again heated and allowed to return to steady state. However, during this series of runs, the test section was heated in increments until the maximum operating temperature of 70ºC was reached. Isothermal runs were conducted at two different isothermal temperatures. These two temperatures were achieved by varying the flow of cooling water into the heat exchanger used to maintain the operating temperature of the working fluid. Through manipulation of the flow of cooling water to the heat exchanger it was possible to conduct isothermal runs at approximate temperatures of 11ºC and 16ºC. In addition, Reynolds number was once again varied. Isothermal runs were made at Reynolds numbers of 5,000, 25,000, and

30,000. (The Reynolds numbers of 25,000 and 30,000 correspond to the maximum flow rate of the system for the two temperatures at which isothermal runs were conducted.)

In all, seven different runs were conducted. Runs were conducted at Reynolds numbers of 5,000 and 30,000 at a temperature of roughly 16ºC. The test section was then cooled. An isothermal run was then conducted at a Reynolds number of 5,000 and a temperature of 11ºC. After this point, the test section was heated up to its maximum working temperature of 70ºC and subsequently cooled back down to 11ºC. Cold runs were then taken at Reynolds numbers of 5,000 and 25,000. The test section was once again heated up to its maximum working temperature and subsequently cooled to 16ºC. Isothermal runs were then conducted at Reynolds numbers of 5,000 and 30,000. Through this mode of testing, it was possible to test for any dependence of the thermocouple output upon operating temperature, heating of the test section, or variation of Reynolds number. It was also possible to test the effectiveness of the correction factors developed. The three figures that follow are deemed representative of the results obtained from this mode of investigation. Figure 3.5 depicts the temperature distribution for the experimental apparatus at an operating temperature of 16ºC and a Reynolds number of 30,000 prior to heating. Figure 3.6 shows the temperature distribution at an operating temperature of 11ºC and a Reynolds number of 5,000 after heating the test section to its maximum operating temperature. Figure 3.7 shows the temperature distribution at an operating temperature of 16ºC and a Reynolds number of 30,000 after heating the test section to its maximum operating temperature for the second time. All three of these figures depict both the raw and corrected thermocouple output.

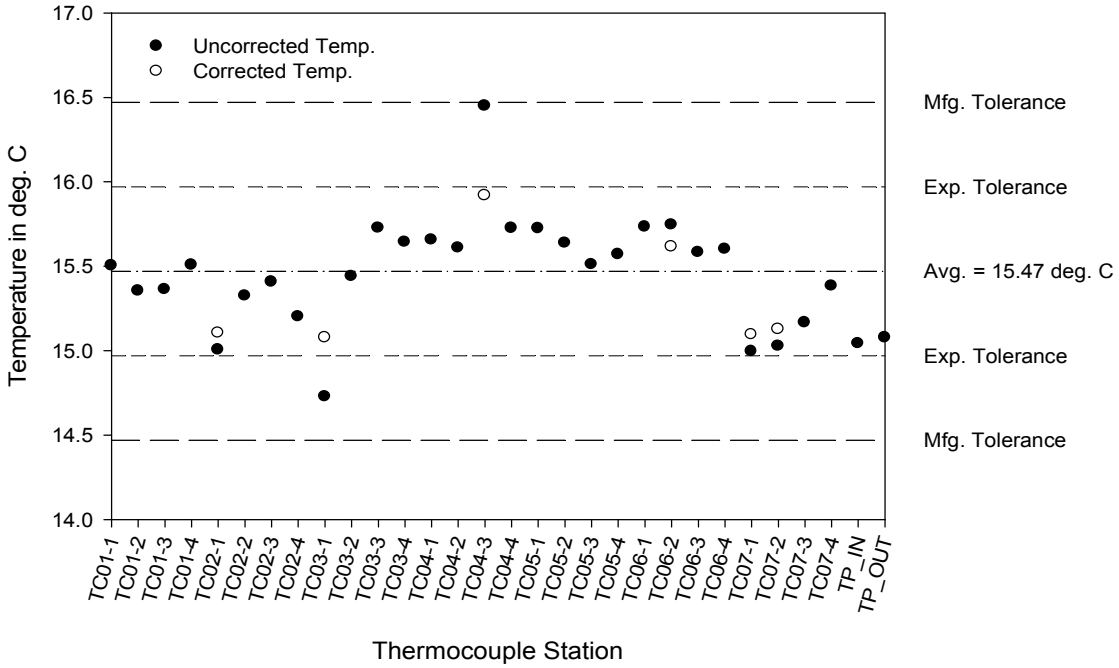

Figure 3.5: Raw and Corrected Thermocouple Data for Re=30,000, Temp. = 16ºC

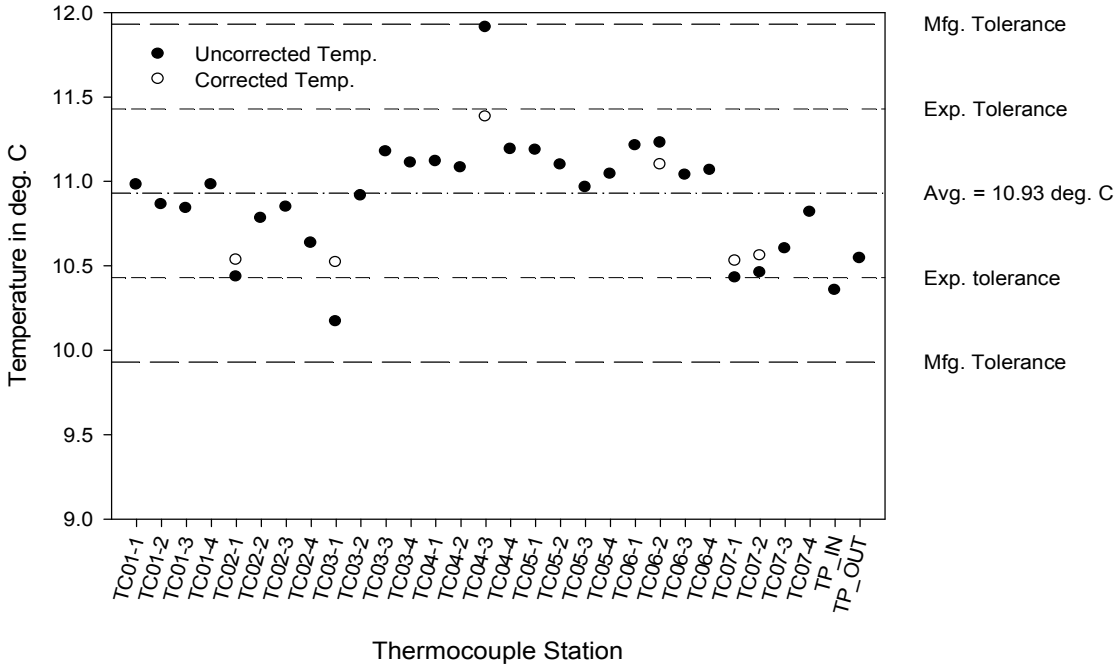

Figure 3.6: Raw and Corrected Thermocouple Data for Re=5,000, Temp. = 11ºC (Post Heating)

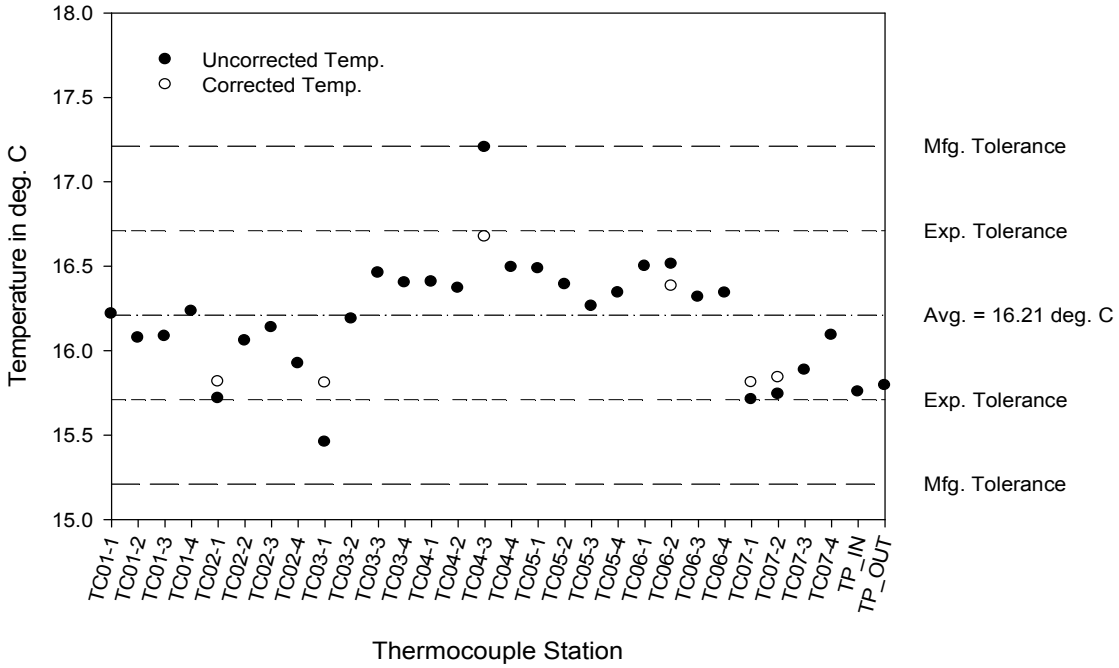

Figure 3.7: Raw and Corrected Thermocouple Data for Re=30,000, Temp. = 16ºC (Post Second Heating)

As demonstrated by these three figures, it was found through this mode of investigation that neither heating of the test section, variation of operating temperature or variation of Reynolds number had any appreciable effects upon the output of the thermocouple array in terms of deviation. Thus, the behavior of the thermocouple was considered highly satisfactory. The correction factors behaved as expected, bringing the temperature values of the outlying thermocouples just within the experimental tolerance generated for the thermocouple array. Based upon the satisfactory performance of the correction factors through this mode of investigation, they were adopted into the LabView data acquisition system and were utilized throughout the remainder of testing conducted with the experimental apparatus.

3.1.3 Coriolis Flow Meters

Two different Micro Motion Coriolis flow meters and corresponding transmitters were used as part of the experimental apparatus. Both of these meters come calibrated from the factory. The two CMF-025 meter and the CMF-100 meter are calibrated to a specification of ±0.1% of mass flow rate when calibrated with water as the working fluid. Despite the fact that these meters are provided with certificates of calibration, it was deemed necessary to perform a calibration on one of the meters to provide assurance of the accuracy of the factory calibration.

Prior to checking the factory calibration, it was first necessary to zero out each of the meters. The meters provide milliamp outputs to the National Instruments data acquisition system, each ranging from 4 to 20mA. It is of great importance to ensure that each of the meters outputs exactly 4mA under zero flow conditions. Valves were included at the inlet and outlet of each meter for exactly this purpose. It was possible to isolate each of the meters from any type of flow by closing off the inlet and outlet valves. With each meter isolated and full of the working fluid intended for measurement, it was possible to trim the milliamp outputs until an accurate zero reading had been established.

The CMF-025 meters was used to assess the accuracy of the factory calibration. Water was used as the working fluid for the purposes of calibration so that direct comparisons could be drawn between the in-house calibration and the factory calibration. The calibration done in the lab consisted of comparing the output amperage and registered mass rate with a mass flow rate obtained through timed manual collection of fluid exiting the system. Through this mode of investigation, it was found that the flow

rates obtained though timed manual collection corresponded with the factory calibration within ±0.1% of rate. Thus, the matter was considered closed.

3.1.4 Void Fraction Section

Calibration of the void fraction section is a necessary step in order to ensure that there is as little error as possible in the liquid mass measurements obtained. Several fittings and lengths of tubing are necessary in order to route fluid to the collection tank. Inherently, these components of the void fraction section will be prone towards trapping some of the fluid that is drained from the void fraction section. In order to account for this phenomenon, the volume of the void fraction section was calculated. The volume obtained through calculation was 277.5cc ($16.93in^3$). With water assumed as the working fluid, the mass associated with this volume would be 276.9g (0.61lb). By measuring the mass of the water drained from the completely filled void fraction section and comparing that mass with the mass that would be drained from the section ideally, it was possible to estimate the amount of fluid that would be trapped in the void fraction section. Through this calibration process, it was found that the amount of liquid drained from the void fraction section at a particular angle of inclination remained relatively consistent through repeated calibration runs. However, it must be noted that due to the shape of the quick closing valves at either end of the void fraction section, larger amounts of fluid are trapped in the void fraction section at higher angles of inclination. Thus, it was necessary to recalibrate the void fraction section at each angle of inclination tested. Once proper estimates of average amount of fluid trapped in the test section at a particular inclination had been obtained, they were added to the mass of fluid drained from the test section in

the form of a correction factor. Table 3.2 shows the mass correction factor applied to the void fraction runs for each of the inclination angles tested as well as the error associated with measurements taken at each inclination angle.

Table 3.2: Void Fraction Correction Factors and Errors Associated with each Tested Angle of Inclination

Inclination Angle (˚)	Avg. Trapped Mass (g)	% Error
0	14.5	0.52252
5	14.6	0.52613
90	17.8	0.64144

From the table, it can be seen that the amount of fluid trapped by the void fraction section remains relatively consistent for the 0˚ and 5˚ inclinations. It can also be seen that the amount of fluid trapped in the void fraction section increases with inclination angle. However, the effect on the error associated with the system remains relatively minimal even when it is oriented in the fully vertical position. Despite the minimal effects upon the error associated with the void fraction collection system calibrations will have to be done for each new angle of inclination in order to ensure that data is collected with the best accuracy possible.

3.2 Experimental Procedure

The experimental setup detailed within the pages of this document is capable of collecting data over a wide range of flow rates, flow patterns, rates of heat addition, and angles of flow inclination. In order to ensure that the data obtained from the experimental setup was of the utmost accuracy and high repeatability throughout the experimental range, it was necessary to develop a consistent experimental procedure.

The development of this experimental procedure also served to help ensure the safety of the user as well as the integrity of the experimental setup. Operation of the experimental setup can be broken down into four different major sections, independent of the type of data being collected. These are Pre-Operation Checks, System Warm Up, Data Collection, and System Shut Down. The experimental setup designed is intended for use in four different research modes, flow visualization, pressure drop measurements, heat transfer measurements, and void fraction measurements. While the general operation of the experimental setup for each of these modes is consistent in many aspects, each of the different research modes necessitates unique procedural aspects pertaining to the collection of data that warrant separate discussion. The remainder of this chapter will present all of procedural aspects associated with the operation of the experimental apparatus for each operational step. The Data Collection section for each research mode will be discussed individually.

3.2.1 Pre-Operation Checks

Prior to system startup, a thorough system wide check is conducted as a precautionary measure. As the system includes high amperage electrical equipment, sensitive data acquisition systems, and large amounts of running water, water leaks are of a major concern. Accordingly, one of the major pre-operation steps is to check the experimental setup and associated plumbing for signs of cracking and or leakage. (Due to its importance, this step is revisited in the System Warm Up section.) Prior to startup, it is also imperative to check the connections between the welder and the heated test section. It should be ensured that these electrical connections are tight and show no signs

of arcing or cracking. The welding cables should also be checked for any signs of deterioration and/or cracking. Should problems be found with the welding cables or associated connections, repair or replacement should be performed prior to system operation. Inline filters for both the air and water delivery systems should be checked for signs of buildup of debris. Should the water filters show excessive buildup, it is necessary to replace them. The air filter/driers can simply be drained if excessive buildup is seen. Water filters should be replaced monthly if the system is under heavy use. Lastly, it is beneficial to check connections between the test loop and the data acquisition system for loose wires or poor connections prior to startup. This helps to shorten delays associated with fault finding should the data acquisition system malfunction. With these checks concluded, it is then safe to proceed with warming up the system.

3.2.2 System Warm Up

The system warm up procedure consists of all of the steps necessary for the initiation of fluid flow through the system. This section will discuss all of the steps necessary for test branch selection, setting proper flow rates through the system, and use of the data acquisition system. The steps for warm up of the system are as follows:

1. Adjust the variable incline test section to the desired angle of inclination using the attached winches.
2. Turn on the flow meters, National Instruments data acquisition system, Validyne carrier demodulator, and power supply for the absolute pressure transducers.

3. Initiate the LabView data acquisition program. A file name for the data will have to be specified for this step. The specified file name should simply be that for a test file. Ensure that data is not being recorded during the startup process. The reason for initiating the data acquisition program at this point is simply to monitor the system conditions.
4. Ensure that all quarter turn shutoff valves for both the water and air delivery systems are closed.
5. Turn on the air compressor cutoff switch and power up the air compressor. (Note that all steps involving the air compressor in the System Warm Up and Data Acquisition sections are only necessary if two-phase flow is desired or if the quick closing valves are to be utilized.)
6. Open main line quarter turn shutoff valve for the air compressor.
7. Adjust the main line air compressor pressure regulator to the desired setting. In order for the quick closing valves to function properly, it is necessary to set the pressure regulator to a minimum pressure of 620kPa (90 psi).
8. Adjust the secondary regulator on the air delivery system to the desired setting. This secondary regulator determines the inlet pressure to the test loop.
9. Open the quarter turn ball valve that controls water flow into the heat exchangers for the water and air delivery systems. Flow through the heat exchangers can be adjusted depending upon the rates of cooling desired.
10. Check pump bypass valve to ensure that it is partially open. Opening this valve allows the pump to circulate water even when flow through the system

is cut off. It is necessary to have this valve open during startup in order to reduce strain on the main water pump.

11. Open inlet and exit valves to the desired branch of the test loop.
12. Connect positive and negative pressure leads for the differential pressure transducer and absolute pressure transducers to the test section intended for use. Proper calibration of the differential pressure transducer should have been conducted prior to this point. The absolute pressure transducers do not require calibration.
13. There are multiple experimental apparatuses connected to the water and air delivery systems. It is necessary to ensure that control valves are set to allow water and air into the proper setup.
14. Open the quarter turn cutoff valves to either side of the flow rate control valves for both the air and water lines.
15. Adjust the water line control valve until the desired mass flow rate is achieved. If very high water mass flow rates are desired, the pump bypass valve can be closed. This should only be done if there is little restriction caused by the water line flow rate control valve.
16. With single phase liquid passing through the desired test section, bleed the inlet and outlet of the differential pressure transducer until all trapped air has been released.
17. Adjust the air line control valve until the desired air mass flow rate has been achieved.

18. Prior to data collection, the system now with water and air running through it should once again be checked for any signs of leakage. Should leakage be found, the system should be shut down until proper repairs can be performed.
19. Stop the running data acquisition program. The program will be restarted with proper settings for the desired mode of research.

At this point, the system warm up procedure has been completed. The few remaining settings that may be altered are specific to the desired mode of research. The steps in the data acquisition process vary depending on the mode of research to be conducted. Thus, the data acquisition process for each research mode will be discussed separately.

3.2.3 Flow Visualization

In order to conduct flow visualization further adjustment to the setup itself is unnecessary. As long as the desired mass flows for air and liquid have been set and the desired flow pattern is being observed, the test section is ready. However, it is necessary to use the data acquisition system to record superficial gas and liquid Reynolds numbers as well as gas and liquid mass flow rates. The setup of lighting, backdrops and photography equipment is of the utmost importance for this mode of research. Figure 2.9, depicting the photography backdrop and lighting arrangement can be used as a reference for this subsection. The procedure for performing flow visualization is as follows:

1. Setup of the photographic equipment should be completed prior to collection of any data. The first step in this process is to place the photographic lighting in the

appropriate orientation. The photographic lights should be placed approximately 0.914 meters (3 ft) from the flow visualization section. The photographic lights should be set at 45˚ angles to the test section. The lights should be set such that they are slightly above the test section so as to reduce glare. It should be noted that as the inclination of the test section is varied, it is necessary to vary the spacing of the lighting. As the angle of the flow visualization section approaches vertical, it will be necessary to position the lighting above and below the section rather than to each side of it. Positioning of the lighting should be varied in order to generate as little glare as possible.

2. In order to further reduce glare, diffusion gels must be mounted in front of the photographic lights. The diffusion gels that have provided the highest quality photos are Roscolux #105 Tough Spun Gel Diffusers. These gels should be affixed to the faces of the photographic lights using rubber spacers in order to prevent the heat of the high output bulbs from melting the gels.
3. The camera should be positioned such that it is slightly behind the lighting and oriented perpendicular to and at the same level as the void fraction section. This is done in order to prevent shadows or reflections of the camera from appearing in the photographs taken. As angles of inclination increase, it will be necessary to position the camera to the side of the photographic lighting.
4. Two cameras have been used for flow visualization with this setup, Nikon D50 digital SLR and a Sony Handycam DCR-VX2100 Digital Video Camera Recorder. The Nikon D50 was used to take still flow visualization images, while the Sony Handycam was used to take flow visualization videos. The Nikon D50

is a CCD camera with a maximum shutter speed of 1/4000th of a second and a resolution of 6.0 megapixels. The Sony Handycam is a 3 CCD video camera with a maximum shutter speed of 1/10,000th of a second and is capable of recording both video and still images at a resolution of 3.8 megapixels. It is not necessary to use these particular cameras. However, a camera with at least comparable shutter speed and resolution should be used. Flow visualization should be conducted with the camera set at its maximum shutter speed.

5. A backdrop must be placed behind the flow visualization section in order to generate sharper images as well as to prevent extraneous lab equipment from appearing in the flow visualization photos taken. It has been found through experimentation that the non-reflective white muslin backdrop provides the sharpest images.
6. It is necessary to place a black backdrop behind the camera and photographer in order to prevent reflections of the photographer, camera, or other objects in the room from appearing the flow visualization photographs or video taken.
7. Lastly, all lighting in the room other than the photographic lighting should be dimmed in order to ensure the highest quality images possible.
8. Once the setup of the photographic equipment is complete, continuation with initialization of the data acquisition program can ensue. For this mode of research, the welder power status should be set to "Off". The flow pattern under observation should be entered into the provided space on the data acquisition program screen. The sampling rate should be set to the desired value. (In general

this value should be set at 6,000 samples per second.) It is once again necessary to enter a file name to which data will be saved in order to initialize the program.

9. The flow must be allowed to stabilize before proceeding with data collection. For non heated flow, this generally takes 2 to 3 minutes.
10. Once flow through the visualization has stabilized, one can proceed with data collection. Data Collection is initiated by clicking the Record Data button on the graphical interface for the data acquisition program. Collecting data with the welder power status set to off will provide superficial Reynolds numbers for both gas and liquid, mass flow rates for both gas and liquid, pressure drop, absolute system pressure, ambient temperate, bulk inlet temperature, and bulk exit temperature. Data should be collected for 2 to 3 minutes in order to ensure that fluctuating values associated with more erratic flow patterns do not cause inaccurate data.
11. While data is being collected, flow visualization should be conducted. If still photos are desired, it is necessary to take several sequential photos in order to ensure that the desired feature in the flow is captured. If video clips are desired, films with a length of approximately 30 seconds are generally sufficient to capture the full range of features associated with a given flow pattern.
12. Having completed the data collection and the flow visualization, the process is complete. The data acquisition program should be stopped. Flow visualization photos and videos should be associated with their accompanying collected data for future reference. It is not necessary to completely restart the system between

each collection of data. The flow rates can simply be adjusted if needed and the process repeated.

The setup of the photographic equipment for flow visualization is not an exact art. Manipulation other than what is specified in this procedure is necessary. The exact setup of the photography equipment has to be adjusted until the clearest image possible is attained. In the following pages, photos of various flow patterns taken at different inclination angles are provided. Images and descriptions of the photographic setup used in each specific flow visualization setting are included as well.

Flow visualization was conducted over a broad range of gas and liquid mass flow rates for inclination angles of 0˚ and 5˚. Figure 3.8 is a photo illustrating the positioning of the lighting, camera, and backdrop used for flow visualization at an inclination angle of 0˚. In the figure, it can be seen that the photographic lights are oriented such that they are slightly above the test section. It can also be noted that the camera is placed slightly

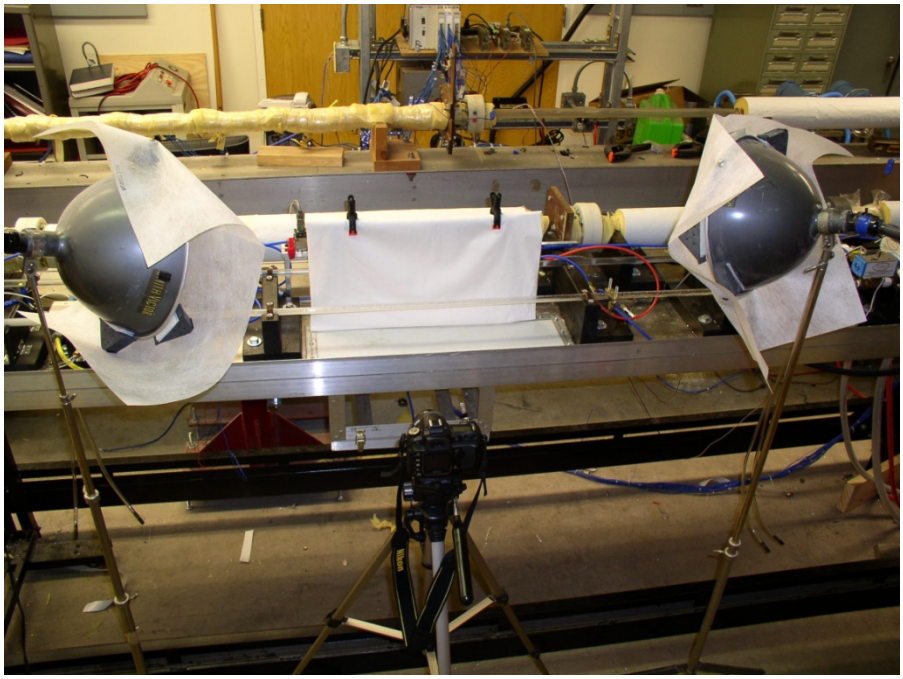

Figure 3.8: Photographic Setup for Flow Visualization at 0˚of Inclination

behind the lighting in order to reduce the possibility of shadows being cast across the test section. The photographic backdrop of white muslin can be seen directly behind the flow visualization section. In addition, it can be seen that the Roscolux diffusion gels are affixed to the front of the photographic lights. Laboratory lighting has been left on in this image in order to make the photographic setup clearly visible. However, under normal operating conditions, the photographic lights would be turned on and the laboratory lights would be fully dimmed.

While numerous flow patterns were encountered during the flow visualization research conducted at this angle of inclination, many of these patterns were transitional. The flow visualization photos presented here are considered representative of three of the major flow patterns encountered; namely, slug flow, plug flow, and annular flow. Figure 3.9 depicts a low energy slug flow at a superficial liquid Reynolds number of 2200 and a superficial gas Reynolds number of 1800. Figure 3.10 depicts plug flow at a superficial liquid Reynolds number of 9300 and a superficial gas Reynolds number of 900. In Figure 3.11, annular flow at a superficial liquid Reynolds number of 5600 and a superficial gas Reynolds number of 18100 is depicted. In this last photo air flow through the flow visualization section is at its maximum.

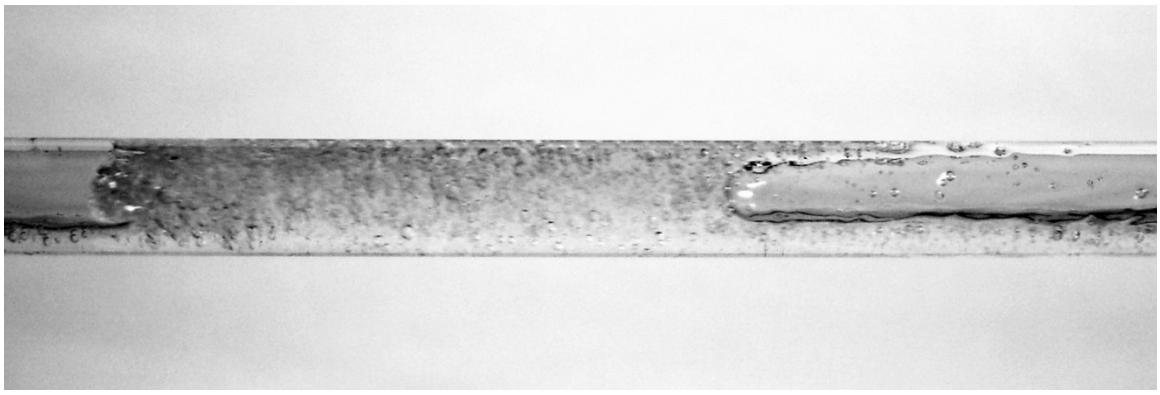

Figure 3.9: Slug Flow at 0˚ Inclination (Re_{SL} = 2200, Re_{SG} = 1800)

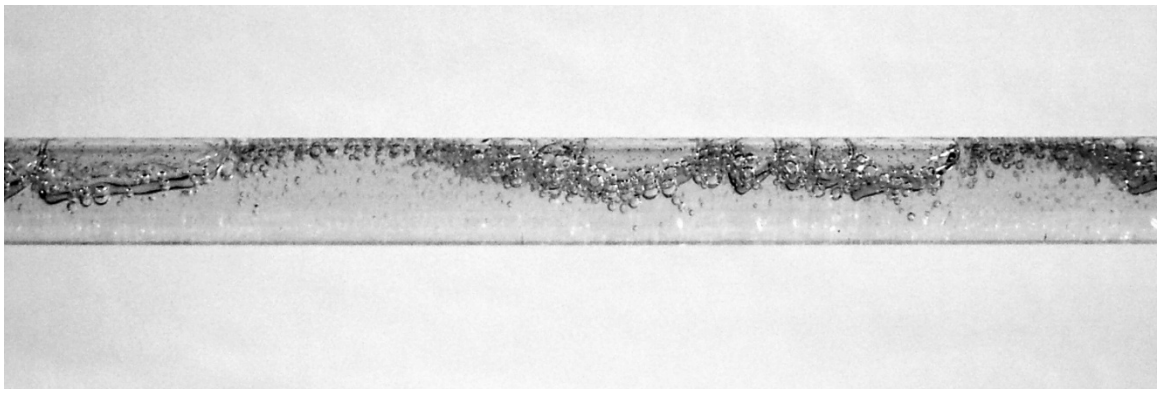

Figure 3.10: Plug Flow at 0° Inclination (Re_{SL} = 9300, Re_{SG} = 900)

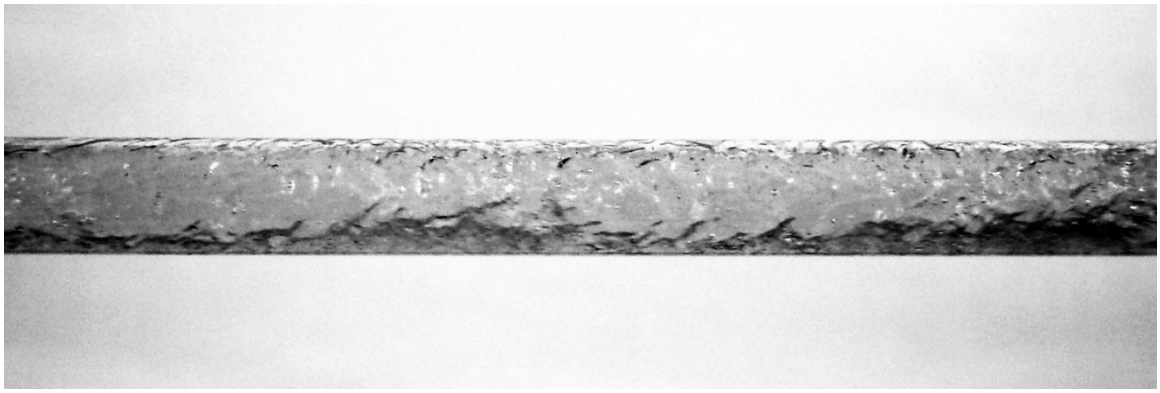

Figure 3.11: Annular Flow at 0° Inclination (Re_{SL} = 5600, Re_{SG} = 18100)

The first feature that can be noticed in all of these photos is that they are in black and white. While the photos were originally taken in color, they have been converted to black and white in a photo editor in order to help make features of the flow patterns more readily apparent. The Nikon D50 does not have the ability to take black and white images. The changes in color in addition to a slight degree of brightening are the only modifications that have been made to the photos.

The second feature that should be noticed in all of these photos is the high degree of clarity. Features of each of the flow patterns such as bubbles and the edges of plugs or slugs are well defined. Visualization of annular flow does not lend itself very well to

crisp features. However, the central core of air surrounded by water can easily be distinguished. These photos are representative of the quality of flow visualization that can be achieved with the relatively simple photographic setup that has been used.

In order to perform flow visualization research at an inclination angle of 5˚, it was necessary to reposition the photographic lighting by a small amount. The light towards the higher end of the flow visualization section had to be raised in order to prevent the generation of shadows and/or glare. There is not any true method for determining the height necessary for the photographic lighting other than to ensure that it is positioned slightly above the flow visualization section. The user simply has to determine the desired position for the lighting through visual inspection. Figure 3.12 is a photo demonstrating the orientation of the lighting, backdrop, and camera used for flow visualization at an inclination angle of 5˚. It can be seen in the photo that the majority of the equipment has remained in approximately the same position as was used for flow

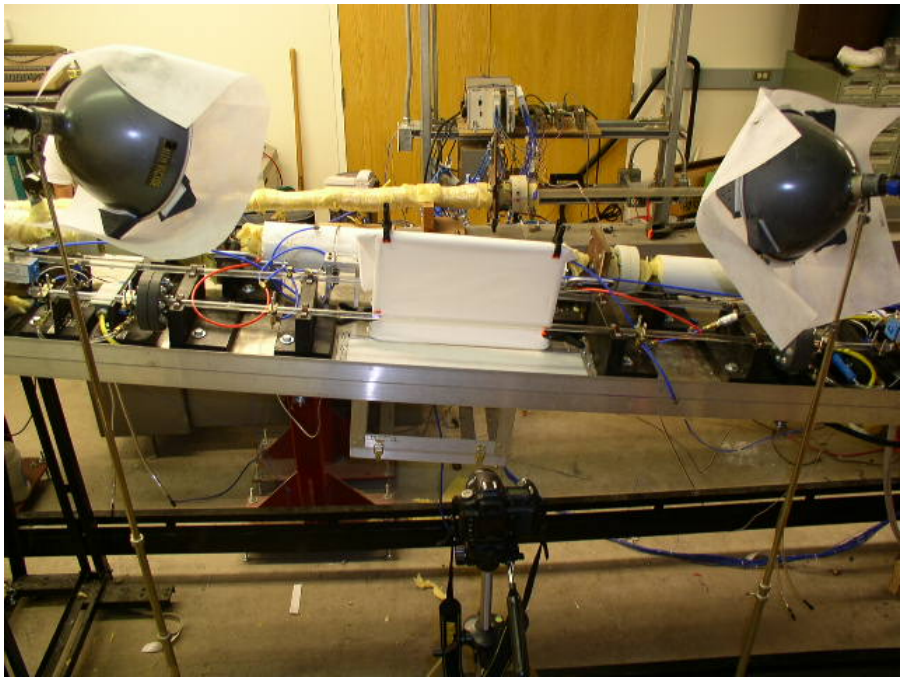

Figure 3.12: Photographic Setup for Flow Visualization at 5˚of Inclination

visualization at 0˚ of inclination. However, the photographic light to the left has been raised in order to account for the new inclination angle.

Flow visualization photos were taken at the 5˚ inclination for the same representative flow patterns presented for the 0˚ inclination. While 5˚ is enough of an incline for gravity effects to begin to present themselves, it is not enough of an inclination for flow patterns associated with more vertical flows to start appearing. Thus, flow visualization is once again presented for slug flow, plug flow, and annular flow. Figure 3.13 depicts a low energy slug flow at a superficial liquid Reynolds number of 2200 and a superficial gas Reynolds number of 1200. Plug flow with a superficial liquid Reynolds number of 11500 and a superficial gas Reynolds number of 900 is depicted in Figure 3.14. Figure 3.15 depicts an annular flow with a superficial liquid Reynolds number of 8600 and a superficial gas Reynolds number of 17900. Once again, the gas flow through the flow visualization section is at its maximum in particular the annular flow depicted.

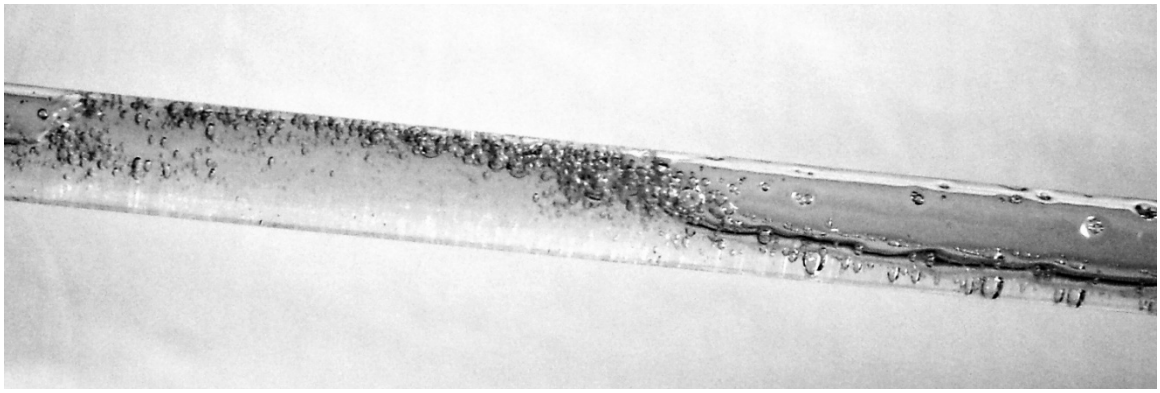

Figure 3.13: Slug Flow at 5˚ Inclination (Re_{SL} = 2200, Re_{SG} = 1200)

The same modifications have been made to this series of photos as those presented for the 0˚ inclination. The photos have been converted to black and white and brightened. It can be seen that the flow visualization photos taken at the 5˚ inclination

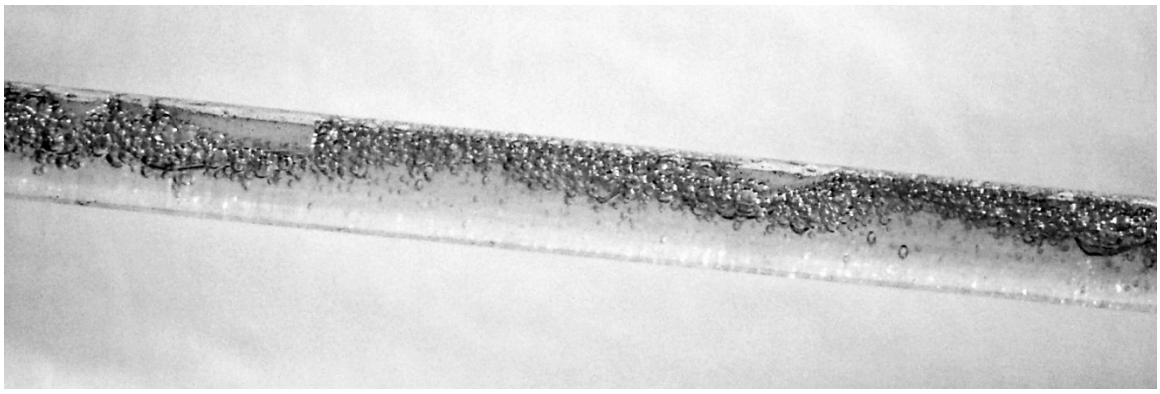

Figure 3.14: Plug Flow at 5˚ Inclination (Re_{SL} = 11500, Re_{SG} = 900)

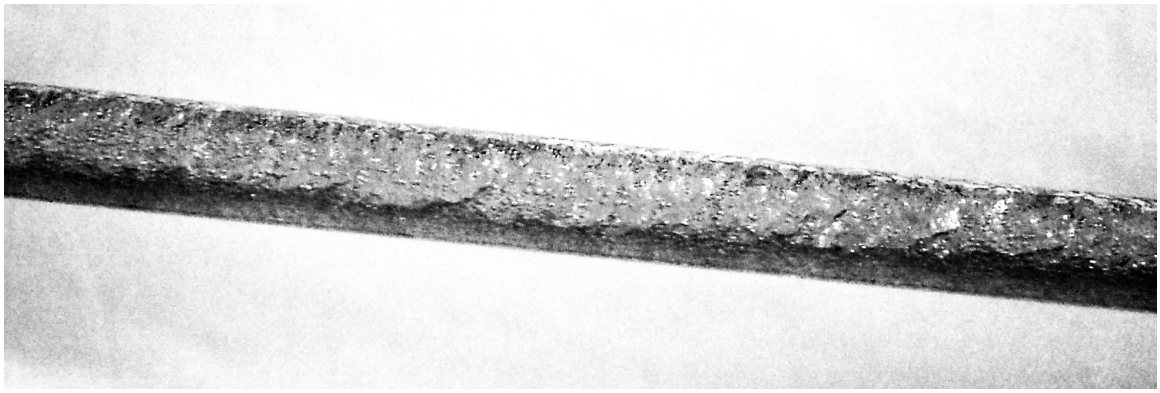

Figure 3.15: Annular Flow at 5˚ Inclination (Re_{SL} = 8600, Re_{SG} = 17900)

angle are of comparable quality and clarity to those taken at the 0˚ inclination. With the lighting properly oriented, the photos are free of shadows or glare.

These representative photos have been presented for the purposes of demonstrating the capabilities of the experimental apparatus as well as to provide a general guide for flow visualization methodology. However, flow pattern mapping has not been conducted as a part of the research presented within this document. Flow pattern mapping is one of the major applications for which the flow visualization section was intended. Research of this type has simply been reserved for a later date.

3.2.4 Pressure Drop Measurements

It is possible to conduct pressure drop measurements using either the heated or non-heated branches of the experimental setup. However, due to the facts that pressure drop measurements are taken in the absence of heating and that it is necessary to associate pressure drop measurements with observed flow patterns, it is preferable to utilize the non-heated branch for this mode of experimentation. In fact, this is one of the major tasks for which the non-heated test branch was intended.

Prior to delving into the procedural discussion for pressure drop measurements, selection of appropriate diaphragms for the Validyne pressure transducer should be discussed. As discussed in the chapter entitled "Calibration of Experimental Setup", there are numerous diaphragms available for use with the Validyne differential pressure transducer. It is necessary that an appropriate diaphragm be selected in order to ensure the accuracy of the pressure drop data recorded. Of main concern is that the diaphragm selected is not too large for the application in which it is being used. It is first necessary to establish an approximate value for the pressure drop that will occur as the flow pattern of interest is passing through the test section. In order to do this, it is necessary to measure the pressure drop across the test section at desired flow conditions, using a diaphragm with a maximum pressure far higher than what is anticipated. (It is of course necessary to calibrate the pressure transducer prior to taking any measurements.) For the purposes of this setup, a diaphragm of 5 psi or larger should be sufficient. This allows an approximate value for pressure drop to be determined without over ranging the pressure transducer. Once this approximate value has been obtained, an appropriate diaphragm can be selected. The expected running pressure of the system should be lower than the

maximum pressure of the diaphragm, but not less than 25% of that maximum pressure. Accuracy begins to drop to an unacceptable level beyond the lowest 25% of the range of each individual diaphragm. After calibration, measurements of pressure drop can ensue. The following is the necessary procedure for conducting a pressure drop run utilizing the experimental apparatus:

1. After the system warm up has been completed, it is necessary to reinitialize the data acquisition program. For this mode of research, the welder power status should be set to "Off". The flow pattern under observation should be entered into the provided space on the data acquisition program screen. The sampling rate must be set to the desired value. (In this mode as in all others, the sampling rate is generally set to 6,000 samples per second.) It is once again necessary to enter a file name to which data will be saved in order to initialize the program.
2. It is necessary to allow the system to stabilize prior to data collection. As this flow is non-heated, the system can be considered stable after 2 to 3 minutes.
3. After allowing the system to stabilize, data collection should be initialized. Of particular interest for this type of data collection are the superficial gas and liquid Reynolds numbers, gas and liquid mass flow rates, inlet and exit temperature, recorded pressure drop, and absolute pressure. Data should be collected for 2 to 3 minutes in order to ensure that errors associated with fluctuations associated with the more erratic flow patterns do not cause inaccuracies.
4. Having completed the data collection, the data acquisition program should be stopped. It is not necessary to restart the system between each data collection run. The data acquisition program can simply be restarted, flow rates readjusted, and

the process can be repeated. Data collection at each flow of interest should be repeated in order to ensure accuracy.

3.2.5 Void Fraction Measurement

This mode of research necessitates the use of the non-heated/void fraction section. The measurement of void fraction using the experimental setup is a relatively delicate process. Accuracy of the void fraction measurement is highly dependent upon the amount of care exercised by the user. Prior to collection of void fraction data, the system should be calibrated for the flow angle desired. The general procedure for the calibration of the void fraction section is discussed in the chapter entitled "Calibration of Experimental Setup". It is necessary to determine the mass of liquid that is inherently retained by the void fraction section at the angle of interest. This mass can be used as a correction factor that is simply added to the liquid mass drained during void fraction data collection at that particular angle of interest. The following is the general procedure for the collection of void fraction data:

1. Having completed the steps in the system warm up, reinitialize the data acquisition program. The welder power status should be set to Off. The flow pattern under observation should be entered into the appropriate space on the data acquisition program screen. The sample rate should be set to the desired value. (Once again, a value of 6,000 samples per second is considered appropriate.) As with all measurements, a file name must be entered in order to initialize the data acquisition program.

2. The system must be allowed to stabilize prior to data collection. This is a non-heated mode of research, necessitating a stabilization period of approximately 2 to 3 minutes.
3. With the system stabilized, data collection should ensue. Values of particular interest for this mode of research are superficial gas and liquid Reynolds numbers, gas and liquid mass flow rates, inlet and exit temperature, ambient temperature, ambient pressure, and system pressure. Data should be collected for 2 to 3 minutes and the data acquisition program stopped. This data is collected for the purposes of comparing collected void fraction data with established correlations.
4. After the first portion of the data collection is completed, it is possible to proceed with measuring the void fraction for the flow of interest. Prior to any void fraction measurements, the initial mass of the collection tank should be measured and recorded. The tank should then be reattached to the experimental apparatus.
5. The first step in void fraction data collection is to trigger the quick closing valves. This is accomplished by flipping the quick closing valve switch attached to the frame of the experimental apparatus to on. This will trap a representative portion of the flow of interest in the void fraction section while simultaneously diverting the continuing flow through the bypass line.
6. The liquid trapped in the void fraction section must now be drained into the collection tank attached to the experimental apparatus. This is accomplished by opening the four quarter turn ball valves attached to the void fraction section drainage ports. After this is done, liquid will begin draining into the collection tank.

7. It is necessary to utilize the air line and nozzle running from the air compressor to blow as much of the fluid as possible out of the void fraction section. The section should always be angled when performing this task. Thus, during experimentation with the test section in its horizontal position, it is necessary to tilt the test section each time liquid is to be drained. An angle of 3˚is generally sufficient to ensure proper drainage of the test section. Air pressure should be supplied via the uppermost drainage port. It will be necessary to disconnect the line running from this void fraction port to the collection tank.
8. With all of the liquid drained, the collection tank should be detached from the experimental apparatus. The new mass of the tank and the mass added to the tank should be recorded. It is not necessary to drain the tank after every run.
9. With the new tank mass measured and recorded, the collection tank should be reattached to the experimental apparatus. With this step, the experimental void fraction run is complete. The process can simply be repeated from this point. The process should be repeated at least two times per data point. Further repeated runs must be conducted for data points in which the collected liquid mass proves highly variable.

3.2.6 Heat Transfer Measurements

This mode of research necessitates use of the heated test section. Running the test section in order to obtain heat transfer data does not require a large degree of adjustment of the setup beyond what is detailed in the system start up procedure. The main differences between this and any other form of experimental run are the use of the welder and the longer times associated with achieving steady state conditions. It should be noted

that it is beneficial to observe flow patterns at the desired gas and liquid mass flow rates in the flow visualization section prior to collecting heat transfer data. This allows correlation between heat transfer results and associated flow patterns. The procedure for the collection of heat transfer data is as follows:

1. Ensure that the welding cables are attached to the welder that is intended for use. If currents ranging from 400 to 750A are desired, the Lincoln DC-600 welder should be used. For currents lower than 400A, the Miller Maxtron 450 welder should be utilized. The amount of amperage supplied to the test section is up to the user. However, it should be noted that better heat transfer data is obtained when the difference between the average bulk temperature and the average wall temperature is relatively high. Care also must be taken that the test section is not overheated. A maximum working temperature of 70˚C (158˚F) has been set for the experimental apparatus. This has been done to help ensure the integrity of components as well as to prevent dry out within the test section.
2. Initialize the data acquisition program. The welder power status should be set to "On". Setting the power status to "On" allows the data acquisition program to collect data from the seven thermocouple stations distributed across the heated test section as well as recording input amperage and voltage. The flow pattern under observation should be entered into the appropriate space on the data acquisition program screen. The sample rate should be set to the desired value. For the purposes of heat transfer measurement, this value should never be below 6,000 samples per second.
3. Allow the system to stabilize for 2 to 3 minutes.

4. After stabilization, power on the desired welder. It will be necessary to switch on the appropriate cutoff switch, power up the welder, and set the welder to the desired amperage. Never turn on the cutoff switches to both welders at the same time. This will cause the in line fuses to burn out.
5. After the welder is powered up, it is once again necessary to allow the flow to stabilize. This can take anywhere from 5 to 20 minutes, depending on the type of flow under observation. The should be considered stable when fluctuations in the temperatures recorded by the inlet and outlet thermocouple probes as well as the temperatures recorded by the initial and final thermocouple stations fall below ±0.5˚C (±0.9˚F).
6. During this period of stabilization, it is also necessary to observe the temperature recorded by the inlet thermocouple. If the temperature recorded by the inlet thermocouple begins to rise higher than desired, further adjustment of the water side heat exchanger is necessary.
7. Once the system has reached steady state, data collection can begin. In general, data collection times of 5 minutes are sufficient to capture accurate data. However, in the case of slug flows where system output proves highly erratic, data should be collected for at least 10 minutes in order to ensure accuracy.
8. Once data collection is completed, the data acquisition program should be stopped and the welder shut down.
9. System cool down is necessary after performing heated runs. Fluid circulating through the test section should be allowed to return to a value close to that of room temperature. It will be necessary to run the data acquisition system in order

to keep track of this temperature value. It will be necessary to allow the welder to cool down as well. The Lincoln welder should be allowed to cool for at least 30 minutes after a high amperage run. The smaller Miller welder should be allowed at least 15 minutes to cool.

10. Once the system has been allowed to cool, this process can be repeated in order to take further data.

3.2.7 System Shut Down

System shut down simply includes all of the steps necessary to shut down equipment and to properly clear the test section. Proper clearing of the test section is necessary in order to prevent the accumulation of organics such as algae in the system. The steps for system shut down are as follows:

1. Stop water flow to the system. Turn off the water pump. Close the water line control valve and all quarter turn ball valves associated with the water delivery system.
2. Adjust the air line control valve until air is flowing through the system at its maximum rate.
3. Use the flowing air to remove all residual water from the system. Ensure that both test branches are completely clear, including the bypass line of the void fraction/flow visualization branch.
4. After the experimental apparatus is completely clear of water, use the air line control valve to shut off air flow to the system. Close all quarter turn cutoff valves associated with the air delivery system.

5. Close the quarter turn cutoff valve that controls water delivery to the water and air side heat exchangers.
6. Power off all equipment, including the National Instruments data acquisition system, Validyne carrier demodulator, and power supply for the absolute pressure transducers.
7. Ensure that the power cutoffs for both welders have been switched off.
8. Lastly, power down the air compressor.

CHAPTER IV

RESULTS AND DISCUSSION

The phase of experimentation documented in this chapter has been primarily associated with the validation of the newly constructed experimental apparatus. Toward this end, data was selectively collected such that comparisons could be made with either known correlations or data collected with the first generation experimental apparatus (Ghajar and Tang, 2008). Experimentation was performed utilizing the three main capabilities of the experimental apparatus, pressure drop measurements, void fraction measurements, and heat transfer measurements. Consequently, it is convenient to subdivide this chapter into three sections detailing the results of each mode of experimentation. As validation of the experimental apparatus is of the greatest concern, detailed comparisons between the collected data and relevant known comparisons and/or data sets will be presented in each section.

4.1 Pressure Drop Measurements

Pressure drop measurements with this experimental apparatus were conducted with the primary concern of ensuring proper behavior with single-phase flow at a horizontal inclination. While it was deemed necessary to ensure proper single-phase behavior, two-phase measurements have been relegated to the body of future research that will be conducted with this experimental apparatus.

Single-phase pressure drop measurements were conducted using distilled water as the working fluid. As the experimental apparatus was not designed to collect data under fully developed laminar flow conditions, the entry length of both test branches restricts experimentation to fully developed turbulent flows. While pressure drop measurements can be conducted using either test branch, experimentation was performed on the flow visualization/void fraction section as a matter of convenience. Experimentation was conducted at Reynolds numbers ranging from 5,000 to 35,000, with the highest Reynolds number corresponding to the maximum liquid mass flow rate. The range of mass flow rates investigated was between 2.6 kg/min (5.8 lb/min) and 16.2 kg/min (35.8 lb/min). Pressure drop runs were conducted with the experimental apparatus operating at steady state in order to ensure the collection of relevant data. Two different diaphragms were used in conjunction with the Validyne differential pressure transducer in order to accurately cover the entire range of pressure drops experienced across the test section. The diaphragms used had maximum differential pressure ranges of 13.8 kPa (2 psi) and 3.5 kPa (0.5 psi). In total, 8 different data points were taken during this mode of experimentation.

For the purposes of comparison, the pressure drop data obtained was converted into friction factor values using the Darcy friction factor equation (Equation 4.1).

$$f = \frac{2\Delta pD}{\rho l V^2} = \frac{\Delta pD^5 \pi^2 \rho}{8 l \dot{m}^2} \tag{4.1}$$

For the purposes of friction factor calculation, pipe diameter (D) and length (L) were simply measured. Pressure drop (Δp) was obtained from the Validyne pressure transducer. Density of water (ρ) was obtained using Equation (4.2), the formula is curve fittted from the density tables of Linstrom and Mallard (2003).

$$\rho = 999.96 + 1.7158 \times 10^{-2} T - 5.8699 \times 10^{-3} T^2 + 1.5487 \times 10^{-5} T^3 \qquad (4.2)$$

In this equation, the necessary units for temperature and density are ˚C and kg/m^3, respectively. Velocity was then calculated from measured values for mass flow rate in combination with other known properties.

The friction values obtained were then compared against the Blasius formula for turbulent flow in smooth pipes (Equation 4.3).

$$f = \frac{0.316}{\mathrm{Re}^{1/4}} \qquad (4.3)$$

It was decided to use the Blasius formula as the correlation for comparison due to its wide use and general acceptance by the engineering community. Figure 4.1 depicts the range of experimental friction factors obtained.

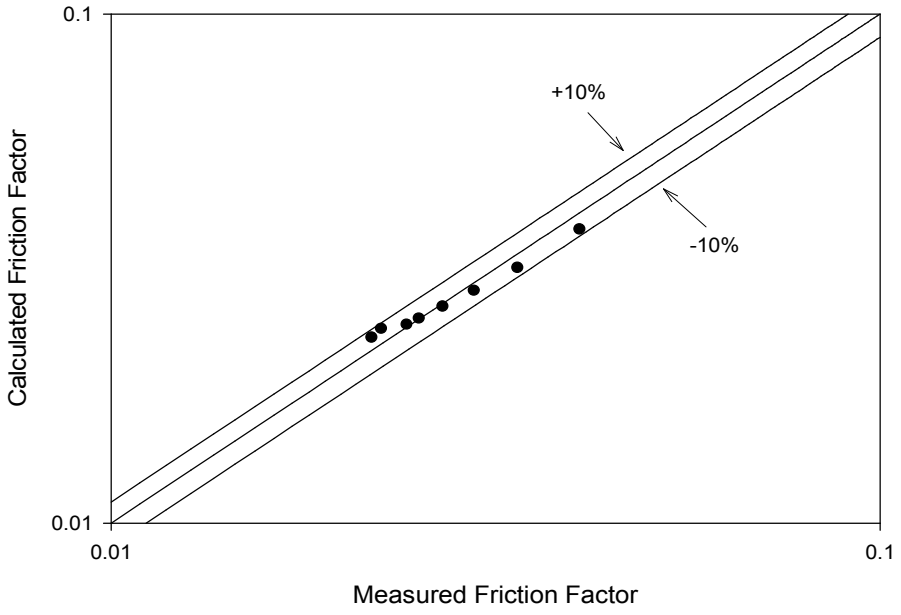

Figure 4.1: Calculated vs. Measured Friction Factor Values for Single-Phase Liquid Water

The error associated with the pressure droop measurements proves to be quite reasonable, within error margins of ±10%. This is well within the anticipated range for the experimental apparatus.

4.2 Void Fraction Measurements

Measurements of void fraction were conducted with the intent of verifying the capabilities of the experimental apparatus. As the apparatus was designed to take void fraction data at any angle of inclination, it was necessary to take void fraction data at multiple inclination angles. For the purposes of verification, it was deemed sufficient to take void fraction data at horizontal and vertical angles as well as an intermediate angle, specifically 5˚. This series of tests allowed for enough of the operational range of the experimental apparatus to be validated that proper behavior at the remaining intermediate angles could be assumed. Void fraction data was collected over a wide range of superficial liquid and superficial gas Reynolds numbers for each angle of inclination. Superficial liquid Reynolds numbers were varied incrementally from 2,000 to 20,000, corresponding to a range of mass flow rates between 1 kg/min (2.2 lb/min) and 25 kg/min (55 lb/min). For each increment of superficial liquid Reynolds number, data was collected at low, medium and high superficial gas Reynolds numbers, covering a range from about 2000 to 20,000 as well. This corresponded to a range of gas mass flow rates between 0.018 kg/min (0.039 lb/min) and 0.25 kg/min (0.55 lb/min). Data at each of these intervals of Reynolds number was repeated as necessary in order to ensure accuracy. The manner in which data was repeated is detailed in the Experimental

Procedure Chapter. Thus, a very broad range of flow patterns as well as flow energies was covered for each inclination angle.

4.2.1 Direct Comparison

The primary means of validation of the results obtained from void fraction experimentation has been direct comparison between the void fraction data obtained from the newly completed experimental apparatus and comparable data sets obtained from outside sources. Woldesemayat and Ghajar (2007) investigated the performance of 68 void fraction correlations within their paper Comparison of void fraction correlations for different flow patterns in horizontal and upward inclined pipes. A second part of the research conducted prior to the publication of this paper involved the compilation of void fraction databases from eight independent sources providing an unbiased data set with a total of 2845 data points. This data set covered a wide range of parameters including numerous inclination angles and working fluids. This data set was compiled for the purposes of evaluating the performance of the various correlations under investigation over as wide a range of parameters as possible. However, for the purposes of validation of the experimental apparatus, it was necessary to ensure that the data sets used were generated with comparable working fluids (i.e. air and water) and at comparable inclinations to the data taken with the experimental apparatus. Hence, only a small number of data points corresponding to inclination angles of 0˚ and 90˚ proved beneficial for the purposes of direct comparison.

Data used for the purposes of direct comparison in the horizontal orientation came from three sources, Franca and Lahey (1992) Spedding and Nguyen (1976), and Minami

and Brill (1987). The data set obtained from Franca and Lahey (1992) was recorded using a test section with a diameter of 19mm (0.75 in) using air and water as the working fluid. Void fraction measurements were conducted using a quick closing valve setup similar to that used in the experimental apparatus presented in this study. In their 1992 paper, Franca and Lahey estimate their experimental uncertainty in void fraction measurements to be ±5%. A total of 6 data points from this data set were used for the purposes of direct comparison. The data set obtained from Spedding and Nguyen (1976) was recorded using a 45.5 mm (1.8 in) pipe with air and water as the working fluids. The experimental uncertainty of their results was not reported in their paper. Once again quick closing valves served as the method of void fraction data collection. For the horizontal inclination, 5 data points taken from Spedding and Nguyen (1976) matched the range investigated using the experimental apparatus. Minami and Brill (1987) recorded their data set with a 77.93 mm (3.068 in) tube with air and water as the working fluids. They also used quick closing valves to measure void fraction. Accuracy of the data obtained was not presented in this paper either, though problems with repeatability were mentioned. A total of 6 data points from the Minami and Brill (1987) data set were used for the purposes of direct comparison.

The data set presented by Spedding and Nguyen (1976) covered a wide range of angles of inclination angles and consequently, data from this source was revisited for the purposes of direct comparison in the vertical orientation. The data of Spedding and Nguyen (1976) yielded a total of 9 data points that were useful for the purposes of direct comparison in the vertical orientation. In addition, data from Sujumnong (1997) was used for the purposes of the direct comparison for the 90˚ inclination angle. The data of

Sujumnong was collected using a 12.7 mm (0.5 in) pipe using air and water as the working fluids. Again in this case, quick closing valves served as the method for capturing void fraction data. Sujumnong (1997) presented the experimental uncertainty associated with their data as generally ranging between ±0.2% and ±8.0%. However, it was noted that for the case of slug flows, the experimental uncertainty associated with the void fraction data could range up to ±20%. Direct comparison was possible with 10 data points taken from Sujumnong (1997).

Direct comparison was made between the experimental data sets obtained from the literature and those taken using the present experimental apparatus on the basis of superficial velocities for both the gas and liquid phases. Thus, data points from the independent data sources were chosen for comparison based on superficial liquid velocity and superficial gas velocity. Superficial velocities were chosen as the means of comparison for a reason that is twofold. By definition, void fraction is the ratio of void or volume of gas to the total volume of the body of interest. By this token, volumetric flow rates would be ideal for comparison purposes if the test section diameters of the experimental setups from which the independent data sets were obtained were identical to that of the experimental apparatus being validated. However, this is not the case. The diameter of test sections used for the various independent databases varies to a relatively large degree. Thus, it is necessary to compare the multiple data sets on a basis that is rooted in the gaseous and liquid volume portions moving through the void fraction test section, but is independent of test section diameter and hence test section area. Comparisons between the independent data sets and the data obtained from the experimental apparatus were therefore necessarily compared on the basis of volumetric

flux. The volumetric flux for the gas and liquid portions of a two-phase flow moving through a particular test section are identical to the superficial gas velocity and superficial liquid velocity for the same flow moving through the same section.

Figure 4.2 depicts the results of the direct comparison for the horizontal orientation. The majority of the experimental data set is predicted within ±15% of the independent data sets. Out of the 17 data points plotted, 14 (or 82%) of the data points are comparable within ±15%. The data from Spedding and Nguyen (1976) seems to be matched the most consistently, while the comparisons with the data sets of Franca and Lahey (1992) and Minami and Brill (1987) generate a small number of points that stray outside the ±15% error bands.

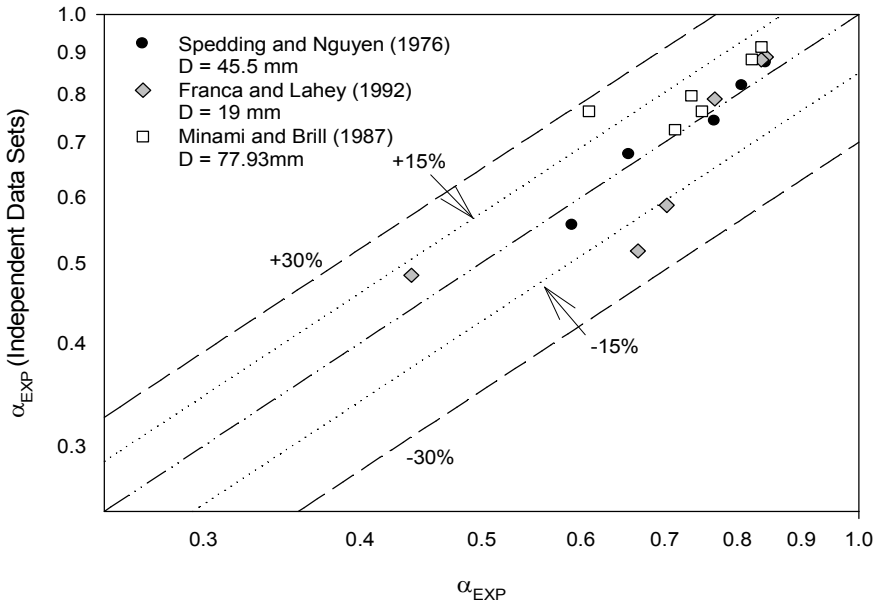

Figure 4.2: Direct Void Fraction Comparison (0˚ Inclination)

Figure 4.3 depicts the results of the direct comparison for the vertical orientation. For this comparison, 95% of the experimental data falls within ±15% of the data from

outside sources. Of the 19 points compared only one does not fall within the ±15% error bands.

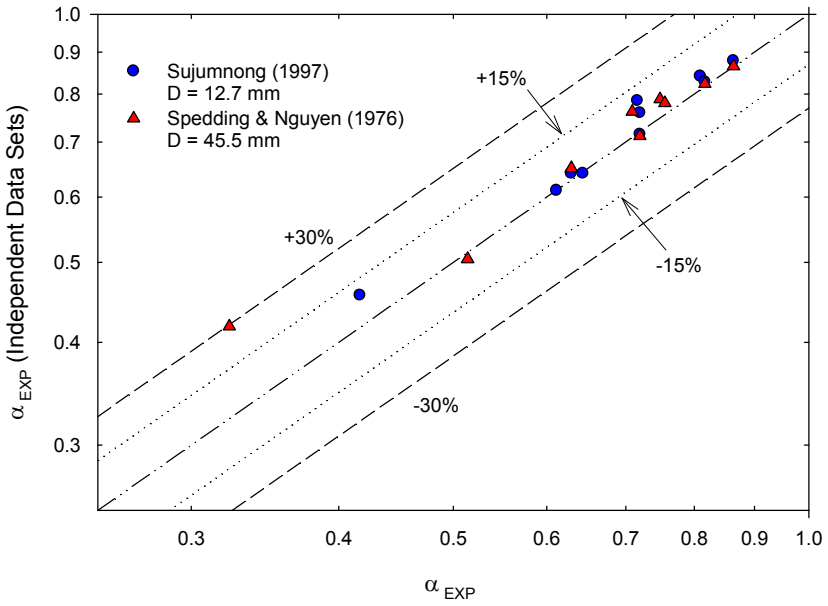

Figure 4.3: Direct Void Fraction Comparison (90° Inclination)

If the direct comparison for both inclinations is viewed as a whole, 32 of 36 total data points compare within ±15%. In other words, 89% of the experimental data compared within 15% of the data from outside sources. This is a quite healthy indication that the experimental apparatus is able to accurately capture void fraction data. As has been previously stated, the direction of current research on the experimental apparatus is towards validation. Future void fraction research at the angles discussed in the previous pages as well as at numerous intermediate angles is intended.

4.2.2 Comparison with Void Fraction Correlations

As a means of further validation, comparisons were made between the experimental data and numerous correlations. This method of comparison has been chosen as a secondary means of validation due to the inherent inaccuracies associated with the many void fraction correlations available. In many cases, void fraction correlations have been generated to provide information about particular flow patterns and were developed using particular fluid combinations and/or particular inclination angles. Many void fraction correlations have also been developed which are intended to encompass a wide range of flow patterns, inclination angles and fluid combinations. However, these general correlations can not encompass this wide range of variables without sacrificing accuracy in particular areas. In general, published accuracies associated with the numerous void fraction correlations available prove somewhat elusive as well. Thus, while the comparison of the experimental data with void fraction correlations does serve to validate the experimental results, it can not be considered as conclusive as the direct comparison.

In order to minimize problems associated with correlation inaccuracies, correlation selection has relied heavily on the extensive investigation of void fraction correlations done by Woldesemayat and Ghajar (2007). The research done by Woldesemayat and Ghajar (2007) compared the performance of 68 different void fraction correlations against 2845 data points obtained from multiple sources and covering a wide range of experimental parameters. Through this research, Woldesemayat and Ghajar (2007) were able to recommend the six best performing of the compared correlations for horizontal, inclined, and vertical flow as well as develop an improved correlation

intended to perform well for any flow inclination. It was chosen to use the top three of these correlations as well as the correlation presented by Woldesemayat and Ghajar (2007) for comparison with the data obtained from the experimental setup at each of the three inclination angles investigated. The top three correlations were those by Toshiba (1989), Rouhani and Axelsson (1970), and Dix (1971). (Dix (1971) and Toshiba (1989) are presented by Coddington and Macian (2002).) The correlation developed by Woldesemayat and Ghajar (2007) during the course of their research was based upon the correlation of Dix (1971). Thus, the correlation of Dix (1971) served to aid in the validation of the experimental data obtained as well as to track any improvements in void fraction prediction by the correlation of Woldesemayat and Ghajar (2007). Table 4.1 presents all of the correlations used for validation purposes.

Figure 4.4 depicts the results of void fraction research compared against each of the aforementioned correlations at a 0˚ inclination angle. From the figure, it can be seen that all four of the correlations predict the entirety of the collected data within the ±30% error bands. The correlations by Rouhani and Axelsson (1970) and Toshiba (1989) seem to perform the best for middle range to high void fraction values. However, as void fraction values decrease, the correlations of Dix (1971) and Woldesemayat and Ghajar (2007) begin to perform increasingly well at middle to lower values of void fraction.

Table 4.1: Void Fraction Correlations used for Comparison Purposes

Toshiba (1989) (Equation 4.4)	$\alpha = \dfrac{U_{SG}}{1.08U_M + 0.45}$
Rouhani and Axelsson (1970) (With Rouhani 1 distribution parameter, C_0) (Equation 4.5)	$\alpha = \dfrac{x}{\rho_G}\left[C_0\left(\dfrac{x}{\rho_G}+\dfrac{1-x}{\rho_L}\right)+\dfrac{U_{GM}}{G}\right]^{-1}$ where $U_{GM} = \left(\dfrac{1.18}{\sqrt{\rho_L}}\right)\left(g\sigma(\rho_L-\rho_G)\right)^{0.25}$ and $C_0 = 1+0.2(1-x)$
Dix (1971) (Equation 4.6)	$\alpha = U_{SG}\left\{U_{SG}\left(1+\left(\dfrac{U_{SL}}{U_{SG}}\right)^{\left(\frac{\rho_G}{\rho_L}\right)^{0.1}}\right)+2.9\left(\dfrac{g\sigma(\rho_L-\rho_G)}{\rho_L^2}\right)^{0.25}\right\}^{-1}$
Woldesemayat and Ghajar (2007) (Equation 4.7)	$\alpha = \dfrac{U_{SG}}{\left\{U_{SG}\left(1+\left(\dfrac{U_{SL}}{U_{SG}}\right)^{\left(\frac{\rho_G}{\rho_L}\right)^{0.1}}\right)+2.9\left[\dfrac{gD\sigma(1+\cos\theta)(\rho_L-\rho_G)}{\rho_L^2}\right]^{0.25}(1.22+1.22\sin\theta)^{\frac{P_{atm}}{P_{system}}}\right\}}$

The lack of performance by the correlation of Woldesemayat and Ghajar (2007) for the horizontal inclination can be easily explained by two factors. The first of these is that the correlation of Woldesemayat and Ghajar (2007) was developed with the intention of covering a very broad range of flow patterns and inclination angles. As previously discussed, this cannot be done without sacrificing accuracy in certain areas. The second factor is that Dix (1971) and through shared ancestry, the correlation of Woldesemayat and Ghajar (2007) tend to overpredict at system pressures less than 1 MPa (145 psi) (Coddington and Macian, 2002). The maximum pressure experienced during void

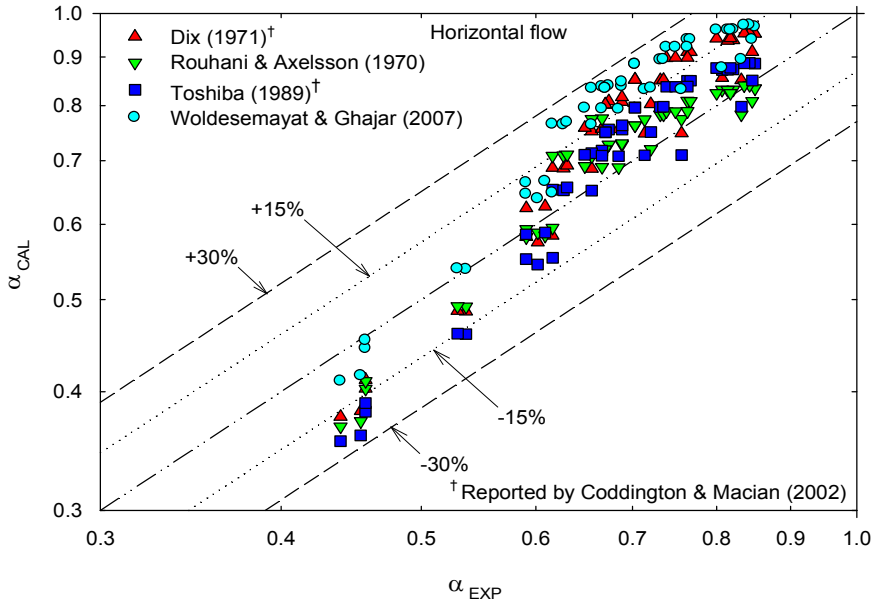

Figure 4.4: Experimental vs. Calculated Void Fraction for 0° Incline

fraction experimentation for any angle of inclination was approximately 0.25 MPa (36 psi), far lower than the range at which Dix (1971) begins to overpredict. Void fraction data was not taken at system pressures above 0.25 MPa (36 psi) as the limits of the system air supply were being approached. For this reason, overprediction from the Woldesemayat and Ghajar (2007) correlation should be anticipated as well.

Pressure limitations on the Rouhani and Axelsson (1970) correlation were not detailed within the paper in which it was presented. The variation of the distribution parameter (C_0) is intended to account for changes in mass flux and flow regime. It should then be expected that the Rouhani and Axelsson (1970) correlation will perform well for the full range of data collected. The only restriction presented for the Toshiba (1989) correlation is that system pressures should be below 10 MPa (1450 psi) (Coddington and Macian, 2002). This is a maximum pressure that is not even remotely

approached by the experimental apparatus. Thus, while the performance of all four correlations is presented for each of the flow inclinations investigated, it should be noted that the performance of the Toshiba (1989) and Rouhani and Axelsson (1970) correlations may better exemplify the overall validity of the void fraction data collected.

The overall performance of each of the four correlations for the 0˚ inclination angle is presented in Table 4.2. From the tabulated data, it can be seen that both the Toshiba (1989) and Rouhani and Axelsson (1970) correlation correctly predict around 90% of the experimental data set within ±15%. This serves as an indicator that the data obtained from the experimental apparatus is quite valid within the acceptable range of error at this angle of inclination.

Table 4.2: Data Points Correctly Predicted within ±15% at 0˚ Inclination

Correlation	# of Data Points	# Points Correctly Predicted	% Correctly Predicted
Toshiba (1989)	45	40	88.89%
Rouhani and Axelsson (1970)	45	41	91.11%
Dix (1971)	45	27	60.00%
Woldesemayat and Ghajar (2007)	45	16	35.56%

Figure 4.5 depicts the comparisons between the experimental void fraction data obtained at 5˚ of inclination against each of the four correlations selected. In the figure, it can be seen that all four of the correlations behave relatively well for this particular incline. A large majority of the data points are predicted within the ±15% error bands by all four of the correlations used. While all of the correlations perform very well, Rouhani and Axelsson (1970) predicts with slightly less accuracy.

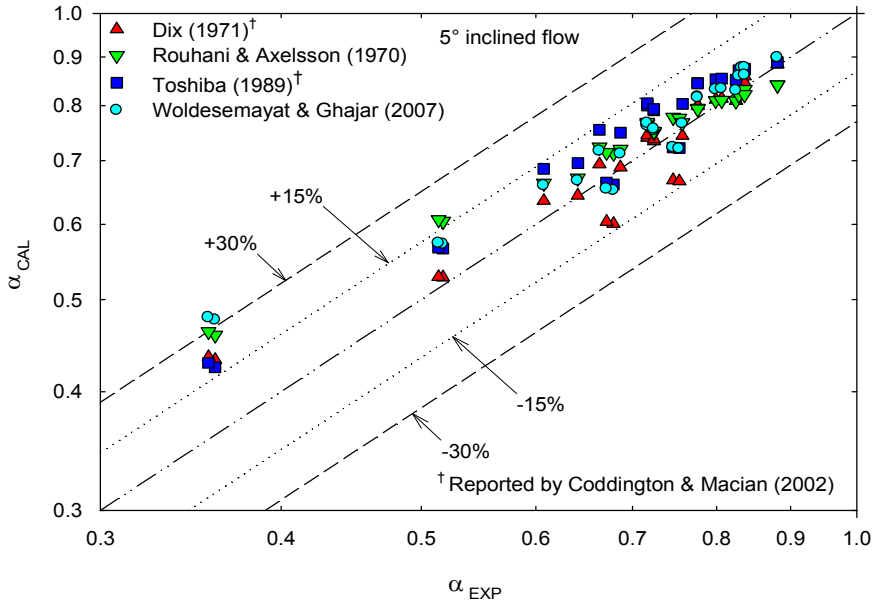

Figure 4.5: Experimental vs. Calculated Void Fraction for 5˚ Incline

Table 4.3 presents the overall performance for each of the correlations used at the 5˚ inclination. From the table, it can be seen that three out of the four correlations predict more than 90% of the data set within ±15%. The slightly lesser performing Rouhani and Axelsson (1970) correlation still predicts 87% of the data set within the same error bands. These percentages of correct prediction definitely help to illustrate the validity of the data taken at the 5˚ inclination.

Table 4.3: Data Points Correctly Predicted within ±15% at 5˚ Inclination

Correlation	# of Data Points	# Points Correctly Predicted	% Correctly Predicted
Toshiba (1989)	31	29	93.55%
Rouhani and Axelsson (1970)	31	27	87.10%
Dix (1971)	31	29	93.55%
Woldesemayat and Ghajar (2007)	31	29	93.55%

Figure 4.6 depicts the comparisons between the experimental void fraction data obtained at 90˚ of inclination and each of the four selected void fraction correlations. Again, it can be seen in this figure that all four of the correlations predict the experimental data set quite well between the ±15% error bands. In the case of the 90˚ inclination, the correlations of Dix (1971) and Woldesemayat and Ghajar (2007) predict the data set with the greatest accuracy.

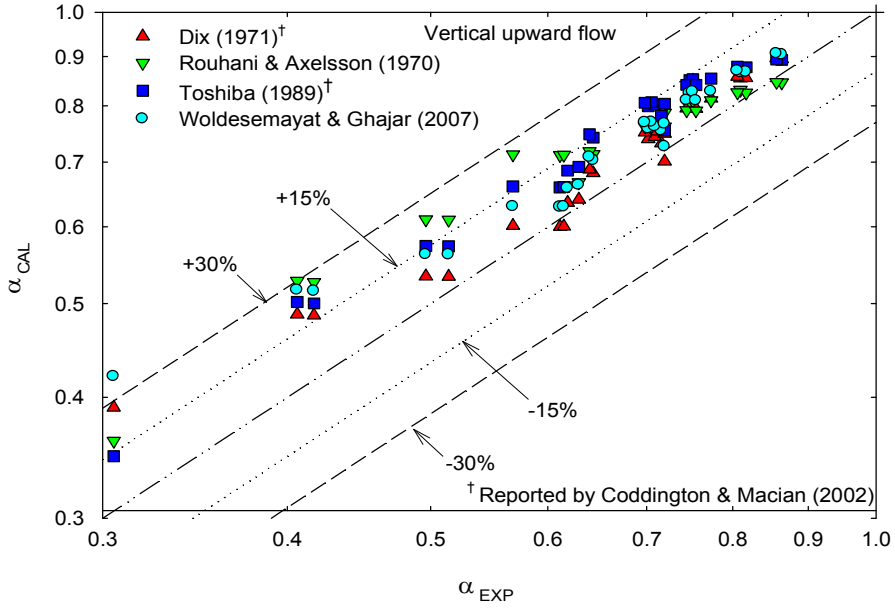

Figure 4.6: Experimental vs. Calculated Void Fraction for 90˚ Incline

Table 4.4 shows the percentage of the experimental data set taken at 90˚ of inclination correctly predicted within ±15%. From the table it can be seen that both the correlations of Dix (1971) and Woldesemayat and Ghajar (2007) predict more than 90% of the data set correctly within an error of ±15%. The correlations of Toshiba (1989) and Rouhani and Axelsson (1970) perform with lesser accuracy, only predicting slightly over 75% of the data set correctly within ±15%. However, this should be attributed more

toward shortcomings of the correlations rather than faults in the data set. In spite of the lesser performance of these two correlations, the data set has been predicted well enough by all four correlations to establish validity.

Table 4.4: Data Points Correctly Predicted within ±15% at 5° Inclination

Correlation	# of Data Points	# Points Correctly Predicted	% Correctly Predicted
Toshiba (1989)	33	25	75.76%
Rouhani and Axelsson (1970)	33	25	75.76%
Dix (1971)	33	30	90.91%
Woldesemayat and Ghajar (2007)	33	30	90.91%

Table 4.5 presents the performance of the four correlations chosen for comparison against the combined data set for the 0°, 5°, and 90° inclinations. It can be seen that the Toshiba (1989) and Rouhani and Axelsson (1970) correctly predict the combined data set within ±15% at percentages of 86.2% and 85.3%, respectively. The correlation research of Woldesemayat and Ghajar (2007) showed that Toshiba (1989) and Rouhani and Axelsson (1970) were able to correctly predict an unbiased data set of 2845 points within ±15% at percentages of 85.3% and 84.2%, respectively. Thus, the performance of the

Table 4.5: Data Points Correctly Predicted within ±15% for all Inclinations

Correlation	# of Data Points	# Points Correctly Predicted	% Correctly Predicted
Toshiba (1989)	109	94	86.2%
Rouhani and Axelsson (1970)	109	93	85.3%
Dix (1971)	109	86	78.9%
Woldesemayat and Ghajar (2007)	109	75	68.8%

experimental data set when compared with these two correlations is quite on par withwhat should be expected. The lesser performances of the correlations of Dix (1971) and Woldesemayat and Ghajar (2007) should not detract from the validity of the experimental data set. As previously explained, the entirety of the data set is below the operational range of these two correlations.

It can be readily seen that experimental apparatus has performed quite well in both the direct comparisons and the correlation comparisons for all of the angles of inclination researched. The direct comparison has shown that 89% of the experimental data compared within ±15% of the experimental data obtained from outside sources. Correlation comparisons have shown that the experimental data set performs at levels comparable to that of contemporary researchers against the top performing correlations presented by Woldesemayat and Ghajar (2007). Having performed well through both modes of comparison, the void fraction data obtained from the experimental setup should be considered quite valid.

4.3 Heat Transfer Measurements

In order to validate the capabilities of the experimental apparatus with respect to heat transfer measurements, data sets were collected for both single-phase liquid and two-phase (gas-liquid) heat transfer. Both of these data sets were collected with the heated section of the experimental setup well insulated in order to reduce heat transfer to the surroundings to the largest possible degree. In both the cases of the single-phase liquid measurements and the two-phase measurements, it was deemed sufficient to collect data at the horizontal orientation for the purposes of validation. Data for both modes of heat

transfer research was reduced using the methodology presented by Ghajar and Kim (2006). The data reduction program used was originally written by Jae-yong Kim (former Ph.D. student) and modified for the purposes of this experimental apparatus by Clement Tang (Ph.D. candidate and fellow member of the research team). This data reduction program calculates local values for both the inside wall surface temperature and inside wall heat flux from measurements of the outside wall temperature, the heat generation within the pipe wall, and the thermophysical properties of the pipe material (electrical resistivity and thermal conductivity), using a finite-difference formulation. Overall values for inside wall temperature, inside wall heat flux, and heat transfer coefficient are then obtained by averaging the appropriate local peripheral values. The remainder of this section will discuss the results of the single-phase liquid heat transfer research and the two-phase heat transfer research independently.

4.3.1 Single-Phase Liquid Heat Transfer Measurements

Single-phase liquid heat transfer measurements were conducted as a preliminary measure to ensure the functionality of the experimental apparatus prior to the collection of two-phase heat transfer data. In this mode of experimentation, distilled water was used as the test fluid. A total of 8 data points were collected for the purposes of validation with respect to single-phase liquid heat transfer. Data was collected across the entire turbulent flow range of which the experimental apparatus is capable. Data was collected in increments of Reynolds number, with values ranging from roughly 9000 to 38,000. Data was collected only at Reynolds numbers above 9000 in order to ensure that the flow through the heated test section was fully turbulent. As the experimental apparatus has

been designed to collect data for turbulent single-phase flows and two-phase flows, the entry length of the heated branch of the experimental apparatus is insufficient for the purposes of collecting data in the laminar region. The upper limit of Reynolds number achieved (i.e. 38,000) represents the maximum capability of the system. The range of Reynolds numbers investigated corresponds to liquid mass flow rates ranging from 4.6 kg/min (10.1 lb/min) to 18.1 kg/min (39.9 lb/min). Once again, the higher of these two values represents the maximum liquid flow rate of which the experimental apparatus is capable. Each of the data points was collected at constant power input to the heated test section, generating a boundary condition of uniform wall heat flux. In the single-phase heat transfer investigation, the values for the uniform wall heat flux ranged from 70,000 W/m^2 (22,190 Btu/h-ft^2) to 90,000 W/m^2 (28,530 Btu/h-ft^2), resulting in a range of heat transfer coefficients between 3600 W/m^2-K (634 Btu/h-ft^2-˚F) and 11,000 W/m^2-K (1937 Btu/h-ft^2-˚F). Experimental Nusselt numbers ranged between 74 and 231. The power input remained relatively constant across the entire range of data collected in this mode of heat transfer research. This was caused by the fact that the welder used to supply power was running at its maximum output throughout the collection of the data set. Running the welder at this output was necessary in order to maximize the difference between the average bulk temperature and the average inner wall temperature, thereby maximizing the accuracy of the data collected.

The single-phase liquid heat transfer data collected was compared against four different single phase Nusselt number correlations in order to establish the validity of the data. The correlations used were those of Dittus-Boelter (1930), Sieder and Tate (1936),

Gnielinski (1976), and Ghajar and Tam (1994). Each of these correlations as well as their working ranges is presented in Table 4.6.

Table 4.6: Single Phase Heat Transfer Correlations

Dittus-Boelter (1930) (Equation 4.8)	$Nu_D = 0.023\,\mathrm{Re}_D^{4/5}\,\mathrm{Pr}^n$ where n = 0.4 for heating	$0.7 \le \mathrm{Pr} \le 160$ $\mathrm{Re_D} \ge 10{,}000$ $L/D \ge 10$
Sieder and Tate (1936) (Equation 4.9)	$Nu = 0.023\,\mathrm{Re}^{0.8}\,\mathrm{Pr}^{1/3}\left(\mu_b/\mu_w\right)^{0.14}$	$0.7 \le \mathrm{Pr} \le 16{,}700$ $\mathrm{Re} \ge 10{,}000$
Gnielinski (1976) (Equation 4.10)	$Nu = \dfrac{(c_f/2)(\mathrm{Re}-1000)\mathrm{Pr}}{1+12.7(c_f/2)^{1/2}\left(\mathrm{Pr}^{2/3}-1\right)}$ where $\dfrac{1}{c_f} = 1.58\ln\mathrm{Re} - 3.28$ (Filonenko Correlation)	$0.5 \le \mathrm{Pr} \le 2000$ $2300 \le \mathrm{Re} \le 5\mathrm{x}10^6$
Ghajar and Tam (1994) (Equation 4.11)	$Nu = 0.023\,\mathrm{Re}^{0.8}\,\mathrm{Pr}^{0.385}\left(x/D_i\right)^{-0.0054}\left(\mu_b/\mu_w\right)^{0.14}$	$3 \le x/D_i \le 192$ $7000 \le \mathrm{Re} \le 49{,}000$ $4 \le \mathrm{Pr} \le 34$ $1.1 \le \mu_b/\mu_w \le 1.7$

As previously stated, Reynolds number was varied between 9000 and 38,000 during the course of experimentation. Thus, for Dittus-Boelter (1930) and the correlation of Sieder and Tate (1936) Reynolds numbers stray slightly lower than the acceptable range. However, no significant effects were seen in the results of comparison with these correlations. Prandtl numbers ranged from 5.9 to 6.2 through the course of experimentation, firmly within the acceptable ranges for all of the correlations used. The L/D ratio for the heated test section is 80, readily satisfying the necessary parameters for the Dittus-Boelter (1930) equation and the correlation of Ghajar and Tam (1994). The ratio of μ_b/μ_w ranged between 1.2 and 1.47 through the course of experimentation, thus

satisfying the constraint of Ghajar and Tam (1994). It can therefore be stated that the data collected for the purposes of single phase heat transfer research is well within the necessary boundaries for the correlations used for the purposes of validation.

Figure 4.7 shows the results of comparison of the experimental results with the four different Nusselt number correlations selected. Prior to the single-phase heat transfer investigation, it had been decided that a deviation of ±20% between experimental and predicted data would be considered acceptable. It can be seen in Figure #.8 that not only has this constraint been satisfied, but the data has been predicted within a deviation of ±10% by all four of the correlations chosen for the purposes of comparison. Thus, having more than satisfied the original desired criteria, the data collected for single-phase liquid heat transfer can be considered valid.

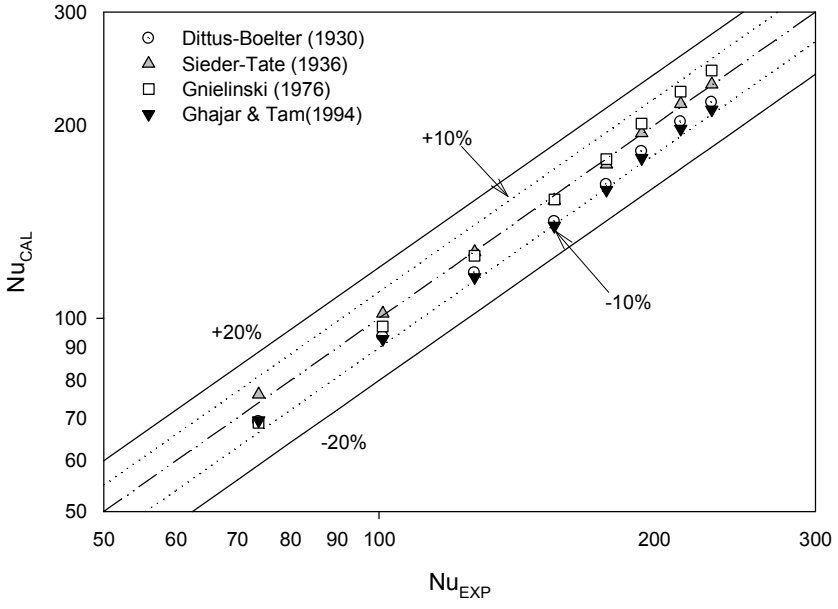

Figure 4.7: Experimental vs. Calculated Nusselt Number for Single-Phase Liquid Heat Transfer (0˚ Incline)

4.3.2 Two-Phase Heat Transfer Measurements

Two-phase heat transfer measurements were conducted with the intention of validation through the use of a direct comparison with heat transfer data from the previous 27.9 mm (1.093 in) diameter experimental apparatus as well as through comparison with the correlation of Ghajar and Tang (2008). In order to facilitate direct comparison with data obtained from the previous experimental setup, data was taken from the new experimental apparatus such that gas and liquid mass fluxes of selected data points from the previous experimental data set were matched as closely as possible. This was done in an attempt to reduce the influence of area and hence pipe diameter upon the comparison as much as possible. Data was collected incrementally through a range of liquid mass fluxes between 180 kg/s-m^2 (37 lb/s-ft^2) and 880 kg/s-m^2 (180 lb/s-ft^2). This corresponds to a range of superficial liquid Reynolds numbers between 2800 and 13000 and a range of mass flow rates between 1.3 kg/min (2.9 lb/min) and 6.5 kg/min (14.3 lb/min). At each liquid mass flux investigated, gas mass flux was varied in order to obtain both a slug flow and an annular flow. It was deemed necessary to perform heat transfer measurements for two well defined flow patterns across the range of capability of the experimental apparatus for the purposes of validation. Through this mode of investigation gas mass flux was varied between 1.8 kg/s-m^2 (0.4 lb/s-ft^2) and 2.6 kg/s-m^2 (5.3 lb/s-ft^2). This corresponds to a range of superficial gas Reynolds numbers between 1200 and 18,000 and a range of mass flow rates between 0.018 kg/min (0.040 lb/min) and 0.18 kg/min (0.40 lb/min). In the two-phase heat transfer investigation, the values for the uniform wall heat flux ranged from 34,700 W/m^2 (11,000 Btu/h-ft^2) to 64,100 W/m^2 (20,300 Btu/h-ft^2), resulting in a range of heat transfer coefficients between 1130 W/m^2-

K (199 Btu/h-ft^2-˚F) and 4530 W/m^2-K (798 Btu/h-ft^2-˚F). Overall, 10 data points were taken for this mode of investigation. Both slug and annular flows were evenly represented with 5 data points being taken for each flow pattern. Of these ten data points, 6 were considered acceptable for direct comparison. In the direct comparison, both the slug and annular flow patterns were evenly represented with 3 data points. Data points were chosen for comparison based on liquid mass flux, gas mass flux, and heat transfer rate.

Figure 4.8 depicts the results of direct comparison between data obtained from the 27.9 mm (1.093 in) diameter setup and the new 1.252cm (0.493in) diameter setup. For the purposes of the two-phase heat transfer data, results are compared on the basis of heat transfer coefficient. As in prior investigations conducted by this research team, the acceptable error for the heat transfer data collected is ±20%. It can be seen from the figure that all collected data points are well within this acceptable range of error.

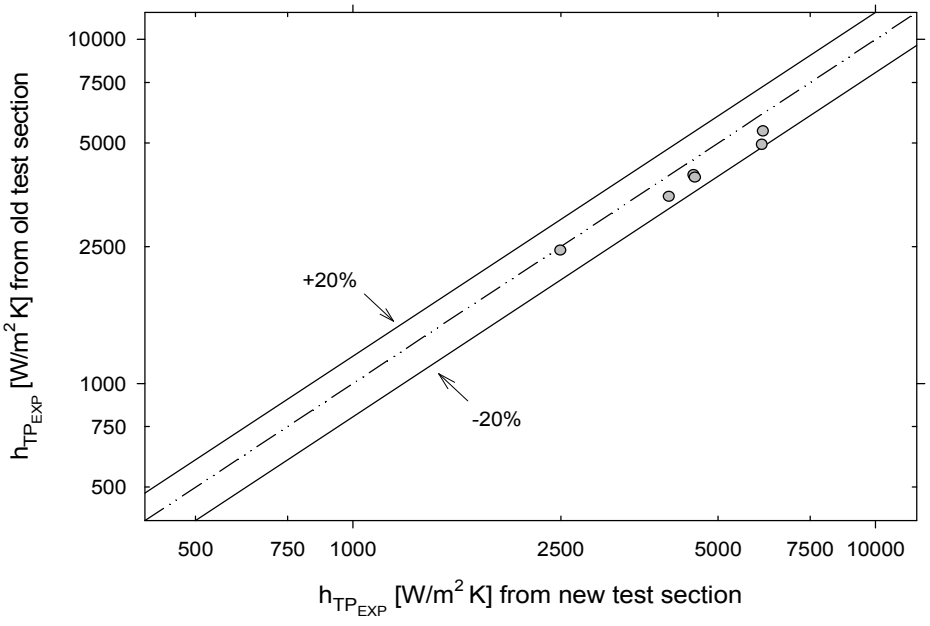

Figure 4.8: Direct Comparison of Two-Phase Heat Transfer Data from Old and New Setups

It may be noted that the heat transfer coefficients recorded by the new experimental setup are slightly higher than those recorded by the previous experimental apparatus. This phenomenon of higher heat transfer coefficients should be considered simply a difference between the two different experimental setups. The comparable data between the new and old experimental setups was quite limited. Further direct comparison is intended and should negate the underprediction seen in the figure. In any case, this mode of comparison has shown that the experimental setup is performing quite well within the predetermined margins of error. The comparison that follows with the correlation of Ghajar and Tang (2008) will serve to better demonstrate the validity of the two-phase heat transfer data collected.

The heat transfer correlation of Ghajar and Tang (2008) is the latest version of a previous correlation developed by Kim et al., (2000). The correlation has been in a state of constant evaluation since that time, with slight modifications being made as new data became available. The most recent form of the correlation presented in Ghajar and Tang (2008) is as follows:

$$h_{TP} = F_P\, h_L \left\{ 1 + C \left[\left(\frac{x}{1-x} \right)^m \left(\frac{1-F_P}{F_P} \right)^n \left(\frac{Pr_G}{Pr_L} \right)^p \left(\frac{\mu_G}{\mu_L} \right)^q \left(I^* \right)^r \right] \right\} \tag{4.12}$$

In this equation the coefficient F_p is a flow pattern factor used to capture the realistic shape of the gas-liquid interface. The equation for F_p is as follows:

$$F_P = \tilde{S}^2_{L,eff} = \left(\frac{S_{L,eff}}{\pi D} \right)^2 = (1-\alpha) + \alpha F_S^2 \tag{4.13}$$

In this equation, the value F_s is a shape factor which is in essence a modified and normalized Froude number. The shape factor is defined as

$$F_S = \frac{2}{\pi}\tan^{-1}\left(\sqrt{\frac{\rho_G\left(V_G - V_L\right)^2}{g\,D\left(\rho_L - \rho_G\right)\cos\theta}}\right) \tag{4.14}$$

The values for void fraction (α) are calculated using the correlation of Spedding and Chen (1984) for the purposes of this investigation. However, it should be noted that the use of other void fraction correlations is possible due to the robustness of the heat transfer correlation developed (Ghajar and Tang, 2008). The correlation of Spedding and Chen (1984) is as follows:

$$\alpha = \left[1 + 2.22\left(\frac{1-x}{x}\right)^{0.65}\left(\frac{\rho_G}{\rho_L}\right)^{0.65}\right]^{-1} \tag{4.15}$$

The value for single-phase liquid heat transfer (h_L) in the two phase heat transfer correlation comes from the Sieder and Tate (1936) correlation. The Sieder and Tate (1936) correlation is as follows:

$$h_L = 0.027\,\mathrm{Re}_L^{4/5}\,\mathrm{Pr}_L^{1/3}\left(\frac{k_L}{D}\right)\left(\frac{\mu_b}{\mu_w}\right)_L^{0.14} \tag{4.16}$$

In the heat transfer correlation, the coefficient I^* is an inclination factor that takes accounts for both the effects of inclination and surface tension. The formulation for the inclination factor is as follows:

$$I^* = \left(1 + \sqrt{Eo}\,\sin\theta\right)\left(1 + 5.0\cos\theta\right) \tag{4.17}$$

In the inclination factor the value Eo corresponds to the Eötvös number. This value also known as the Bond number (Bo) represents the hydrodynamic interaction of buoyancy and surface tension forces that occur in two-phase flow (Ghajar and Tang, 2008). The Eötvös number takes the following form:

$$Eo = \frac{(\rho_L - \rho_G)gD^2}{\sigma} \tag{4.18}$$

In the heat transfer correlation, the values of the constant C and the exponents m, n, q, and r are adjustable for the purposes of improvement of the accuracy of prediction for particular sets of data. In Ghajar and Tang (2008) the following values for the constant and exponents were proposed: C = 0.3, m = 0.3, n = 0.01, p = 0.01, q = 0.01 and r = 1.0. These are the values used in the reduction of the two-phase heat transfer data presented in this chapter.

Ghajar and Tang (2008) validated their correlation against a set of 986 experimental data points for different flow patterns, inclination angles, and gas-liquid combinations. The investigation spanned superficial liquid Reynolds numbers between 750 and 127,000 and superficial gas Reynolds numbers between 14 and 209,000. Through this validation it was shown that the correlation was able to predict a very high percentage (over 93%) of the data points within an error margin of ±30%.

Figure 4.9 depicts the results of comparison of the experimental heat transfer coefficients and the heat transfer coefficients calculated using the correlation of Ghajar and Tang (2008). It can be seen that the majority (90%) of the data points are predicted by the correlation within error margins of ±20%. Thus, the data is predicted by the correlation of Ghajar and Tang (2008) very well within the acceptable margins of error. It can also be seen that there is neither a consistent overprediction nor underprediction. Having met these two criteria, the two-phase heat transfer data collected with the experimental apparatus can be considered valid.

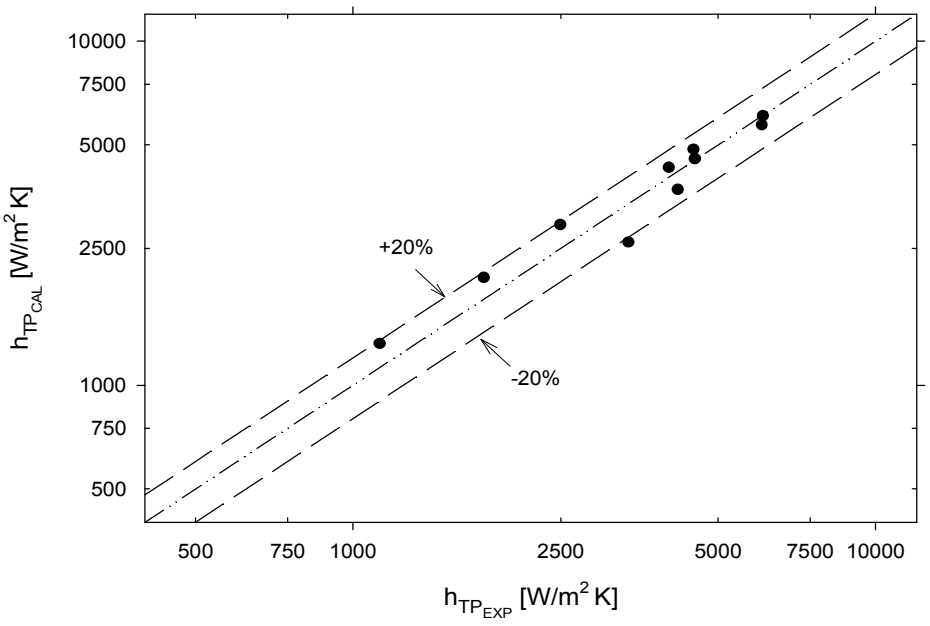

Figure 4.9: Comparison of Two-Phase Heat Transfer Data from New Setup with Correlation of Ghajar and Tang (2008)

CHAPTER V

CONCLUSIONS AND RECOMMENDATIONS

This document has been intended to detail the design, construction, and validation of the experimental apparatus that has been presented within the preceding chapters. The experimental apparatus has been developed for the purposes of two-phase flow pressure drop, void fraction, and non-boiling heat transfer measurements as well as flow visualization at any angle of inclination between positive and negative 90˚. It is the first experimental apparatus that has been developed with all of these capabilities. The experimental setup has been validated for single-phase pressure drop measurements, void fraction measurements, single-phase heat transfer measurements, and two-phase non-boiling heat transfer measurements. Validation of single-phase pressure drop capabilities consisted of comparison between collected data converted to friction factor and the Blasius friction factor formula for turbulent flow in smooth pipes. This mode of validation achieved highly satisfactory results. Void fraction data was compared against multiple correlations and independent data sets at multiple inclinations with highly satisfactory results as well. Horizontal single-phase heat transfer data obtained from the experimental apparatus was compared against four established correlations and proved quite accurate. Horizontal two-phase non-boiling heat transfer data was compared both against the correlation of Ghajar and Tang (2008) and data obtained from the previous experimental apparatus. Both modes of validation proved quite satisfactory. Examples

of the quality of the flow visualization possible with this setup in addition to methodology have been presented. Having performed well at all of the desired types of measurements, the device can be considered a valid and highly versatile addition to the Oklahoma State University heat transfer laboratory. Future plans are centered around the use of this experimental apparatus to continue to test the correlation of Ghajar and Tang (2008) as well as the correlation of Woldesemayat and Ghajar (2007). It is also intended to develop robust correlations for both two-phase non-boiling heat transfer and void fraction for inclination angles between positive and negative 90º. In addition, the flow visualization capability will be utilized to develop flow pattern maps for inclination angles between positive and negative 90º.

Through the use of this experimental apparatus, a few different aspects have come to light that can be improved upon. Thus, recommendations for the further improvement of the experimental apparatus can be made. The first of these is that both more accurate systems of control and flow rate metering for the gas side of the experimental apparatus should be installed. The Parker metering valve used on the gas side of the experimental apparatus should be replaced with a more precise valve that will allow for better control of the gas inlet to the system at low mass flow rates. In order to more accurately measure the gas inlet to the system at these low mass flow rates, a new meter with enhanced capabilities at low mass flow rates should also be installed. Currently, the Oklahoma State University heat transfer research team is in contact with Micro Motion with the intention of procuring this meter. It may also be necessary to install a more precise control valve on the liquid side of the experimental apparatus for the purposes of more accurate control at low liquid mass flow rates. The installation of a new meter on the

liquid side of the experimental apparatus should not be necessary. Through the use of the experimental apparatus, it was also found that cycling of the air compressor used for the supply of air caused fluctuations in the mass flow of air inlet to the system. In some cases, this phenomenon caused erroneous readings. Thus, changes in air mass flow rate had to be monitored in order to ensure the accuracy of the data obtained. Utilization of an air compressor with a larger tank would serve to reduce the effects of cycling upon the readings obtained from the experimental apparatus. It should be noted that while there is always room for improvement, the experimental apparatus has been shown to more than satisfy all of the criteria chosen for the purposes of validation.

REFERENCES

Boussman,W.S., 1994, Studies of Two-Phase Gas-Liquid Flow in Microgravity, *Ph.D. Dissertation,* University of Houston, also: NASA Contractor Report 195434 (1995).

Boussman, W. S., and Dukler, A. E., 1994, Ground Based Studies of Gas-Liquid Flows in Microgravity using Lear Jet Trajectories, *Proceedings of 32nd Aerospace Sciences Meeting and Exhibit,* Reno, NV, Paper No. AIAA 94-0829.

Coddington, P., and Macian, R., 2002, A Study of the Performance of Void Fraction Correlations used in the Context of Drift-Flux Two-Phase Flow Models, *Nuclear Engineering Design,* Vol. 215, pp. 199-216.

Dittus, F. W., and Boelter, L. M. K., 1930, Publications on Engineering, Vol. 2, p. 443, University of California, Berkley.

DOE, 2001, University of Tulsa Embark on Wax Deposition Study, *Oil and Gas Journal,* Vol. 99, p. 56.

Dukler, A, E., Fabre, J. A., McQuillen, J. B., and Vernon, R., 1988, Gas-Liquid Flow at Microgravity Conditions: Flow Patterns and their Transitions, *International Journal of Multiphase Flow,* Vol. 14, pp. 389-400.

Fore, L. B., Witte, L. C., and McQuillen, J. B., 1996, Heat Transfer to Annular Gas-Liquid Mixtures at Reduced Gravity, *Journal of Thermophysics and Heat Transfer,* Vol. 10, pp. 633-639.

Fore, L. B., Witte, L. C., and McQuillen, J. B., 1997, Heat Transfer to Two-Phase Slug Flows under Reduced-Gravity Conditions, *International Journal of Multiphase Flow,* Vol. 23, pp. 301-311.

Franca, F., and Lahey Jr., R. T., 1992, The Use of Drift-Flux Techniques for the Analysis of Horizontal Two-Phase Flows, *International Journal of Multiphase Flow,* Vol. 18, pp 787-801.

Furuholt, E. M., 1988, Multiphase Technology: Is it of Interest for Future Field Developments?, *Presented at Society of Petroleum Engineers European Petroleum Conference,* Oct. 17-19, London, England, Paper No. 18361.

Gao, S., House, W., Chapman, W., 2005, Characterization of Hydrate Formation in Black Oil using NMR, *Proceedings of 2005 Offshore Technology Conference,* May 2-5, Houston, TX, Paper No. OTC 17152.

Ghajar, A. J., and Kim, J., 2006, Calculation of Local Inside-Wall Convective Heat-Transfer Parameters from Measurements fo Local Outside-Wall Temperatures along an Electrically Heated Circular Tube, *Heat Transfer Calculations,* edited by Myer Kutz, McGraw-Hill, New York, NY, pp. 23.3-23.27, 2006.

Ghajar, A. J., and Tam, L. M., 1994, Heat Transfer Measurements and Correlations in the Transition Region for a Circular Tube with Three Different Inlet Configurations, *Experimental and Thermal Fluid Science,* Vol. 8, No. 1, pp. 79-90.

Ghajar, A. J., and Tang, C. C., 2008, Importance of Non-Boiling Two-Phase Flow Heat Transfer in Pipes for Industrial Applications, *Proceedings of the 11th Conference on Process Integration, Modeling, and Optimization for Energy Saving and Pollution Reduction (PRES'2008),* Aug. 24-28, Prague, Czech Republic.

Gnielinski, V., 1976, New Equations for Heat and Mass Transfer in Turbulent Pipe and Channel Flow, *Int. Chem. Eng.*, Vol. 16, pp. 359-368.

Kim, D., Ghajar, A. J., and Dougherty, R. L., 2000, Robust Heat Transfer Correlation for Turbulent Gas-Liquid Flow in Vertical Pipes, *Journal of Thermophysics and Heat Transfer,* Vol. 14, pp. 574-578.

Kim, D., Ghajar, A. J., Doughtery, R. L., and Ryali, V. K., 1999, Comparison of 20 Two-Phase Heat Transfer Correlations with Seven Sets of Experimental Data, Including Flow Pattern and Tube Inclination Effects, *Heat Transfer Engineering,* Vol. 20, No. 1, pp. 15-40.

Kline, S. J., and McClintock, F. A., 1953, Describing Uncertainties in Single-Sample Experiments, *Mechanical Engineering,* Vol. 1, pp. 3-8.

Linstrom, P. J., and Mallard, W. G., (eds.) 2003, NIST Chemistry WebBook, NIST Standard Reference Database No. 69, *National Institute of Standards and Technology,* http://webbook.nist.gov.

Minami, K. and Brill, J. P., 1987, Liquid Holdup in Wet Gas Pipelines, *SPE Production Engineering,* Vol. 5, pp. 36-44.

Rite, R. W., and Rezkallah, K. S., 1994, Heat Transfer in Two-Phase Flow through a Circular Tube at Reduced Gravity, *Journal of Thermophysics and Heat Transfer,* Vol. 8, pp. 702-708.

Rouhani, S. Z., and Axelsson, E., 1970, Calculation of Void Volume Fraction in the Sub Cooled and Quality Boiling Regions, *International Journal of Heat and Mass Transfer,* Vol. 13, pp. 383-393.

Sieder, E. N., and Tate, G. E., 1936, Heat Transfer and Pressure Drop of Liquids in Tubes, *Ind. Eng. Chem.* Vol. 28, No. 12, p. 1429-1435.

Shiu, K. C. and Beggs, H. D., 1980, Predicting Temperatures in Flowing Oil Wells, *Journal of Energy Resources Technology,* Vol. 102, pp. 2-11.

Singh, P., Venkatesan, R., and Fogler, H. S., 2000, Formation and Aging of Incipient Thin Film Wax-Oil Gels, *AIChE Journal,* Vol. 46, pp. 1069-1074.

Spedding, P. L., and Chen, J. J. J., 1984, Holdup in Two-Phase Flow, *International Journal of Multiphase Flow,* Vol. 10, pp. 307-339.

Spedding, P. L., and Nguyen, V. T., 1976, Data on Holdup, Pressure Loss, and Flow Patterns for Two-Phase Air-Water Flow n and Inclined Pipe, Report Eng. 122, University of Aukland, Aukland, New Zealand.

Sujumnong, M., 1997, Heat Transfer, Pressure Drop, and Void Fraction in Two-Phase, Two-Component Flow in a Vertical Tube, *Ph. D. Dissertation,* The University of Manitoba, Winnipeg, Manitoba, Canada.

Wang, L., Huang, X.-H., and Lu, Z., 2004, Immiscible Two-Component Two-Phase Gas-Liquid Heat Transfer on Shell Side of a TEMA-F Heat Exchanger, *Heat and Mass Transfer,* Vol. 40, pp. 301-306.

Woldesemayat, M. A., and Ghajar, A. J., 2007, Comparison of Void Fraction Correlations for Different Flow Patterns in Horizontal and Upward Inclined Pipes, *International Journal of Multiphase Flow,* Vol. 33, pp. 347-370.

Woo, G. T., Garbis, S. J., and Gray, T. C., 1984, Long-Term Control of Paraffin Deposition, *Proceedings of 59th Annual SPE Conference,* Sept. 16-19, Houston, TX, Paper No. SPE 13126.

Yong, F., 1996, Chemical Removal of Formation Damage from Paraffin Deposition: Part 1-Soluability and Dissolution Rate, *Proceedings of SPE International Symposium on Formation Damage Control,* Feb., Lafayette, LA, Paper No. SPE 31128.

Zhao, L., and Rezkallah, K. S., 1993, Gas-Liquid Flow Patterns at Microgravity Conditions, *International Journal of Multiphase Flow,* Vol. 19, pp. 751-763.

APPENDIX A

LIST OF EXPERIMENTAL EQUIPMENT

Water Transport

Bell and Gosset series 1535 Model 3545 D10 Coupled Centrifugal Pump (Main Pump)

Aqua-Pure AP12T water purification system

Oberdorfer Model 600 F13 pump (pump for filtration system)

Bio Logic BIO-1.5 UV filter

ITT Standard Model BCF 4063 one shell and two-tube pass heat exchanger

Standard gate valve (for flow control)

Air Transport

Ingersoll-Rand T30 Model 2545 Industrial Air Compressor

1379kPa (200psi) regulator / filter-drier assembly

Copper coil heat exchanger submerged in flowing water

Secondary filter drier assembly

Parker Model 24NS 82(A)-V8LN-SS Needle Valve (for flow control)

Coriolis Mass Flow Meters

Micro Motion Elite Series Model CMF100 coupled with Micro Motion Model RFT9739 Field Mount Transmitter (water side flow rate measurement)

Micro Motion Elite Series Model CMF025 coupled with Micro Motion Model 1700 Transmitter (air side flow rate measurement)

Data Acquisition

National Instruments SCXI 1000 Chassis

(2) National Instruments SCXI 1102s 32 channel modules

National Instruments SCXI 1125 8 channel module

(2) National Instruments SCXI 1303 32 Channel Isothermal Terminal Blocks

National Instruments SCXI 1313 8 Channel High Voltage Attenuator Terminal Block

CPU of choice for recording of data

Pressure Transducer

Validyne Model DP-15 pressure transducer

Validyne Model CD15 carrier demodulator

Diaphragm numbers 26, 32, and 36, corresponding to maximum pressures of 3.5kPa (0.5psi), 14.0kPa (2.0psi), and 35.0kPa (5.0psi),

Heated Test Branch

Kolflo Model 3/8-40C-4-3-3V-2 3 vane static mixer (at inlet)

Kolflo ½-80-4C-3-2 3 vane static mixer (at outlet)

Miller Maxtron 450 arc welder (lower current supply)

Lincoln Idealarc DC-600 three phase rectified electric welder (higher current supply)

Empro Model B-1000-50 shunt (current readings)

Test Section: Schedule 40 IPS Alloy 304 Stainless Steel; Length 101.6cm (40in), Diameter 12.52mm (0.493in)

Flow Visualization Sections: Optical Clarity Polycarbonate Tubing; Diameter 1.27cm (0.50in)

(28) Omega CO1-T Thermocouples (thermocouple array)

(2) Omega TMQSS-06U-6 Thermocouple Probes (inlet and outlet)

Omega EXTT-T-24-SLE Thermocouple Wire

Omegabond 101 Two-Part Thermocouple Epoxy (for adhering of thermocouple array)

Micro-Lok Fiber Glass Pipe Insulation (7.62cm (3in) thickness) (test section insulation)

Flow Visualization / Void Fraction Branch

Kolflo Model 3/8-40C-4-3-3V-2 3 vane static mixer (at inlet) *

Kolflo ½-80-4C-3-2 3 vane static mixer (at outlet) *

*Note: Same static mixers employed for both test sections.

(2) Omega Model TMQSS-06U-6 Thermocouple Probes (inlet and outlet)

Omega EXTT-T-24-SLE Thermocouple Wire

(3) W. E. Anderson Model ABV1DA101 Pneumatic Ball Valves

(3) Dynaquip Controls Model 145750.01 solenoid controllers

Flow Visualization Section: Optical Clarity Polycarbonate Tubing; Length 152.4cm (60in), Diameter 1.27cm (0.50in)

Photographic Equipment

Nikon D50 digital SLR (still photos)

Sony Handycam DCR-VX2100 Digital Video Camera Recorder (videos)

(2) 500 Watt photographic lights

(2) Roscolux #105 Tough Spun Gel Diffusers

APPENDIX B

UNCERTAINTY ANALYSIS

The main objective of this study has been to evaluate the performance of the newly designed experimental apparatus. As a part of this performance evaluation, it was necessary to conduct a thorough uncertainty analysis. Three main parameters were investigated through the course of the study as a part of the evaluation process. These parameters are friction factor, void fraction, and heat transfer coefficient. The uncertainty associated with each of these parameters has been investigated using the methods proposed by Kline and McClintock (1953). The uncertainty associated with each of these parameters will be discussed individually in the order in which the associated results were presented in the Results and Discussion Section (i.e. friction factor, void fraction, and heat transfer coefficient).

B.1 Friction Factor

The Darcy friction factor was used as the primary basis of evaluation of the single-phase pressure drop measurements conducted with the experimental apparatus. The Darcy friction factor is defined as:

$$f = \frac{\Delta p \frac{D}{l}}{\frac{\rho V^2}{2}} = \frac{2\Delta p D}{\rho l V^2} \tag{B.1}$$

In this equation, it is necessary to substitute in relations for the area and velocity squared terms. These relations are as follows:

$$A = \frac{\pi D^2}{4} \tag{B.2}$$

$$V^2 = \frac{16\dot{m}^2}{\rho^2 \pi^2 D^4} \tag{B.3}$$

If we then substitute these relations back into Equation (B.1), we get:

$$f = \frac{2\Delta p D^5 \rho \pi^2}{16 l \dot{m}^2} \tag{B.4}$$

Thus, it can be seen that the friction factor is a function of the pressure drop, test section inner diameter, density, test section length, and mass flow rate. The uncertainty in the Darcy friction factor can then be calculated using the following relation:

$$w_f = \left[\begin{array}{l} \left(\frac{\partial u_f}{\partial \Delta p} w_{\Delta p} \right)^2 + \left(\frac{\partial u_f}{\partial \rho} w_\rho \right)^2 \\ + \left(\frac{\partial u_f}{\partial l} w_l \right)^2 + \left(\frac{\partial u_f}{\partial \dot{m}} w_{\dot{m}} \right)^2 + \left(\frac{\partial u_f}{\partial D} w_D \right)^2 \end{array} \right]^{\frac{1}{2}} \tag{B.5}$$

The entire function can then be divided by friction factor in order to give a percentage error as follows:

$$\frac{w_f}{f} = \left[\left(\frac{1}{\Delta p} w_{\Delta p} \right)^2 + \left(\frac{1}{\rho} w_\rho \right)^2 + \left(\frac{1}{l} w_l \right)^2 + \left(\frac{2}{\dot{m}} w_{\dot{m}} \right)^2 + \left(\frac{5}{D} w_D \right)^2 \right]^{\frac{1}{2}} \tag{B.6}$$

The appropriate values can then be substituted into this equation in order to generate the experimental uncertainty. Table B.1 presents the measurement device or method used to obtain each variable as well as the uncertainties associated with each of these devices.

Table B.1: Uncertainties Associated with Friction Factor

Instrument / Method	Parameter Measured	Associated Uncertainty
Validyne Pressure Transducer	Pressure Drop (Δp)	±0.25% FS
Fitted Equation (Linstrom & Mallard (2003))	Density (ρ)	±0.06%
Dial Calipers	Length (l)	±0.127mm
MicroMotion Coriolis Flow Meter	Mass Flow Rate ($\dot{m}$)	±1.8% (worst case)
Dial Calipers	Diameter (D)	±0.127mm

In order to simplify calculations, all of the associated uncertainties were converted into percentages of reading. This accomplished, it was possible to obtain a worst case uncertainty for friction factor of ±3.85%.

B.2 Void Fraction

By definition the void fraction of a trapped portion of two-phase flow is as follows:

$$\alpha = 1 - \frac{V_{liq}}{V_{tot}} \tag{B.7}$$

For the purposes of this study, it was convenient to measure the mass of the liquid quantities involved rather than the volume. Thus it was necessary to convert the void fraction correlation to a mass relation rather than a volume relation. With the knowledge that the density of water is readily approximated as 1g/cc, the following relation was generated for the void fraction of the experimental apparatus:

$$\alpha = 1 - \frac{m_{liq}}{m_{tot}} \tag{B.8}$$

In this equation, m_{liq} represents the mass of the liquid drained into the collection tank. The term m_{tot} represents the total mass of liquid that can be contained within the test section. The value m_{tot} has an estimated uncertainty of ±2.0g.

The uncertainty associated with the mass of the liquid drained from the test section of the experimental apparatus is directly related to the angle of inclination at which the measurements are taken. As part of the measurement of this value, it is necessary to zero the test section with respect to the fluid inherently trapped within the system. The associated uncertainty in the zero values varies with inclination angle. For the purposes of this uncertainty investigation, this value was taken at its maximum (referred to as m_{cal}) of 17.8g with an associated uncertainty of ±2.0g.

Each of the zero values was obtained by averaging a series of measurements of the losses associated with draining the test section when it was completely filled with fluid. The uncertainties were developed based upon the variability of the data that was used to obtain the averages.

It should also be noted that the measurement of the mass of the fluid in the collection tank was found by subtracting the measured mass of the empty tank (m_{tk}) from the combined measured mass of the tank and drained liquid (m_{tk+liq}). Each of these masses is measured using a scale with a resolution of 1g. Hence, they each have associated uncertainties of ±0.5g. If these measured masses and the correction factor are introduced into the void fraction equation, the following relation is generated:

$$\alpha = 1 - \frac{m_{tk+liq} - m_{tk} + m_{cal}}{m_{tot}} \tag{B.9}$$

where

$$m_{liq} = m_{tk+liq} - m_{tk} + m_{cal} \tag{B.10}$$

The uncertainties associated with the variables that make up m_{liq} are additive. Thus, for the worst case scenario, the maximum uncertainty associated with the value of m_{liq} is ±3.0g.

The uncertainty associated with the void fraction measurement can be calculated from the following relation:

$$w_\alpha = \left[\left(\frac{\partial \alpha}{\partial m_{liq}} w_{m_{liq}} \right)^2 + \left(\frac{\partial \alpha}{\partial m_{tot}} w_{m_{tot}} \right)^2 \right]^{\frac{1}{2}} \tag{B.11}$$

or

$$w_\alpha = \left[\left(\frac{1}{m_{tot}} w_{m_{liq}} \right)^2 + \left(\frac{m_{liq}}{m_{tot}^2} w_{m_{tot}} \right)^2 \right]^{\frac{1}{2}} \tag{B.12}$$

The uncertainty associated with the void fraction values obtained is dependent upon the range of the void fraction being measured. In other words, percentage accuracy is lost to a small degree with decreasing void fraction values. This dependency of uncertainty upon void fraction values necessitated that test runs at both high and low void fraction be used for the purposes of uncertainty analysis. For the purposes of this investigation, a worst case scenario value was generated at a void fraction value of 0.28 and a best case uncertainty was developed at a void fraction value of 0.86. The values for the sample test runs are presented in Table B.2.

Table B.2: Selected Void Fraction Runs for Uncertainty Analysis

Condition	Run #	α	m-liq (g)	m-tot (g)
High VF	RN0086VF	0.8639	20	277.5
Low VF	RN0115VF	0.2836	181	277.5

If the selected values are then substituted into the uncertainty equation, a value of uncertainty in void fraction of ±0.0108 or ±1.25% is obtained for the high void fraction condition. For the low void fraction condition, an uncertainty value of ±0.01174 or ±4.16% is attained.

B.3 Heat Transfer Coefficient

Nusselt number was used as the primary means of evaluation for the heat transfer data obtained from the experimental apparatus. However, the uncertainty associated with the heat transfer coefficient has been investigated in order to present uncertainty results that are directly comparable with those presented by other researchers in this area. In order to simplify calculation, this uncertainty analysis will be conducted with the assumption of single phase heat transfer. This will give an acceptable estimate of the uncertainty generated by the equipment utilized in obtaining the necessary values to calculate the heat transfer coefficient. The heat transfer coefficient is defined as the following:

$$h = \frac{\dot{q}''}{\overline{T}_{wi} - \overline{T}_b} = \frac{\dot{q}''}{\Delta T} \tag{B.13}$$

The uncertainty in the heat transfer coefficient can be obtained from the following relation:

$$w_h = \left[\left(\frac{\partial h}{\partial \dot{q}''} w_{\dot{q}''} \right)^2 + \left(\frac{\partial h}{\partial \Delta T} w_{\Delta T} \right)^2 \right]^{\frac{1}{2}} \tag{B.14}$$

This equation can be rewritten with proper values substituted as the following:

$$w_h = \left[\left(\frac{1}{\Delta T} w_{\dot{q}''} \right)^2 + \left(\frac{-\dot{q}''}{\Delta T^2} w_{\Delta T} \right)^2 \right]^{\frac{1}{2}} \tag{B.15}$$

From this uncertainty relation, it can be seen that it is necessary to develop uncertainties for both the quantity ($\overline{T}_{wi} - \overline{T}_b$) and the heat flux. The uncertainty associated with the ΔT value can be assumed to be the sum of the uncertainties associated with the average wall inner temperature and the bulk temperature. The equation for the average wall inner temperature is as follows:

$$\overline{T}_{wi} = \dot{q} R_t + \overline{T}_{wo} \tag{B.16}$$

The uncertainty associated with the wall inner temperature can be calculated using the following relation:

$$w_{\overline{T}_{wi}} = \left[\left(\frac{\partial \overline{T}_{wi}}{\partial \dot{q}} w_{\dot{q}} \right)^2 + \left(\frac{\partial \overline{T}_{wi}}{\partial R_t} w_{R_t} \right)^2 + \left(\frac{\partial \overline{T}_{wi}}{\partial \overline{T}_{wo}} w_{\overline{T}_{wo}} \right)^2 \right]^{\frac{1}{2}} \tag{B.17}$$

If proper values are then substituted into the equation, the following uncertainty relation is obtained:

$$w_{\overline{T}_{wi}} = \left[\left(R_t w_{\dot{q}} \right)^2 + \left(\dot{q} w_{R_t} \right)^2 + \left(w_{\overline{T}_{wo}} \right)^2 \right]^{\frac{1}{2}} \tag{B.18}$$

It should be noted in this equation that both the inner wall temperature and the outer wall temperature are averages. The outer wall temperature at each station was taken to be the average of the readings of the four thermocouples at that station. Figure 2.7 can be used

as a reference for the thermocouple positioning along the test section length as well as at each station. Thus, for the temperature at each station, we have the relation:

$$\overline{T}_{wosn} = \frac{\overline{T}_{wo-1} + \overline{T}_{wo-2} + \overline{T}_{wo-3} + \overline{T}_{wo-4}}{4} \tag{B.19}$$

In this equation, $\overline{T}_{wosn}$ indicates the average outer wall temperature at a given station number. $\overline{T}_{wo-1}$ through $\overline{T}_{wo-4}$ represent the average outer wall temperatures for each of the four thermocouples at particular station.

The uncertainty associated with all of the thermocouples attached to the heated test section has been reduced to within ±0.5˚C through the calibration process. Since the uncertainties of the thermocouples are considered identical, the uncertainty in the average temperature at each station can be assumed to be ±0.5˚C as well. There are seven total thermocouple stations in place across the length of the test section. In order to obtain a value for the average wall outer temperature, a numerical average of the average temperatures obtained for each station was taken as follows:

$$\overline{T}_{wo} = \frac{\overline{T}_{wos1} + \overline{T}_{wos2} + \overline{T}_{wos3} + \overline{T}_{wos4} + \overline{T}_{wos5} + \overline{T}_{wos6} + \overline{T}_{wos7}}{7} \tag{B.20}$$

Once again, the uncertainty associated with the outer wall average temperature can be assumed as ±0.5˚C.

It is also necessary to calculate an uncertainty for the thermal resistance of the heated test section. The equation for thermal resistance is as follows:

$$R_t = \frac{\ln(D_o / D_i)}{2\pi k l} \tag{B.21}$$

The uncertainty associated with the thermal resistance can be calculated from the following relation:

$$w_{R_t} = \left[\left(\frac{\partial R_t}{\partial D_o} w_{D_o} \right)^2 + \left(\frac{\partial R_t}{\partial D_i} w_{D_i} \right)^2 + \left(\frac{\partial R_t}{\partial k} w_k \right)^2 + \left(\frac{\partial R_t}{\partial l} w_l \right)^2 \right]^{\frac{1}{2}} \tag{B.22}$$

Substituting in appropriate values, this relation can be rewritten as:

$$w_{R_t} = \left[\begin{array}{l} \left(\frac{1}{2\pi D_o kl} w_{D_o} \right)^2 + \left(\frac{-1}{2\pi D_i kl} w_{D_i} \right)^2 \\ + \left(\frac{-\ln\left(D_o / D_i \right)}{2\pi k^2 l} w_k \right)^2 + \left(\frac{-\ln\left(D_o / D_i \right)}{2\pi k l^2} w_l \right)^2 \end{array} \right]^{\frac{1}{2}} \tag{B.23}$$

In order to evaluate the uncertainty in thermal resistance as well as the uncertainty associated with other needed variables, it was necessary to utilize values from specific single-phase heat transfer test runs. The values with measured and/or manufacturer prescribed uncertainties associated with this random test run are shown for the best case heat transfer coefficient uncertainty are shown in Table B.3. Table B.4 depicts the calculated uncertainties associated with this test run. Table B.5 shows the measured and/or manufacturer prescribed uncertainties associated with the worst case heat transfer coefficient uncertainty. In Table B.6 the calculated uncertainties associated with the worst case heat transfer uncertainty are depicted. Substituting in appropriate values, it was possible to find that the uncertainty associated with the thermal resistance remained relatively constant at ±02.18E-5K/W or between ±0.60% of the thermal resistance value. It should be noted that as the value for the thermal conductivity was obtained from a best fit curve of tabulated data, the uncertainty associated with this value was considered negligible.

It was next necessary to calculate an uncertainty for the heat transfer rate. While an enthalpy based relation for heat transfer rate is generally more desirable for single phase flow, the following relation based on voltage and amperage input is more representative of the finite-differencing calculations that are necessary for developing heat transfer rates for two-phase flows.

$$\dot{q} = V_D I \tag{B.24}$$

The uncertainty equation can be written as follows:

$$w_{\dot{q}} = \left[\left(\frac{\partial \dot{q}}{\partial V_D} w_{V_D} \right)^2 + \left(\frac{\partial \dot{q}}{\partial I} w_I \right)^2 \right]^{\frac{1}{2}} \tag{B.25}$$

Substituting in proper values for the partial derivatives yields:

$$w_{\dot{q}} = \left[\left(I w_{V_D} \right)^2 + \left(V_D w_I \right)^2 \right]^{\frac{1}{2}} \tag{B.26}$$

Both the measured amperage and voltage drop have uncertainties of ±1.0%. This uncertainty is associated with the inherent error of the National Instruments data acquisition system used to capture these values. For the test cases investigated, the error associated with the heat transfer rate calculated from the measured power input ranged between ±39.9W and ±51.36W or between±1.41% and ±1.49% of the calculated value. As a means of verifying the validity of the power input to the system, the following enthalpy based equation was used.

$$\dot{q} = \dot{m} C_p \left(T_{b,out} - T_{b,in} \right) \tag{B.27}$$

For each run, the difference between the enthalpy based calculation and the input power calculation of the heat transfer rate was assumed to be the error associated with losses due to convection and/or storage within the test section itself. For the test runs conducted

up to this point, this heat balance error has ranged between -3.44% and -6.89%. The error associated with the heat balance is added to the error associated with the measured power input in order to obtain a total uncertainty in the heat transfer rate. For the data collected to date, the total uncertainty in the heat transfer rate has varied between -2.03% and -8.31%. It should be noted that it is not physically possible to obtain a positive error in heat transfer rate as heat would have to be added to the system from some outside source.

Having calculated the uncertainties in outer wall average temperature, thermal resistance, and heat transfer rate it is possible to calculate the uncertainty in inner wall average temperature. Substituting the proper values into Equation (B.18) yields an uncertainty in inner wall temperature between -0.570˚C and -1.154˚C or between -0.98% and -2.19% of the measured value.

Prior to calculating an uncertainty in heat transfer coefficient, it was also necessary to calculate an uncertainty in heat flux. The equation for the heat flux associated with the system is the following:

$$\dot{q}'' = \frac{V_D I}{\pi D_i L} \tag{B.28}$$

The following uncertainty relation can be derived for the equation:

$$w_{\dot{q}''} = \left[\left(\frac{\partial \dot{q}''}{\partial V_D} w_{V_D} \right)^2 + \left(\frac{\partial \dot{q}''}{\partial I} w_I \right)^2 + \left(\frac{\partial \dot{q}''}{\partial D_i} w_{D_i} \right)^2 + \left(\frac{\partial \dot{q}''}{\partial l} w_l \right)^2 \right]^{\frac{1}{2}} \tag{B.29}$$

Substituting in the proper variables for the partial derivatives yields the following equation:

$$w_{\dot{q}''} = \left[\left(\frac{I}{\pi D_i l} w_{V_D} \right)^2 + \left(\frac{V_D}{\pi D_i l} w_I \right)^2 + \left(\frac{-V_D I}{\pi D_i^2 l} w_{D_i} \right)^2 + \left(\frac{-V_D I}{\pi D_i l^2} w_l \right)^2 \right]^{\frac{1}{2}} \quad \text{(B.30)}$$

Utilizing the proper values in combination with this equation yields an uncertainty in heat flux of between -1826W/m^2 and -7113W/m^2 or -2.06%.and -8.33% of value.

Having calculated all of the intermediate uncertainty values, it was possible to calculate the overall uncertainty associated with the heat transfer coefficient. The uncertainty values obtained ranged between -1.40% and -3.80% of calculated values. The tabulated values for the best and worst case uncertainties associated with heat transfer coefficient are shown in Tables B.3 through B.6.

Table B.3: Measured Values and Associated Uncertainties (Best Case – Run 002)

Variable	Value	Uncertainty	Uncertainty (% value)
Test Section Inner Diameter (D_i) (m)	0.0125	1.270E-05	0.10%
Test Section Outer Diameter(D_o) (m)	0.0171	1.270E-05	0.07%
Test Section Length (l) (m)	1.016	3.175E-03	0.31%
Thermal Conductivity (k) (W/m-K)	13.438	NA	NA
Voltage Drop (V_d) (V)	4.95018	0.050	1.00%
Applied Amperage (I) (A)	716.558	7.166	1.00%
Mass Flow Rate ($\dot{m}$) (kg/s)	0.190659	9.533E-04	0.50%
Avg. Bulk Temperature (T_b) (ºC)	25.922	0.500	1.93%
Inlet - Outlet Bulk Temp.(ΔT_b) (ºC)	4.29634	1.000	23.28%
Specific Heat (C_p) (J/kg-K)	4167.234	NA	NA
Inner Wall Temp - Avg. Bulk Temp	32.493	NA	NA

Table B.4: Calculated Values and Associated Uncertainties (Best Case – Run 002)

Variable	Value	Uncertainty	Uncertainty (% value)
Outer Wall Average Temperature (T_o) (ºC)	45.458	0.500	1.10%
Inner Wall Average Temperature (T_i) (ºC) (upper)	58.414	-0.570	-0.98%
Inner Wall Average Temperature (T_i) (ºC) (lower)	58.414	-0.807	-1.38%
Thermal Resistance (R_i) (K/W)	0.0037	2.181E-05	0.60%
Heat Balance Error (q_{err}) (W)	NA	-122.0872907	-3.44%
Input Heat Transfer Rate (q_{in}) (W) (upper)	3547.09	-71.924	-2.03%
Input Heat Transfer Rate (q_{in}) (W) (lower)	3547.09	-172.251	-4.86%
Heat Flux (q") (W/m^2) (upper)	88745.9	-1826.202	-2.06%
Heat Flux (q") (W/m^2) (lower)	88745.9	-4327.129	-4.88%
Heat Transfer Coefficient (h) (W/m^2-K) (upper)	7562.32	-106.066	-1.40%
Heat Transfer Coefficient (h) (W/m^2-K) (lower)	7562.32	-172.662	-2.28%

Table B.5: Measured Values and Associated Uncertainties (Worst Case – Run 005)

Variable	Value	Uncertainty	Uncertainty (% value)
Test Section Inner Diameter (D_i) (m)	0.0125	1.270E-05	0.10%
Test Section Outer Diameter(D_o) (m)	0.0171	1.270E-05	0.07%
Test Section Length (l) (m)	1.016	3.175E-03	0.31%
Thermal Conductivity (k) (W/m-K)	13.465	NA	NA
Voltage Drop (V_d) (V)	4.43211	0.044	1.00%
Applied Amperage (I) (A)	636.547	6.365	1.00%
Mass Flow Rate ($\dot{m}$) (kg/s)	0.076468	3.823E-04	0.50%
Avg. Bulk Temperature (T_b) (ºC)	27.505	0.500	1.82%
Inlet - Outlet Bulk Temp.(ΔT_b) (ºC)	8.40994	1.000	11.89%
Specific Heat (C_p) (J/kg-K)	4149.659	NA	NA
Inner Wall Temp - Avg. Bulk Temp	36.438	NA	NA

Table B.6: Calculated Values and Associated Uncertainties (Worst Case – Run 005)

Variable	Value	Uncertainty	Uncertainty (% value)
Outer Wall Average Temperature (T_o) (ºC)	53.658	0.500	0.93%
Inner Wall Average Temperature (T_i) (ºC) (upper)	63.942	-0.605	-0.95%
Inner Wall Average Temperature (T_i) (ºC) (lower)	63.942	-0.803	-1.26%
Thermal Resistance (R_t) (K/W)	0.0036	2.177E-05	0.60%
Heat Balance Error (q_{err}) (W)	NA	-131.6336004	-4.67%
Input Heat Transfer Rate (q_{in}) (W) (upper)	2821.25	-91.735	-3.25%
Input Heat Transfer Rate (q_{in}) (W) (lower)	2821.25	-171.532	-6.08%
Heat Flux (q") (W/m^2) (upper)	70585.8	-2310.942	-3.27%
Heat Flux (q") (W/m^2) (lower)	70585.8	-4305.518	-6.10%
Heat Transfer Coefficient (h) (W/m^2-K) (upper)	3604.95	-86.436	-2.40%
Heat Transfer Coefficient (h) (W/m^2-K) (lower)	3604.95	-136.968	-3.80%

It should be noted that the uncertainty associated with the heat transfer coefficient is highly dependent upon two different factors. These are the heat balance error and the difference between the average inner wall temperature and the average bulk temperature. The calculated heat balance error serves as the major criteria for the retention of collected data. Minimization of the heat balance error causes notable increases in the accuracy of the data obtained. In cases of collection of single-phase heat transfer data, it is required that the heat balance error is kept below -8%. Inherently, higher heat balance errors are associated with the collection of two-phase heat transfer data. This is due to the fact that the inlet and exit temperature probes are not necessarily in contact with both phases of the flow. For this mode of data collection, the restriction on acceptable heat balance error is relaxed to a value of -20%.

Maximizing the difference between the average inner wall temperature and the average bulk temperature inherently increases the accuracy of the heat transfer coefficient value obtained. This can be seen readily if Equations (B.13) through (B.15) are referenced. It is not possible to directly monitor the average bulk temperature or the

average inner wall temperature. However, the outer wall temperatures at each station and the inlet and outlet bulk temperatures can be measured directly. If the difference between the temperature at one of the later stations and the bulk temperature at the inlet or outlet is maximized, it can be assumed that the difference between the average inner wall temperature and the average bulk temperature has been maximized as well. Special care must be taken to keep this temperature differential as high as possible in order to ensure the accuracy of the data collected.

VITA

Wendell L. Cook

Candidate for the Degree of

Master of Science

Thesis: AN EXPERIMENTAL APPARATUS FOR MEASUREMENT OF PRESSURE DROP, VOID FRACTION, AND NON-BOILING TWO-PHASE HEAT TRANSFER AND FLOW VISUALIZATION IN PIPES FOR ALL INCLINATIONS

Major Field: Mechanical Engineering

Biographical:

Personal Data: Born in Brownsville, Texas on September 30, 1980, the son of George and Susan Cook

Education: Graduated from the Science Academy of South Texas, Mercedes, Texas in May, 1999; received Bachelor of Science degree in Mechanical Engineering from Oklahoma State University, Stillwater, Oklahoma in December, 2004. Completed the requirements for the Master of Science in Mechanical Engineering at Oklahoma State University, Stillwater, Oklahoma in December, 2008.

Experience: School of Mechanical and Aerospace Engineering as a teaching assistant. Oklahoma State University School of Mechanical and Aerospace Engineering, 2005 to 2008.

Name: Wendell L. Cook Date of Degree: December, 2008

Institution: Oklahoma State University Location: Stillwater, Oklahoma

Title of Study: AN EXPERIMENTAL APPARATUS FOR MEASUREMENT OF PRESSURE DROP, VOID FRACTION, AND NON-BOILING TWO-PHASE HEAT TRANSFER AND FLOW VISUALIZATION IN PIPES FOR ALL INCLINATIONS

Pages in Study: 131 Candidate for the Degree of Master of Science

Major Field: Mechanical Engineering

Scope and Method of Study: This study has been conducted in order to present the design, construction, and validation of a state-of-the-art experimental apparatus for the purposes of measurement of pressure drop, void fraction, and non-boiling two-phase heat transfer and flow visualization in pipes with inclination angles ranging between positive and negative ninety degrees. Methods of validation for each intended capability of the experimental apparatus have included comparison of the data obtained with established correlations. In addition, void fraction measurements have been compared against experimental data obtained from four independent sources. In the cases of single-phase heat transfer and two-phase non-boiling heat transfer, direct comparisons have been made between data obtained with the newly completed experimental apparatus and data previously collected at the Oklahoma State University heat transfer laboratory. Examples of the flow visualization capabilities as well as methodology have been presented.

Findings and Conclusions: Validations of the experimental apparatus for each of the intended modes of data collection including pressure drop, void fraction, and non-boiling two-phase heat transfer have proved highly satisfactory. In addition flow visualization was conducted using the experimental apparatus with excellent results. Having validated the functionality of this experimental apparatus, it is intended that it be utilized to further test correlations that have been developed for two-phase non-boiling heat transfer in pipes and void fraction. It is intended that the experimental apparatus be utilized to continue to develop these equations so that they are applicable for any angle of inclination between positive and negative ninety degrees. It is also intended that the device be used for generating flow maps for inclinations between positive and negative ninety degrees. The device should be considered both a highly capable and versatile addition to the Oklahoma State University heat transfer laboratory.

ADVISER'S APPROVAL: Dr. Afshin J.Ghajar